

ABSTRACT

SUMIYOSHI, TAISUKE. Synthesis and Reactivity of Ruthenium(II) and Platinum(IV) Complexes. (Under the direction of Dr. T. Brent Gunnoe.)

Late transition metals and non-dative heteroatomic ligand complexes (non-dative heteroatomic ligand = imido, oxo, amido, hydroxo, and alkoxo) have a potential application toward C-H activation. However, these complexes are synthetically and catalytically challenging, and there are more things to learn about these systems.

Complexes possessing a soft donor η^6 -arene and hard donor acetylacetonate ligand, $[(\eta^6\text{-}p\text{-cymene})\text{Ru}(\kappa^2\text{-}O,O\text{-acac-}\mu\text{-CH})_2][\text{OTf}]_2$ (OTf = trifluoromethanesulfonate; acac = acetylacetonate) and $[(\eta^6\text{-}p\text{-cymene})\text{Ru}(\kappa^2\text{-}O,O\text{-acac})(\text{THF})][\text{BAr}'_4]$ {Ar' = 3,5-(CF₃)-C₆H₃}, were prepared and fully characterized. The lability of the $\mu\text{-CH}$ linkage for complex $[(\eta^6\text{-}p\text{-cymene})\text{Ru}(\kappa^2\text{-}O,O\text{-acac-}\mu\text{-CH})_2][\text{OTf}]_2$ and the THF ligand of $[(\eta^6\text{-}p\text{-cymene})\text{Ru}(\kappa^2\text{-}O,O\text{-acac})(\text{THF})][\text{BAr}'_4]$ allow access to the unsaturated cation $[(\eta^6\text{-}p\text{-cymene})\text{Ru}(\kappa^2\text{-}O,O\text{-acac})]^+$. The reaction of $[(\eta^6\text{-}p\text{-cymene})\text{Ru}(\kappa^2\text{-}O,O\text{-acac})(\text{THF})][\text{BAr}'_4]$ with KTp {Tp = hydridotris(pyrazolyl)borate} produces $[\text{TpRu}(\eta^6\text{-}p\text{-cymene})][\text{BAr}'_4]$. The azide complex $[(\eta^6\text{-}p\text{-cymene})\text{Ru}(\kappa^2\text{-}O,O\text{-acac})(\text{N}_3\text{Ar})][\text{BAr}'_4]$ forms upon reaction of $[(\eta^6\text{-}p\text{-cymene})\text{Ru}(\kappa^2\text{-}O,O\text{-acac})(\text{THF})][\text{BAr}'_4]$ with N₃Ar (Ar = *p*-tolyl), and reaction of $[(\eta^6\text{-}p\text{-cymene})\text{Ru}(\kappa^2\text{-}O,O\text{-acac})(\text{THF})][\text{BAr}'_4]$ with CHCl₃ at 100 °C yields the chloride-bridged binuclear complex $[(\eta^6\text{-}p\text{-cymene})\text{Ru}]_2(\mu\text{-Cl})_3[\text{BAr}'_4]$. The details of solid-state structures of $[(\eta^6\text{-}p\text{-cymene})\text{Ru}(\kappa^2\text{-}O,O\text{-acac-}\mu\text{-CH})_2][\text{OTf}]_2$, $[\text{TpRu}(\eta^6\text{-}p\text{-cymene})][\text{BAr}'_4]$ and $[(\eta^6\text{-}p\text{-cymene})\text{Ru}]_2(\mu\text{-Cl})_3[\text{BAr}'_4]$ are disclosed.

Synthesis of platinum (IV) complexes such as $(\text{NCN})\text{Pt}(\text{Me})_2\text{X}$ and $(\text{NCN}')\text{Pt}(\text{Me})_2\text{X}$ { $\text{NCN} = 2,6\text{-}(\text{pzCH}_2)_2\text{C}_6\text{H}_3$; $\text{NCN}' = 2,6\text{-}(3,5\text{-Me}_2\text{pzCH}_2)_2\text{C}_6\text{H}_3$; $\text{X} = \text{triflate}$ } were prepared, and tested to insert oxygen atom from oxidants into Pt-CH₃ bonds. Also, $[(\text{NCN}')\text{Pt}(\text{Me})_2(\text{THF})][\text{BAr}'_4]$ ($\text{Ar}' = 3,5\text{-}(\text{CF}_3)_2\text{C}_6\text{H}_3$) complex have ligand exchange with oxidants such as pyridine-*N*-oxide and trimethylamine-*N*-oxide to yield $[(\text{NCN}')\text{Pt}(\text{Me})_2(\text{O-py})][\text{BAr}'_4]$ and $[(\text{NCN}')\text{Pt}(\text{Me})_2(\text{O-NMe}_3)][\text{BAr}'_4]$.

Synthesis and Reactivity of Ruthenium(II) and Platinum(IV) Complexes

by

Taisuke Sumiyoshi

A dissertation submitted to the Graduate Faculty of

North Carolina State University

In partial fulfillment of the

Requirements for the degree of

Master of Science

Chemistry

Raleigh, NC

2007

Approved by:

James D. Martin

Christian Melander

Elon Ison

T. Brent Gunnoe
Chair of Advisory Committee

DEDICATION

Beauty in nature and collapse in science.

BIOGRAPHY

Taisuke Sumiyoshi was born on June 15th, 1979 in Zama, Kanagawa province, Japan. He had grown up in the city until high school in Japan, and he became interested in environmental and social problems. He entered LeesMcRae College at western part of North Carolina in the United State in 1998. Why North Carolina remains unknown even today. After transferring to Western Carolina University, he graduated from the university with B.S. degree in chemistry and minor in mathematics in 2003. During the study, he met a farm family, Hamiltons, and realized people must live on soil, water, and some wind. Therefore, he came North Carolina State University for graduate work in science of chemistry to attempt understanding nature in 2004. He worked on Master of Science with direction of T. Brent Gunnoe. As he studied in the graduate school, he realized there is a conflict between absolute world (nature) and relative world (human society), which cannot be mixed. For 12 years, he has had the environmental/social problem on his mind, and it ends up with a really simple answer. People just have to choose either nature or this society.

ACKNOWLEDGMENTS

I like to thank my advisor Dr. T Brent Gunnoe. He taught me how to think in chemistry. Also, all the professors I had interact with help my research and understanding science. Thank you.

I thank Hamilton family and all Fairview people, especially Susie and William. Thank you for always welcoming me to stay and show me the local and small-scale farm. I don't know how I could survive in mountains without you. I learned an adventure mind from you. "Open your heart and there is nothing to worry about." Infinite joy in Fairview!

I thank Mike and Aiko Ward for always supporting and encouraging me. Whenever I am tired, they let me rest my wings to recharge my battery. "This life is bonus!" What a positive attitude! You are my goal.

I thank Elizabeth and Fred for sharing an idea of feeding a community. Life is quite beautiful on the soil and water. I enjoyed their goat's milk!

I thank existence of Appalachian Mountains. Mother Nature!

I thank families of Basso, Jones, Neal, and Stumpf for making my life in Raleigh enjoyable. It all started from Fleet Feet in Raleigh, so I like to thank Fleet Feet owners, Bob and Kathy. I had no time to think about bad things because they kept me busy with running and happy hours. I cannot think good life here without them. Running was a big part of me in Raleigh. Thank you, Stephanie, Shawna, Julie, Candice, and Anne, for running with me. I will never forget how fun it was!!

I thank Gunnoe group for helping me all kinds of things. I don't know how much trouble I made, but thank them for looking after me. Especially, I like to thank Mr. Delp for

welcoming to stay last half year. I cannot thank enough for this. I'm glad that Copper learned how to sit! Nice back move, Atreyu!

I thank this country, the United States of America, for giving me an opportunity to come to schools and meet people.

Finally, I thank my family for giving me good health. That's best thing I got in my life, so I will take care of it. Thank you for all your supports, encouragements, and worries. I have realized the value to have my family since I moved to the US. I am sorry Grandma. I'm too late. I wish you heard me to say... Somehow I grew up without you around, and I became little bit idealistically crazy. I will go on the way I believe.

I am always so grateful to have my family and friends around. Anywhere I go, I always have good people around. I am just too lucky. Thank you, everyone! Good food, good wine, and good friends surrounded by beautiful nature...that's true heaven.

TABLE OF CONTENTS

LIST OF TABLES.....	ix
LIST OF FIGURES.....	x
LIST OF SCHEMES.....	xiii
LIST OF CHARTS.....	xvi
CHAPTER ONE.....	1
1.1 Late transition metals with anionic heteroatomic ligands.....	1
1.2 Bonding between transition metals and non-dative heteroatomic ligands.....	3
1.3 Synthesis of late transition metal amides and alkoxo complexes.....	5
1.4. Reactivity of late transition metals complexes with heteroatomic ligands.....	6
1.4.1 Basicity of Ru(II) anilido, amido and hydroxo, alkoxo and related complexes.....	8
1.4.2 Nucleophilicity of late transition metals and heteroatomic ligands complexes.....	15
1.4.2.a Arylamination and olefin hydroamination.....	16
1.4.3 C-H activation.....	19
1.4.3.a Activation of C-H bonds via 1,2-addition across metal-heteroatom bonds....	21
1.4.3.b Regeneration of metal non-dative ligand system.....	23
1.5 Late transition metal imido and oxo complexes.....	25
1.5.1 Examples of late transition metal imido and oxo species.....	25
1.5.2 Reactivity of late transition metal imido and oxo species.....	26
1.6 Summary.....	28
REFERENCES.....	30
CHAPTER TWO.....	34

2.1 Introduction.....	34
2.1.1 Background of metal imido and oxo species.....	34
2.1.2 Various metal complexes with <i>p</i> -cymene and acetylacetonate ligands.....	35
2.2 Synthesis and characterization of $[(\eta^6\text{-}p\text{-cymene})\text{Ru}(\kappa^2\text{-}O, O\text{-acac-}\mu\text{-CH})_2][\text{OTf}]_2$	37
2.2.1 Reaction of $[(\eta^6\text{-}p\text{-cymene})\text{Ru}(\kappa^2\text{-}O, O\text{-acac-}\mu\text{-CH})_2][\text{OTf}]_2$ with <i>p</i> -tolylazide and PhI=NTs.....	43
2.3 Synthesis and characterization of $[(\eta^6\text{-}p\text{-cymene})\text{Ru}(\kappa^2\text{-}O, O\text{-acac})(\text{THF})][\text{BAr}'_4]$	45
2.3.1 Reaction of $[(\eta^6\text{-}p\text{-cymene})\text{Ru}(\kappa^2\text{-}O, O\text{-acac})(\text{THF})][\text{BAr}'_4]$ with PhI=NTs and trimethylamine- <i>N</i> -oxide.....	49
2.3.2 Reactivity of $[(\eta^6\text{-}p\text{-cymene})\text{Ru}(\kappa^2\text{-}O, O\text{-acac})(\text{THF})][\text{BAr}'_4]$ with <i>p</i> -tolyl-azide..	53
2.3.3 Hydrogenation Catalysis.....	54
2.4 Synthesis and characterization of $[\text{TpRu}(\eta^6\text{-}p\text{-cymene})][\text{BAr}'_4]$	55
2.5 Reaction of $[(\eta^6\text{-}p\text{-cymene})\text{Ru}(\kappa^2\text{-}O, O\text{-acac})(\text{THF})][\text{BAr}'_4]$ in Chloroform and Methylene Chloride.....	59
2.6 Electrochemistry.....	62
2.7 Summary.....	64
2.8 Experimental procedures.....	64
REFERENCES	73
CHAPTER THREE	76
3.1 Saturated hydrocarbon C-H activation across M-X bonds of late transition metal complexes with non-dative heteroatomic ligands.....	76
3.1.1 C-H activation by Ru(II)-hydroxo/anilido and Ir(III)-methoxo complexes.....	76

3.1.2 Platinum (IV) complexes.....	78
3.1.3 Synthesis of platinum (IV) triflate complexes.....	79
3.1.4 Synthesis of platinum (IV) cationic species.....	81
3.2 Attempted conversion of Pt-R to Pt-OR.....	89
3.2.1 Attempted oxygen atom insertion into Pt ^{IV} -Me bonds.....	91
3.3 Summary.....	96
3.4 Experimental procedures.....	97
REFERENCES.....	103

LIST OF TABLES

Table 1.1. Kinetic data for the reaction of bromoethane with Cu ^I and Ru ^{II} complexes.....	16
Table 2.1. Selected bond distances (Å) and angles (°) for [(η ⁶ - <i>p</i> -cymene)Ru(κ ² - <i>O,O</i> -acac-μ-CH)] ₂ [OTf] ₂ (1).....	40
Table 2.2. Crystal data and structure refinement for complexes 1 , 5 and 7	40
Table 2.3. Selected bond distances (Å) and angles (°) for [TpRu(η ⁶ - <i>p</i> -cymene)][BAr' ₄] (5).....	59
Table 2.4. Selected bond distances (Å) and angles (°) for {[(η ⁶ - <i>p</i> -cymene) ₂ Ru] ₂ (μ-Cl) ₃ }[BAr' ₄] (7).....	62
Table 2.5. The redox potentials for the various Ru(II) complexes.....	63
Table 3.1. Selected bond distances (Å) and angles (°) for [(NCN')Pt(Me) ₂ (THF)][BAr' ₄] (3).....	85
Table 3.2. Selected crystallographic data for complexes 3 and 4	86
Table 3.3. Selected bond distances (Å) and angles (°) for [(NCN')Pt(Me) ₂ (NH ₃)][BAr' ₄] (4).....	89

LIST OF FIGURES

Figure 1.1. Proposed transition state of hydrogenation using ruthenium(II) complexes.....	2
Figure 1.2. Filled $d\pi$ and $p\pi$ orbital interaction.....	3
Figure 1.3. Resonance structure of M-X bond.....	4
Figure 1.4. Potential impact of π -bonding on geometry around X (e.g., X = NR ₂).....	7
Figure 1.5. Variation of bond distances for anilido complexes TpRu{P(OMe) ₃ } ₂ (NHPPh) and TpRu(PPh ₃)(CO)(NHPPh).....	13
Figure 1.6. Various pathways of metal-mediated C-H activation.....	20
Figure 1.7. C-H bond cleavage 1,2-addition cross metal-heteroatom bond.....	21
Figure 1.8. Energy differences at transition state between C-H activation with M-X vs. M- C.....	23
Figure 1.9. Stability of metal oxo-aryl or alkyl complexes.....	24
Figure 2.1. Molecular orbital diagram of π -bonding on d ⁴ and d ⁰ formally octahedral metal imido or oxo complex.....	35
Figure 2.2. Two potential coordination modes for acetylacetonate are κ^2 -O,O and κ^1 -C.....	36
Figure 2.3. ¹ H NMR spectrum of [(η^6 - <i>p</i> -cymene)Ru(κ^2 -O,O-acac- μ -CH)] ₂ [OTf] ₂ (1) in CDCl ₃	38
Figure 2.4. ¹³ C NMR spectrum of [(η^6 - <i>p</i> -cymene)Ru(κ^2 -O,O-acac- μ -CH)] ₂ [OTf] ₂ (1) in CDCl ₃	39
Figure 2.5. ORTEP (scaled to enclose 30% probability) of [(η^6 - <i>p</i> -cymene)Ru(κ^2 -O,O-acac-	

$\mu\text{-CH})_2[\text{OTf}]_2$ (1).....	35
Figure 2.6. ^1H NMR spectrum of $[(\eta^6\text{-}p\text{-cymene})\text{Ru}(\kappa^2\text{-}O,O\text{-acac})(\text{THF})][\text{BAr}'_4]$ (2) in CDCl_3	46
Figure 2.7. ^{13}C NMR spectrum of $[(\eta^6\text{-}p\text{-cymene})\text{Ru}(\kappa^2\text{-}O,O\text{-acac})(\text{THF})][\text{BAr}'_4]$ (2) in CDCl_3	47
Figure 2.8. ^1H NMR spectrum of reaction product from the addition of PMe_3 to 2 in CDCl_3	48
Figure 2.9. ^1H NMR spectrum of releasing free THF by addition of NCMe into 2 in CDCl_3	49
Figure 2.10. ^1H NMR spectrum of reaction of 2 and $\text{PhI}=\text{NTs}$ in the presence of styrene...	51
Figure 2.11. ^1H NMR spectrum of $[(\eta^6\text{-}p\text{-cymene})\text{Ru}(\kappa^2\text{-}O,O\text{-acac})(\text{N}_3\text{Ar})][\text{BAr}'_4]$ (6) in CDCl_3	54
Figure 2.12. ^1H NMR of $[\text{TpRu}(\eta^6\text{-}p\text{-cymene})][\text{BAr}'_4]$ (5).....	57
Figure 2.13. ^{13}C NMR of $[\text{TpRu}(\eta^6\text{-}p\text{-cymene})][\text{BAr}'_4]$ (5).....	57
Figure 2.14. ORTEP (30% probability) of $[\text{TpRu}(\eta^6\text{-}p\text{-cymene})][\text{BAr}'_4]$ (5).....	58
Figure 2.15. ^1H NMR of $\{[(\eta^6\text{-}p\text{-cymene})_2\text{Ru}]_2(\mu\text{-Cl})_3\}[\text{BAr}'_4]$ (7).....	60
Figure 2.16. ORTEP (50% probability) of $[(\eta^6\text{-}p\text{-cymene})_2\text{Ru}]_2(\mu\text{-Cl})_3[\text{BAr}'_4]$ (7).....	61
Figure 3.1. Key steps of C-H activation by M-X system (X = OR NR ₂ , etc.).....	76
Figure 3.2. Coordination mode of NCN ligand and anticipate ^1H NMR features of CH_2 groups.....	80
Figure 3.3. ^1H and ^{13}C NMR spectra of $(\text{NCN})\text{Pt}(\text{Me})_2\text{OTf}$ (1) in CDCl_3	80
Figure 3.4. ^1H and ^{13}C NMR spectra of $(\text{NCN}')\text{Pt}(\text{Me})_2\text{OTf}$ (2) in CDCl_3	81

Figure 3.5. ^1H NMR spectra of $[(\text{NCN}')\text{Pt}(\text{Me})_2(\text{THF})][\text{BAr}'_4]$ (3) in CDCl_3	82
Figure 3.6. ^{13}C NMR spectra of $[(\text{NCN}')\text{Pt}(\text{Me})_2(\text{THF})][\text{BAr}'_4]$ (3) in CDCl_3	82
Figure 3.7. ORTEP (scaled to enclose 50% probability) of $[(\text{NCN}')\text{Pt}(\text{Me})_2(\text{THF})][\text{BAr}'_4]$ (3) (BAr'_4 anion is not depicted).....	84
Figure 3.8. ^1H NMR and ^{13}C NMR spectra of $[(\text{NCN}')\text{Pt}(\text{Me})_2(\text{NH}_3)][\text{BAr}'_4]$ (4) in CDCl_3	88
Figure 3.9. ORTEP (scaled to enclose 30% probability) of $[(\text{NCN}')\text{Pt}(\text{Me})_2(\text{NH}_3)][\text{BAr}'_4]$ (4) (BAr'_4 anion is not depicted).....	88
Figure 3.10. The migration of alkyl or aryl groups to terminal oxo ligands in transition metal complexes.....	90
Figure 3.11. Metal oxo complex in orbital occupancy.....	90
Figure 3.13. The reaction of $(\text{NCN}')\text{Pt}(\text{Me})_2\text{OTf}$ (2) with H_2O_2 and the observation of resonance due to methanol.....	93
Figure 3.14. The reaction of $(\text{NCN}')\text{Pt}(\text{Me})_2\text{OTf}$ (2) with <i>tert</i> -butyl peroxide and the observation of resonance due to methanol.....	94
Figure 3.12. ^1H NMR spectrum of $[(\text{NCN}')\text{Pt}(\text{Me})_2(\text{ONCH}_3)][\text{BAr}'_4]$ (5) in CDCl_3	96
Figure 3.13. ^1H NMR spectrum of $[(\text{NCN}')\text{Pt}(\text{Me})_2(\text{O-pyridine})][\text{BAr}'_4]$ (6) in CDCl_3	96

LIST OF SCHEMES

Scheme 1.1. $\text{TpOsCl}_2(\text{NHPH})$ is not protonated by HCl	8
Scheme 1.2. Deprotonation of phenylacetylene- CH with TpRu(II) amido.....	9
Scheme 1.3. Deprotonation of 1,4-cyclohexadiene C-H bond with TpRu(II) amido.....	10
Scheme 1.4. Proposed mechanism for the reaction of Ru(II) amido with 1,4 cyclohexadiene	11
Scheme 1.5. Effect of ancillary ligands on basicity of parent amido ligand.....	11
Scheme 1.6. Delocalization of the amido lone pair into the phenyl π^* system.....	12
Scheme 1.7. Relative bond rotation barriers for $\text{Ru-N}_{\text{amido}}$ and/or $\text{N}_{\text{amido-C}_{\text{phenyl}}}$ in series of TpRu(L)(L')NHPH complexes.....	14
Scheme 1.8. Rotation barrier of $\text{N}_{\text{amido-C}_{\text{phenyl}}}$ bond for $(\text{IPr})\text{Cu}^{\text{I}}\text{NHPH}$ complex.....	15
Scheme 1.9. Nucleophilicity study of $\text{TpRu}(\text{PMe}_3)_2\text{NHPH}$ and $(\text{NHC})\text{Cu}(\text{NHPH})$	15
Scheme 1.10. Metal catalyzed arylamination and hydroamination reaction.....	16
Scheme 1.11. Propose mechanism on $(\text{BINAP})_2\text{Pd}$ -catalyzed amination of bromobenzene..	17
Scheme 1.12. $(\text{NHC})\text{CuXR}$ catalyze C-X formation ($\text{X} = \text{NR}'$, O or S).....	18
Scheme 1.13. Proposed catalytic cycle $(\text{NHC})\text{Cu(I)}$ -anilido hydroamination complexes.....	19
Scheme 1.14. Formation of intermediate copper catalyst and its reactivity.....	19
Scheme 1.15. Proposed mechanism of 1,2-addition pathway for early and late transition metal systems.....	22
Scheme 1.16. Proposed mechanism for "oxy" functionalization of C-H bonds.....	25
Scheme 1.17. Aziridination and amination catalyzed by metal-imido complex.....	27

Scheme 1.18. Intermediates of aziridination: two-electron insertion and one electron insertion.....	27
Scheme 2.1. Metathesis reaction to yield $[(\eta^6\text{-}p\text{-cymene})\text{Ru}(\kappa^2\text{-}O, O\text{-acac-}\mu\text{-CH})_2][\text{OTf}]_2$ (1).....	38
Scheme 2.2. Ligand exchange of $[(\eta^6\text{-}p\text{-cymene})\text{Ru}(\kappa^2\text{-}O, O\text{-acac-}\mu\text{-CH})_2][\text{OTf}]_2$ (1) with acetonitrile.....	42
Scheme 2.3. Competition between coordination of acac-CH and OTf.....	42
Scheme 2.4. Equilibria for coordination of THF as a function of counterion.....	43
Scheme 2.5. Potential reaction to yield $[(\eta^6\text{-}p\text{-cymene})(\kappa^2\text{-}O, O\text{-acac})\text{Ru}=\text{N}(\text{Ar})]^+$	44
Scheme 2.6. Possible decomposition pathways.....	44
Scheme 2.7. Reaction of 1 with <i>p</i> -tolylazide.....	45
Scheme 2.8. Reaction of 1 with PhI=NTs.....	45
Scheme 2.9. Synthesis of $[(\eta^6\text{-}p\text{-cymene})\text{Ru}(\kappa^2\text{-}O, O\text{-acac})(\text{THF})][\text{BAR}'_4]$ (2).....	46
Scheme 2.10. Ligand exchange reaction of 2 with PMe_3	47
Scheme 2.11. Ligand exchange reaction of 2 with NCMe.....	49
Scheme 2.12. Reaction of 2 with PhI=NTs.....	50
Scheme 2.13. Reaction of 2 and PhI=NTs in the presence of styrene.....	51
Scheme 2.14. Reaction of 2 with trimethylamine- <i>N</i> -oxide.....	52
Scheme 2.15. Reaction of 2 and trimethylamine- <i>N</i> -oxide with presence of styrene.....	52
Scheme 2.16. Ligand exchange of THF with <i>p</i> -tolyl-azide.....	54
Scheme 2.17. Reaction of 2 with KTp.....	56
Scheme 2.18. Product of 2 in CHCl_3 in at 100 °C.....	60

Scheme 3.1. Proposed mechanism for H/D exchange between Ru ^{II} -OH and C ₆ D ₆	77
Scheme 3.2. Proposed mechanism for C-H activation of benzene by (κ^2 -acac- O,O) ₂ Ir ^{III} (OMe)(py).....	78
Scheme 3.3. Synthesis of Pt-OTf complexes.....	79
Scheme 3.4. Synthesis of [(NCN')Pt(Me) ₂ (THF)][BAr' ₄] (3).....	82
Scheme 3.5. Synthesis of [(NCN')Pt(Me) ₂ (NH ₃)][BAr' ₄] (4).....	87
Scheme 3.6. Baeyer-Villiger-type reaction for oxygen atom insertion into the Re-CH ₃ bond.....	91
Scheme 3.7. Proposed O-atom insertion reaction to (NCN')Pt(Me) ₂ OTf (2).....	91
Scheme 3.8. The reactions of complex 3 with trimethylamine- <i>N</i> -oxide and pyridine- <i>N</i> - oxide.....	95

LIST OF CHARTS

Chart 2.1. Template of $[(\eta^6\text{-arene})\text{Ru}^{\text{II}}(\kappa^2\text{-O,O-acac})]^+$	35
Chart 2.2. Possible $[(\eta^6\text{-}p\text{-cymene})(\kappa^2\text{-O,O-acac})\text{Ru}^{\text{IV}}]$ oxo and imido complexes.....	37
Chart 2.3. Hydrogenation of ethyl benzene catalyzed by complex 2	55

CHAPTER 1: Introduction

1.1 Late transition metals with anionic heteroatomic ligands

Homogeneous single-site catalysts have had a significant impact on the commodity chemical industry as well as fine chemical synthesis in the past few decades. In general, characteristics of efficient catalyst systems include control of selectivity including regioselectivity and stereoselectivity, high overall yield, mild reaction conditions and low waste production. For instance, since 2002 six Nobel prizes have been awarded for work in homogeneous catalysis: Sharpless, Noyori and Knowles (2002), asymmetric hydrogenation¹ and Schrock, Grubbs and Chauvin (2005), olefin metathesis.^{2,3} An most important aspect of homogeneous catalysis is that the structure of the catalyst precursor can be determined in detail, and various intermediates are often observable in the catalytic cycle, which allows for understanding of the nature of its reactivity, and can lead to the rational design of improved catalysts.

The reactivity of late transition metals with non-dative heteroatomic ligands can vary substantially based on metal identity and oxidation state. The developments of catalytic cycles and enzymatic chemistry that are based on non-dative heteroatomic ligands have increased interest in the area of chemistry. For example, transformation of 1,4-fatty dienes to alkyl hydroperoxides involving hydrogen atom abstraction from allylic hydrogen by Fe^{III} hydroxide is an important biological catalytic reactions (eq 1).^{4, 5} Catalytic C-O and C-N bond formation with olefins can also involve metal amido, hydroxo and related systems (eq 2 and eq 3).⁶⁻⁹ Transition metal heteroatom systems are useful for hydrogenation of ketones

1.2 Bonding between transition metals and non-dative heteroatomic ligands

Bonds between a transition metal and an anionic heteroatomic ligand can be comprised of σ - and π -bonding components. The σ -bonding is between of electropositive metal electronegative N- or O- based ligand and hence can have substantial ionic character. If the metal has an empty orbital of π -symmetry, formal donation of a lone pair or the heteroatomic ligand imparts multiple bond character. However, late transition metals in low oxidation states have high d-electron counts. In the case where all $d\pi$ orbitals are filled, both π and π^* molecular orbitals are occupied and there is no net π -bond between the metal and heteroatomic ligand (Figure 1.2). π basic non-dative heteroatomic ligands cannot have interactions with filled d-orbitals on the metal, and M-X bond consists of a formal σ bond and non- π -bonding (Figure 1.2). The non-bonding interaction π destabilize M-X bond to some degree by the repulsion between the correct symmetry of filled $p\pi$ and $d\pi$ orbitals. This repulsion increases by closer orbital energy levels. For example, overlapping of filled-orbitals of F-F results in net destabilization of the bond.

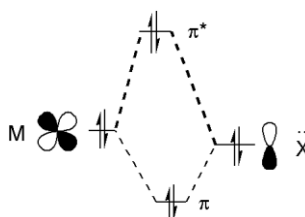


Figure 1.2. Filled $d\pi$ and $p\pi$ orbital interaction.

E-C theory describes bond dissociation energy (BDE) of a sigma bond with four components, E (electrostatic), C (covalent), T (transference) and R (receptance), where A and B are acceptor and donor end of bond (eq 7).

$$\text{BDE} = E_A E_B + C_A C_B + T_A R_B \quad (7)$$

First, bond energy can be divided into two components: heterolytic and homolytic. From heterolytic viewpoint, $E_A E_B$ presents electrostatic part of bonding, and $C_A C_B$ describes the covalent component of bonding. Both bonding consists of two electrons. T and R describe how much energy requires shifting from homolytic (neutral radical) to heterolytic (charge ionic) bond. Herein, $E_A E_B$ and $T_A R_B$ terms become more important for ionic bond. On the other hand, covalent bond like C-C bond is dictated by $C_A C_B$ term.

Because late transition metals are more electropositive than heteroatoms such as nitrogen, oxygen or sulfur, the bonds are expected to be relatively polar character. E-C theory suggests greater bond polarity increases $E_A E_B$ and $T_A R_B$ terms, which can lead to strong bonds. Thus, strength of M-X (X = O, N or S) bond can increase with greater electronegativity of X atom. Moreover, putting electron-withdrawing substituents on X concentrates negative charge on X atom (Figure 1.3). Thus, the energy of polar M-X bonds increases by Coulomb contribution, and M-X complexes possess in relatively strong bonds.

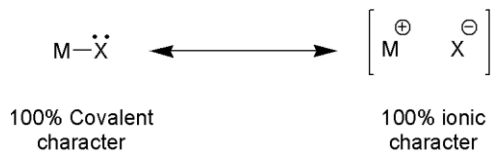
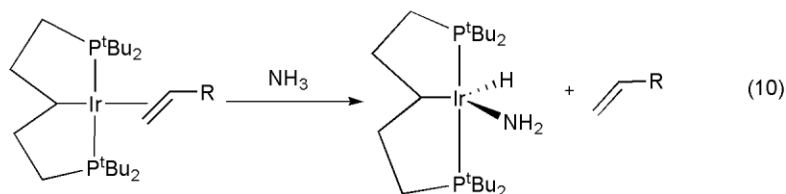
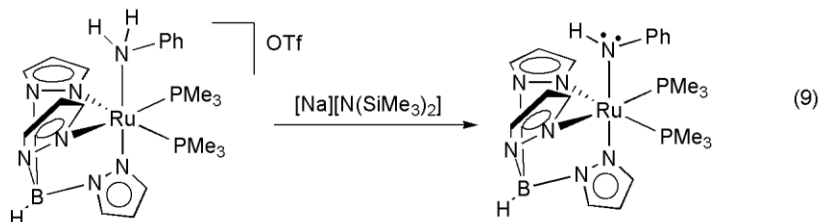
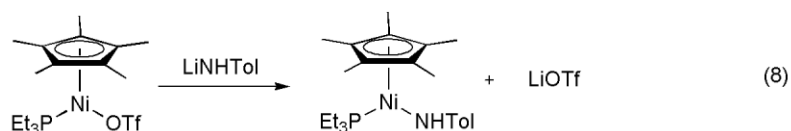


Figure 1.3. Resonance structure of M-X bond.

Until relatively recently, examples of late transition metal complexes with anionic heteroatomic ligands were rare compared to systems in high oxidation states. This was rationalized by Pearson's Hard-Soft Acid-Base theory, which predicts a bond mismatch between "soft" late transition metals and "hard" donor O- or N- ligands, and hence, inherently weak M-X (X = OR, NR₂, etc.) bonds. However, focused efforts toward the preparation of such systems have suggested that this deserved to be reconsidered due to the experimental observation that late transition metals with non-dative ligands bonds are strong.^{18, 19} Importantly, M-X systems are reactive and present diverse patterns of reactivity.²⁰⁻²²

1.3 Synthesis of late transition metal amides and alkoxo complexes

Amido (NR₂), hydroxo (OH) and related ligands formally bear a mono-anionic charge. There are multiple synthetic routes to produce late transition metal hydroxo, alkoxo, and amido complexes. In general, most of the complexes are synthesized through metathesis, deprotonation or oxidative addition. The metathesis technique involves a metal halide complex and addition of an alkali metal alkoxide, hydroxide, or amide to form a metal alkoxo, hydroxo or amido and an alkali halide salt as a byproduct (eq 8).²³⁻²⁸ In the deprotonation pathway, a base is used to deprotonate an N-H or O-H group of a coordinated amine, alcohol or water (eq 9).^{29, 30} Hartwig, Goldman et al. successfully synthesized an Ir(III) parent amido complex through oxidative addition of ammonia to Ir^I (eq 10).³¹



1.4. Reactivity of late transition metals complexes with heteroatomic ligands

Late transition metals in low oxidation states have high d- electron counts. In cases where the $d\pi$ orbitals are filled, π -basic ligands, such as non-dative heteroatomic ligands (e.g., NH_2 , NHPh , OH and OMe) cannot π donate because of filled d-orbitals on the metal (Figure 1.2). In this scenario, both π and π^* molecular orbitals are filled (Figure 1.4). Also, because of M-X bond polarity, the disruption of π -bonding is expected to result in highly nucleophilic and /or basic heteroatomic ligands.

The relationship among basicity of X atoms, orientation around X atoms and valance electrons of transition metals is important for reactivity of M-X systems. The Figure 1.4 shows the potential impact of π -bonding on geometric features. In mode A, there is no π -bonding between the metal and X, the X atom is sp^3 hybridized, and a pyramidal ligand X

results. In mode B with π -bonding between the metal and X, a planar geometry around X results.

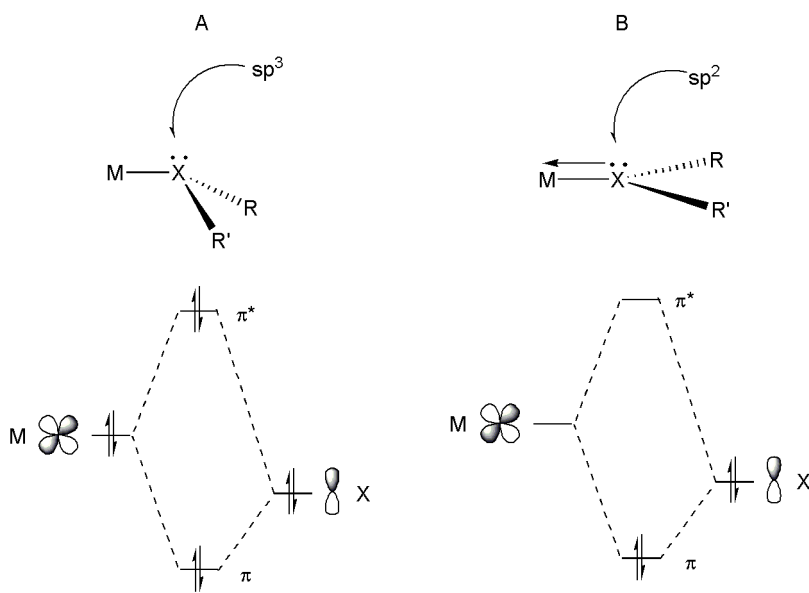
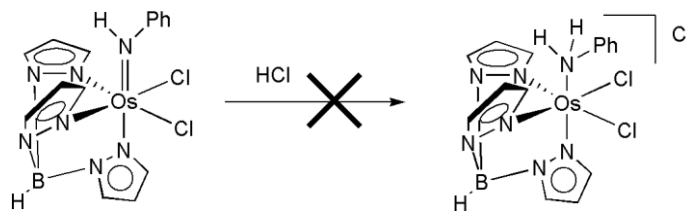


Figure 1.4. Potential impact of π -bonding on geometry around X (e.g., X = NR₂).

The potential impact on amido-to-metal π -bonding has been demonstrated by Mayer et al.³² His research group isolated and characterized the Os(IV) (d^4) complex, TpOsCl₂(NHPh), and studied the reactivity with acids including HCl/Et₂O, acetic acid, H₂O and other proton sources. It is important to note that a solid-state X-ray diffraction study reveals substantial N-Os multiple bond character. This anilido complex does not react with an excess of HCl/Et₂O (Scheme 1.1), which was demonstrated to be a thermodynamic effect by deprotonation of [TpOsCl₂(NH₂Ph)][OTf] by chloride. This suggests that the lone pair of the phenyl amido ligand has strongly π donated to the metal center, and the bond is considered as double bond like B type orientation shown in Figure 1.4 above.

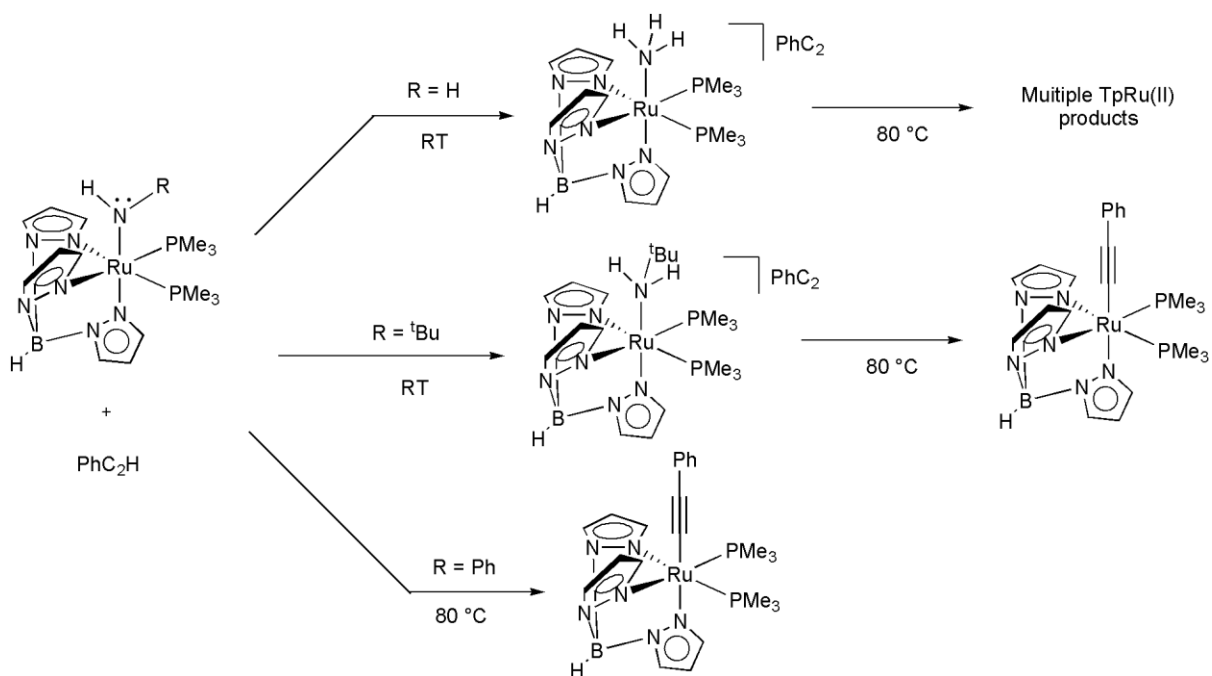


Scheme 1.1. $\text{TpOsCl}_2(\text{NHPh})$ is not protonated by HCl .

1.4.1 Basicity of Ru(II) anilido, amido and hydroxo, alkoxo and related complexes

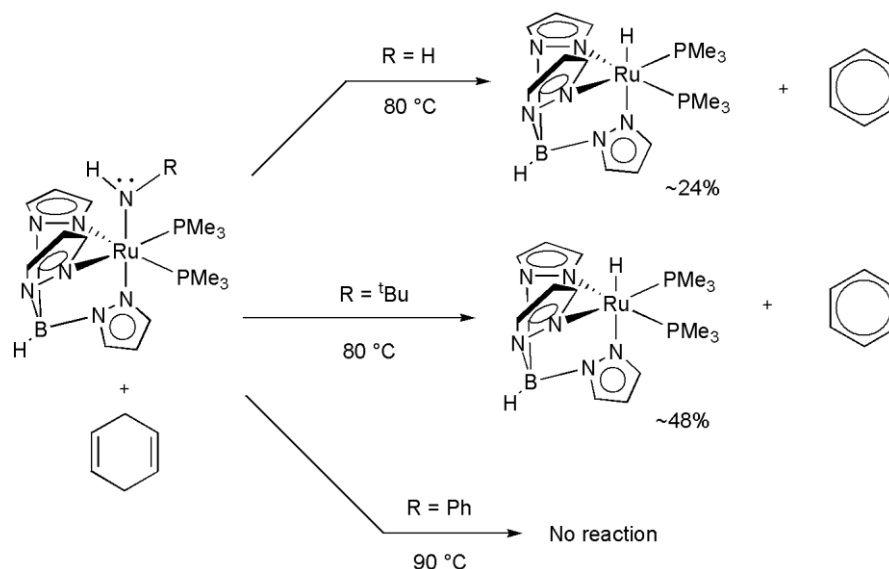
The combination of late transition metals in low oxidation states and non-dative heteroatomic ligands can result in highly basic heteroatomic ligands. As discussed above, the enhanced basicity is a result of the disruption of π -bonding in combination with polar metal-heteroatom bonds. In order to understand the extent to which the basicity of the non-dative heteroatomic ligand can be varied and exploited for synthetic purposes, our group has been exploring the reactivity of late transition metal systems with formally anionic ligands. As an entry point, we began studying $\text{TpRu}(\text{L})(\text{L}')\text{X}$ (Tp = hydridotris(pyrazolyl)borate; $\text{L} = \text{L}' = \text{P}(\text{OMe})_3$ or PMe_3 or $\text{L} = \text{CO}$ and $\text{L}' = \text{P}(\text{Ph})_3$; $\text{X} = \text{NH}_2$, NH^tBu or NHPh) systems.²⁹ $\text{TpRu}(\text{L})(\text{L}')\text{X}$ complexes possess pseudo-octahedral geometry about the Ru(II) (d^6) metal center. Therefore, all the d-orbitals that potentially can π -bonding with the heteroatomic ligands are filled. Also, the reactivity of the non-dative heteroatomic ligands is potentially tunable with variety of ancillary ligands (L/L') that affect the electronics of the metal center.

Initial reactivity studies including establishment of the range of acids that would react with the Ru(II) systems. The amido complexes $\text{TpRu}(\text{L})(\text{L}')\text{NHR}$ react with weakly acidic C-H bonds (Scheme 1.2 and Scheme 1.3).



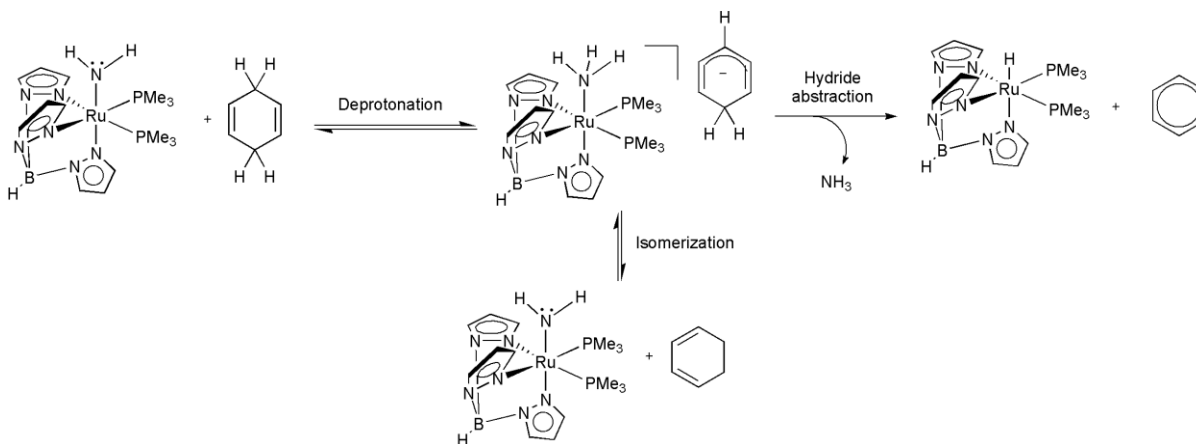
Scheme 1.2. Deprotonation of phenylacetylene-CH with TpRu(II) amido.

For example, both $\text{TpRu}(\text{PMe}_3)_2\text{NH}_2$ and $\text{TpRu}(\text{PMe}_3)_2\text{NH}^t\text{Bu}$ react with phenylacetylene at room temperature to produce the ion pair $[\text{TpRu}(\text{PMe}_3)_2(\text{NH}_2\text{R})][(\text{C}_2\text{Ph})]$ ($\text{R} = \text{H}$ or *tert*-butyl), and heating releases amine and produces the acetylide complexes $\text{TpRu}(\text{PMe}_3)_2(\text{C}_2\text{Ph})$ (Scheme 1.2). In contrast, $\text{TpRu}(\text{PMe}_3)_2\text{NHPh}$ does not react with phenylacetylene at room temperature. The experiment requires heating the solution of the anilido complex with 10 equiv of phenylacetylene to approximately 80 °C to observe production of $\text{TpRu}(\text{PMe}_3)_2(\text{C}_2\text{Ph})$ and aniline. The attenuated basicity of Ph amido is most likely due to the delocalization of the amido lone pair to phenyl π^* orbitals.



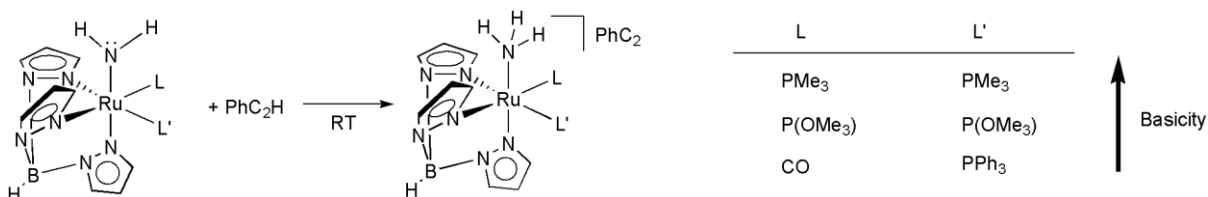
Scheme 1.3. Deprotonation of 1,4-cyclohexadiene C-H bond with TpRu(II) amido.

At elevated temperature, TpRu(PMe₃)₂(NHPh) (R = H or *tert*-butyl) systems react with 1,4-cyclohexadiene to give benzene, amine (NH₂R) and TpRu(PMe₃)₂H. Hence, 1,4-cyclohexadiene is converted benzene via net removal of 2H⁺/2e⁻. In addition, prior to benzene formation, the isomerization of 1,4-cyclohexadiene to 1,3-cyclohexadiene is observed. The first step of the reaction is proposed to involve acid/base chemistry. Scheme 1.4 depicts a reaction pathway that accounts for these observations. Initial proton transfer forms a Ru(II) amine complex with cyclohexadienyl counter ion as an intermediate, and net hydride abstraction after amine dissociation would yield benzene and the ruthenium hydride complex (Scheme 1.4). The failure of TpRu(PMe₃)₂NHPh to react with 1,4-cyclohexadiene suggests that a hydrogen atom abstraction pathway is unlikely.



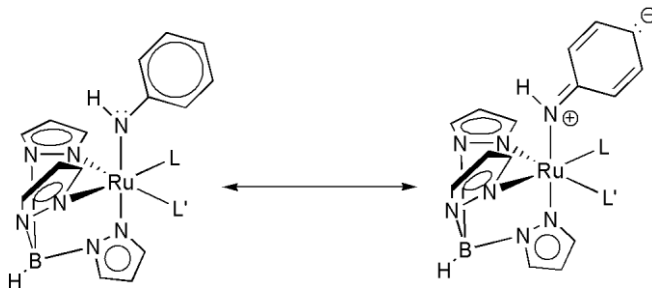
Scheme 1.4. Proposed mechanism for the reaction of Ru(II) amido with 1,4-cyclohexadiene.

Ancillary ligand effects were also observed in the reaction of TpRu(L)(L')NH_2 with phenylacetylene. The qualitative kinetic trend for the deprotonation of the phenylacetylene C-H bond corresponds to the donating abilities of the ancillary ligands. The basicity was increased as greater donation ability of the ancillary ligand for the systems: $\text{TpRu(PMe}_3)_2\text{NH}_2 \geq \text{TpRu(P(OMe}_3)_2\text{NH}_2 > \text{TpRu(PPh}_3)_2\text{(CO)NH}_2$ (Scheme 1.5). Also, sterics could be important factor for the basicity. Comparison between ancillary ligand effect and π -donating ligand effect, ancillary ligands give less impact on the basicity. That suggests Ru(II) d^6 systems present π -conflict between filled metal $d\pi$ orbital and lone pair electrons on amido ligands, and the lone pair electron on the π -donating ligands do not have significant affect from electron density of metal center.



Scheme 1.5. Effect of ancillary ligands on basicity of parent amido ligand.

A comparison of [Ru]-NHR (R = H, *tert*-Bu or Ph) shows the Ph amido to be the least basic non-dative ligand among those three. It is anticipated that the phenyl group serves to delocalize the amido lone pair using π^* orbitals of the phenyl ring, thus decreasing the basicity of the lone pair (Scheme 1.6).



Scheme 1.6. Delocalization of the amido lone pair into the phenyl π^* system.

An X-ray crystal diffraction study of $\text{TpRu}\{\text{P}(\text{OMe})_3\}_2(\text{NHPh})$ showed that the $\text{N}_{\text{amido}}\text{-C}_{\text{phenyl}}$ bond length is 1.365(2) Å, which is 0.086 Å shorter than the $\text{N}_{\text{amido}}\text{-C}_{\text{phenyl}}$ bond length of $[\text{TpRu}\{\text{P}(\text{OMe})_3\}_2(\text{NH}_2\text{Ph})][\text{OTf}]$ and consistent with resonance structure shown in scheme 1.6. When two anilido complexes such as $\text{TpRu}\{\text{P}(\text{OMe})_3\}_2(\text{NHPh})$ and $\text{TpRu}(\text{PPh}_3)(\text{CO})(\text{NHPh})$ complexes were compared, inverse correlation between $\text{N}_{\text{amido}}\text{-C}_{\text{phenyl}}$ and $\text{Ru-N}_{\text{amido}}$ bond lengths was observed (Figure 1.5). Although sterics may be affective to the bond distances, this data is consistent with delocalization of the amido lone pair into the phenyl π^* system as well as π -conflict between filled metal $d\pi$ orbital and the lone pair electrons on amido ligands. Moreover, electron denser metal center may creates π -conflict with π -donating ligand to cause longer $\text{Ru-N}_{\text{amido}}$ bond length so that the lone pair

electrons tend to delocalize into phenyl π^* orbitals, which result in shorter $N_{\text{amido}}-C_{\text{phenyl}}$ bond distance.

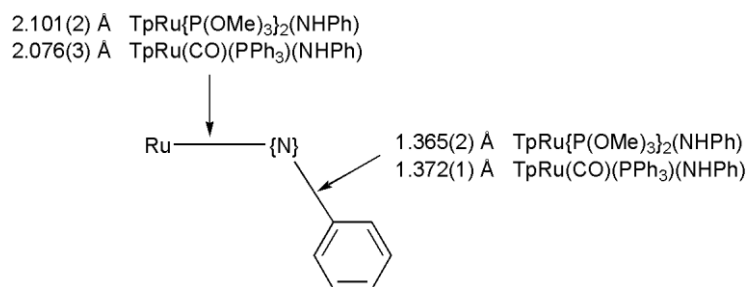
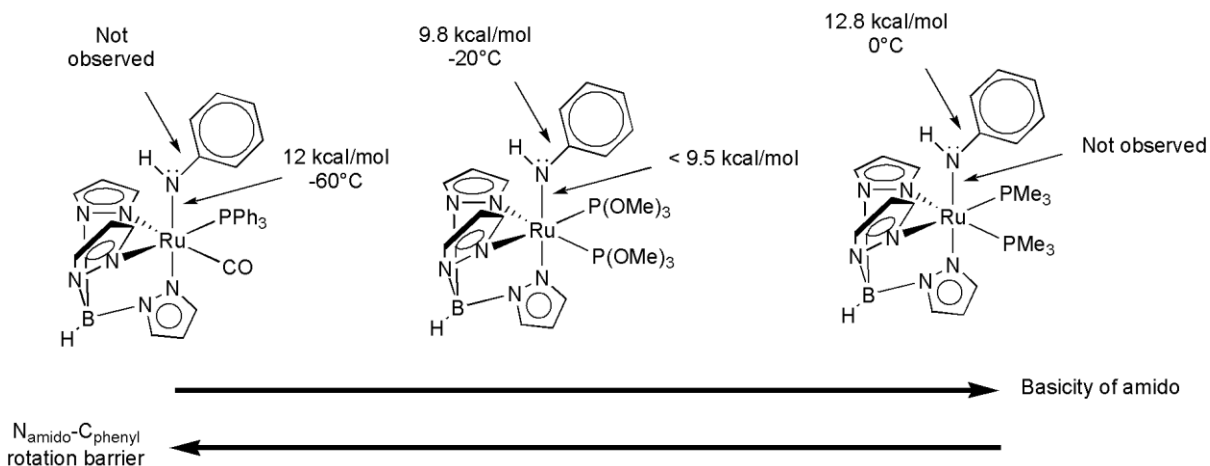


Figure 1.5. Variation of bond distances for anilido complexes $TpRu\{P(OMe)_3\}_2(NHPh)$ and $TpRu(PPh_3)(CO)(NHPh)$.

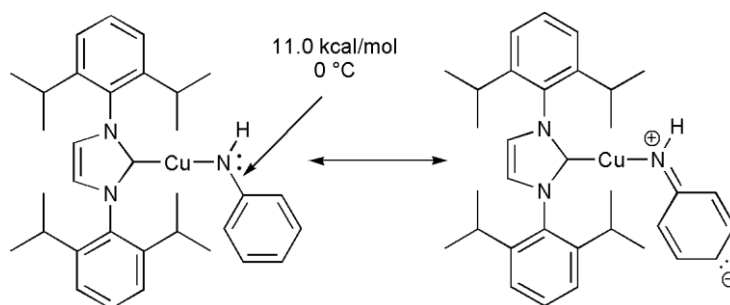
Amido-to-phenyl electron donation should increase the $N_{\text{amido}}-C_{\text{phenyl}}$ bond order. Hence, determination of the $N_{\text{amido}}-C_{\text{phenyl}}$ rotational barrier should track with the extent of this bonding interaction. We used variable temperature 1H NMR spectroscopy to determine the rotational barriers. For example, single resonances are observed for ortho and meta protons of the amido phenyl at elevated temperature, and both ortho and meta resonances broaden and decoalesce at reduced temperature. Hindered rotation around $N_{\text{amido}}-C_{\text{phenyl}}$ is consistent with these observation of broadening, decoalescence and coalescence for ortho and meta protons, and the rotational barrier was calculated. The rotational barrier of the $N_{\text{amido}}-C_{\text{phenyl}}$ bond becomes greater as the electron density of Ru is increased (Scheme 1.7). For example, the PMe_3 ligand is stronger electron donor than the $P(OMe)_3$ ligand, so π -conflict between metal $d\pi$ orbital and the lone pair electrons on anilido ligand are expected to increase and enhance the delocalization of the amido lone pair into the phenyl π^* system. Considering steric factors, the rotational barrier increases in the order complexes, $TpRu\{P(OMe)_3\}_2(NHPh) < TpRu(PMe_3)_2(NHPh) < TpRu(PPh_3)(CO)(NHPh)$. In another

respect, the more electron rich metal center enhances the basicity of the lone pair electrons on anilido ligand.



Scheme 1.7. Relative bond rotation barriers for $\text{Ru}-N_{\text{amido}}$ and/or $N_{\text{amido}}-C_{\text{phenyl}}$ in series of $\text{TpRu}(\text{L})(\text{L}')\text{NHP}$ complexes.

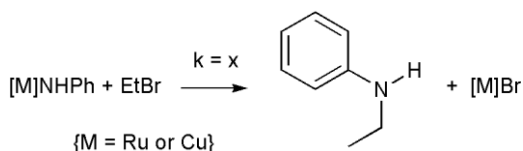
The same principle can be applied to $\text{Cu}(\text{I})$ -amido complexes. The monomeric $(\text{IPr})\text{Cu}^{\text{I}}(\text{NHP})$ complex $\{\text{IPr} = 1,3\text{-bis}(2,6\text{-diisopropylphenyl})\text{imidazol-2-ylidene}\}$ was isolated, characterized and studied by Dr. Elizabeth Blue in the Gunnoe group.³³ Variable temperature ^1H NMR spectroscopy was used to study the dynamics of the complex $(\text{IPr})\text{Cu}(\text{NHP})$ (Scheme 1.8). As the temperature is lowered from room temperature, the amido phenyl resonances broaden and decoalesce into two doublets, which corresponds to slow rotation of $N_{\text{amido}}-C_{\text{phenyl}}$ bond. The ΔG^\ddagger for this process was calculated to be ~ 11 kcal/mol at 0°C . Thus, $\text{Cu}(\text{I})$ phenyl amido's basic lone pair of electrons delocalize into π^* system of phenyl.



Scheme 1.8. Rotation barrier of $N_{\text{amido}}-C_{\text{phenyl}}$ bond for $(\text{IPr})\text{Cu}^{\text{I}}\text{NHPH}$ complex.

1.4.2 Nucleophilicity of late transition metals and heteroatomic ligands complexes

Coordination of late transition metals in low oxidation states to non-dative heteroatomic ligands limits ligand-to-metal π -donation. The nature of these systems increases nucleophilic character as well as basicity.^{21, 22, 29, 30, 34-40} Both anilido complexes $\text{TpRu}(\text{PMe}_3)_2\text{NHPH}$ and $(\text{NHC})\text{Cu}(\text{NHPH})$ act as nucleophile and react with bromoethane through $S_{\text{N}}2$ reactions to produce $\text{TpRu}(\text{PMe}_3)_2\text{Br}$, $(\text{NHC})\text{Cu}(\text{Br})$ and ethylaniline (Scheme 1.9 and Table 1.1).³³ However, the copper(I) anilido complexes react more rapidly with bromoethane than the $\text{TpRu}(\text{II})$ anilido complex. Potentially, steric environment difference between six-coordinated Ru complex and two-coordinated Cu may attenuate/enhance the nucleophilicity. For example, complex $(\text{IMes})\text{Cu}(\text{NHPH})$ shows greater nucleophilicity than $(\text{IPr})\text{Cu}(\text{NHPH})$. In fact, amido ligand coordinated to low oxidation state late transition metal exhibit the nucleophilic reactivity.



Scheme 1.9. Nucleophilicity study of $\text{TpRu}(\text{PMe}_3)_2\text{NHPH}$ and $(\text{NHC})\text{Cu}(\text{NHPH})$.

Table 1.1. Kinetic data for the reaction of bromoethane with Cu^I and Ru^{II} complexes.^a

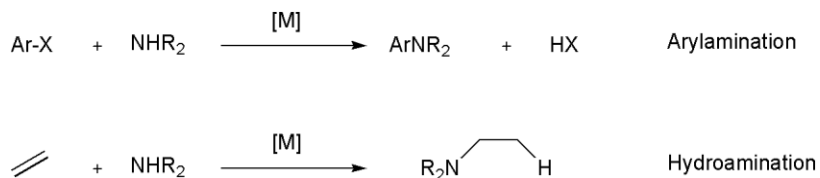
Complexes	k_{obs} (s ⁻¹)	$t_{1/2}$ (min)	ΔG^b
(IMes)Cu(NHPh)	$3.3(3) \times 10^{-4}$	35(3)	22.0
(IPr)Cu(NHPh)	$2.4(2) \times 10^{-4}$	49(4)	22.2
(SIPr)Cu(NHPh)	$1.1(1) \times 10^{-4}$	109(8)	22.6
TpRu(PMe ₃) ₂ (NHPh)	$8.6(3) \times 10^{-6}$	22 ^c	29.0

^a All reactions at room temperature except TpRu(PMe₃)₂(NHPh), which was acquired at 80 °C. ^b Kinetic barrier in kilocalories per mole. ^c In hours.

1.4.2.a Arylamination and olefin hydroamination

One of the potential applications for late transition metals with non-dative heteroatomic ligands systems is to initiate C-X (X = N, O and S) bond formation (Scheme 1.10). Olefin hydroamination provides an atom economical route for the formation of C-N bonds.⁴¹⁻⁴⁵ Related reactions for alcohols and thiols provide routes to O-C/S-C bond formation.^{15, 46, 47} Examples of late transition metal catalysts for olefin hydroamination have been reported. For example, palladium complexes catalyze "Markovnikov" hydroamination of olefins, and a rhodium system catalyzes "anti-Markovnikov" hydroamination of olefins.^{48.}

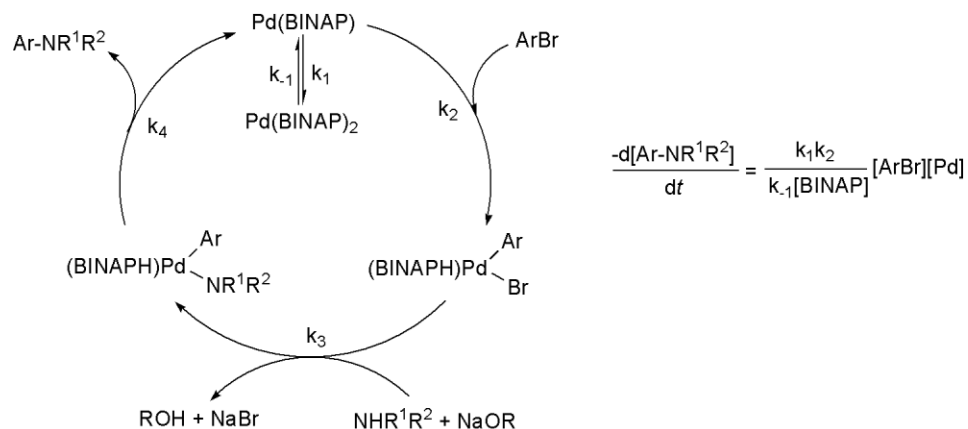
49



Scheme 1.10. Metal catalyzed arylamination and hydroamination reaction.

Palladium systems also catalyze aromatic C-N bond formation through arylamination transformation from aryl halides and amines to arylamines.^{17, 50-54} Buchwald et al. and

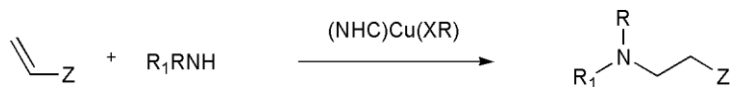
Hartwig et al. have attempted to understand the mechanism of the transformation using $(\text{BINAP})_2\text{Pd}$ (BINAP = 1,1'-binaphthalene-2,2'-diylbis(diphenylphosphine)) catalyst. The proposed mechanism and rate equation has shown in Scheme 1.11, which is the most consistent based on a number of kinetic studies, studies of stoichiometric oxidative addition, and reactivity of arylpalladium halide and arylpalladium amido complexes. Several measured data matches the reaction rate equation: the zero-order dependence of the rate on the concentration of amine, first-order dependence of concentration of bromoarene, and inverse independent relationship with concentration of BINAP ligand. The experiment of stoichiometric oxidative addition provides strong evidence, which bromoarene reacts with $(\text{BINAP})\text{Pd}$ where comes from $(\text{BINAP})_2\text{Pd}$ lying off the catalytic cycle.



Scheme 1.11. Proposed mechanism on $(\text{BINAP})_2\text{Pd}$ -catalyzed amination of bromobenzene.

Although Pd, Ru and Rh catalysts have been successful as catalysts for C-X formation processes, those metals are relatively expensive. In addition, they each suffer from limited substrate scope. There is a potential advantage to use of Cu as a catalyst from an economical viewpoint. The Gunnoe group has successfully synthesized monomeric Cu(I)

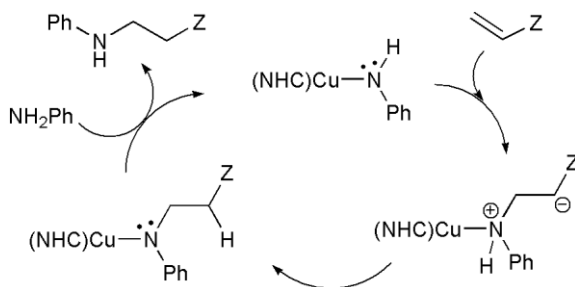
complexes, (NHC)CuX {NHC = IPr, IMes and SIPr; IMes = 1,3-bis(2,4,6-trimethylphenyl)imidazol-2-ylidene, SIPr = 1,3-bis(2,6-diisopropylphenyl)imidazolin-2-ylidene; X = NPh, NHCH₂Ph, OEt, OPh, SPh and SCH₂Ph}. These complexes catalyze the hydroamination^{55, 56}, hydroalkoxylation^{55, 56} and hydrothiolation⁵⁷ of electron-deficient olefins (Scheme 1.12).



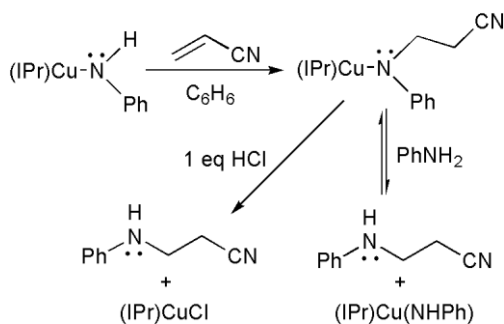
Scheme 1.12. (NHC)CuXR catalyze C-X formation (X = NR', O or S).

Gunnoe et al. have developed the scope of reactivity and mechanism for olefin hydroamination reaction catalyzed by Cu(I) anilido complexes,⁵⁶ Intermolecular nucleophilic addition pathway is likely occurring and producing anti-Markovnikov compound based on kinetic studies and observation of intermediate species (Scheme 1.13). Although there is lack of evidence for zwitterionic intermediate, indirect suggestion of formation of zwitterionic intermediate is significantly slower reaction rate with secondary amine comparing with primary amine. The stoichiometric reaction of (IPr)Cu(NHPh) and acrylonitrile result in formation of (IPr)Cu(N(Ph)CH₂CH₂CN) confirmed by ¹H NMR spectroscopy (Scheme 1.14), which is one of the intermediate form in catalytic cycle shown in scheme 1.13. In addition, the treatment of (IPr)Cu(N(Ph)CH₂CH₂CN) with 1 equiv of HCl produces 3-anilinopropionitrile and (IPr)CuCl. Also, stoichiometric reaction of (IPr)Cu(N(Ph)CH₂CH₂CN) and aniline result in formation of 3-anilinopropionitrile and (IPr)Cu(NHPh). In situ ¹HNMR spectroscopy study provides an evidence that catalyst resting state is (IPr)Cu(N(Ph)CH₂CH₂CN) in hydroamination of acrylonitrile using (IPr)Cu(NHPh)

complex. $(\text{IPr})\text{Cu}(\text{N}(\text{Ph})\text{CH}_2\text{CH}_2\text{CN})$ can coordinate to aniline to produce three coordinated $(\text{IPr})\text{Cu}(\text{N}(\text{Ph})\text{CH}_2\text{CH}_2\text{CN})(\text{NH}_2\text{Ph})$ complex, and intramolecular proton transfer give off Cu catalyst and hydroamination product. $(\text{IPr})\text{Cu}(\text{N}(\text{Ph})\text{CH}_2\text{CH}_2\text{CN})$ complex is proposed as the rate determining step of overall catalytic cycle.



Scheme 1.13. Proposed catalytic cycle $(\text{NHC})\text{Cu}(\text{I})$ -anilido hydroamination complexes.



Scheme 1.14. Formation of intermediate copper catalyst and its reactivity.

1.4.3 C-H activation

Our society has been dependent on fossil fuel for last a few hundred years, and people in our planet are expecting to consume more energy and materials next a few decades. We gain most of our energy source, commodity and fine chemicals from limited fossilized resources. In order to maximize energy and materials output, the most abundant natural gas

and petroleum such as alkanes and saturated hydrocarbons are crucial in the next decade. Herein, the development of metal mediated carbon-hydrogen bond activation and functionalization can have a dramatic impact on future energy production as well as production of commodity chemicals.

Over the past few decades, there has been research in the area of organometallic homogeneous catalysis for metal mediated C-H bond activation.⁵⁸⁻⁷⁵ Studies of stoichiometric metal mediated C-H activation have resulted in elucidation of several pathways by which metals can cleave C-H bonds (Figure 1.6). The pathway of C-H activation is dependent on the metal system and can vary depending on electrophilicity / electron density or a function of ancillary ligands of metal center, oxidation state, metal identity, and nucleophilicity of ligands.

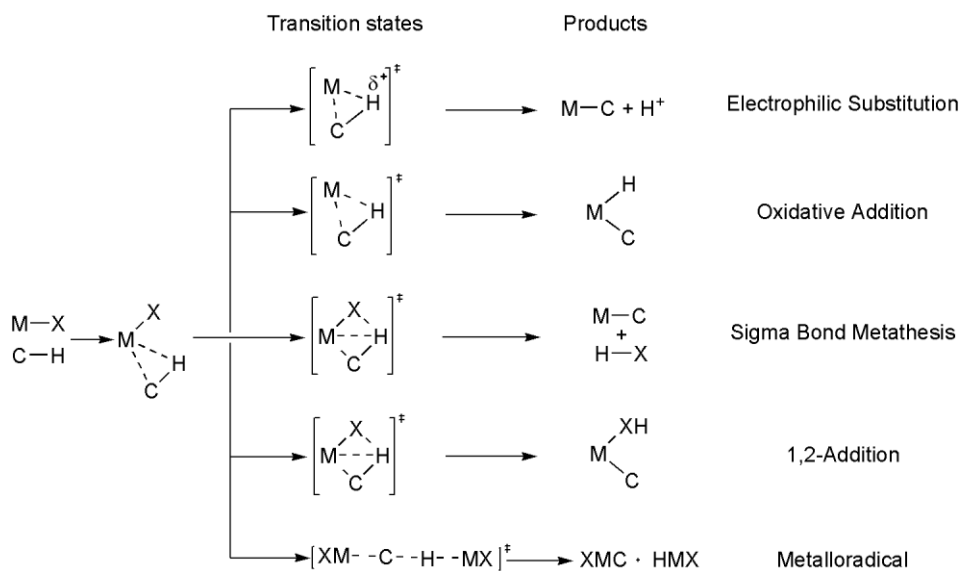


Figure 1.6. Various pathways of metal-mediated C-H activation.

There are three key steps for the transformation in functionalizing alkane C-H: rate of conversion, stability of a homogeneous catalyst, and selectivity of product formation. It is challenging to meet all three requirements.

1.4.3.a Activation of C-H bonds via 1,2-addition across metal-heteroatom bonds

One of the first strategies on development of catalysts toward C-H activation through 1,2-addition includes Lewis acidic metal center and basic character of heteroatomic-based ligand (Figure 1.7). Lewis acidic metal can provide a coordination site for non-polar C-H bond like hydrocarbon to weaken the C-H bond as well as potential regioselectivity. And, highly basic non-dative heteroatomic ligand abstract H^+ from the C-H bond intramolecularly, which might be a reasonable picture for non-polar C-H bonds activation by 1,2-addition cross metal-heteroatomic complex.

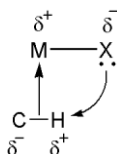
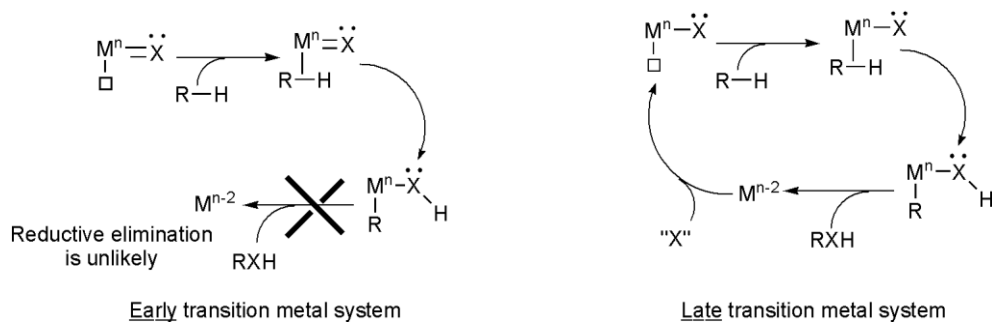


Figure 1.7. C-H bond cleavage 1,2-addition cross metal-heteroatom bond.

These early transition metal systems, successfully activate hydrocarbon C-H bonds.⁷⁶ And, they are a single step (i.e., N-C reductive elimination) from a functionalized product. However, it only activates a stoichiometric ratio of C-H bonds, because reductive elimination of the organic molecule is unlikely to occur for early transition metal systems (Scheme 1.15). Therefore, the redox flexibility of late/middle transition catalyst can potentially affords more systems to catalytically produce organic compounds.

Low valent late transition metal complexes with heteroatomic anionic ligand such as amido, hydroxo and alkoxo and related ligands are potentially useful for hydrocarbon C-H activation.⁷⁷⁻⁸⁰ Our starting hypothesis for these systems was that C-H activation could proceed thru a 1,2-addition type pathway (Figure 1.7). The first key step is that the transition metal center provides an open coordination site to interact with C-H bond (intermolecular organic substrates) and enhance C-H acidity (similar to known chemistry upon coordination of dihydrogen⁸¹⁻⁸⁵). Intramolecular bond breaking and bond forming occur at the basic heteroatomic atom ("X") abstracting the proton from the coordinated C-H bond and forming a M-C bond.

In our knowledge, catalytic cycle C-H functionalization by 1,2-addition pathway has never observed. There are, however, some aspects might incorporate into a catalytic cycle, and proposed catalytic cycle for 1,2-addition of C-H bond to metal non-dative heteroatom bond is shown in scheme 1.15; First step in this catalysis, 1,2-addition of C-H bond across M-X bond. Second, reductive eliminate ($+2e^-$) C-X group. Third, metal is oxidized ($-2e^-$) by X source and regenerate M-X bond. The first step has been studied and provide us some evidences that 1,2-addition might be occurring. Although reductive elimination for early transition metal is unlikely to take place because of electropositive character, late transition metal systems are able to do reductive elimination from aryl amine complexes.^{52, 54} For example, Pd(BINAP)aryl-amine complex reductively eliminate aniline to give off Pd(BINAP).^{86, 87} The third step will be discussed in section 1.4.3.b.



Scheme 1.15. Proposed mechanism of 1,2-addition pathway for early and late transition metal systems.

In σ -bond metathesis pathway (Figure 1.6), C_1 -H bond crossing M - C_2 transition state formation leads the reaction net proton transfer from C_1 to C_2 . In our model, the most important factors for C-H activation are the electrophilicity of metal center and basicity/nucleophilicity of the X ligand. Hence, we view the description of metal-heteroatom multiple bonding as a central feature. We anticipate that the transition state of C-H activation by M-X species should be more facile than by M-C species because of basicity/nucleophilicity of X atom (Figure 1.8).

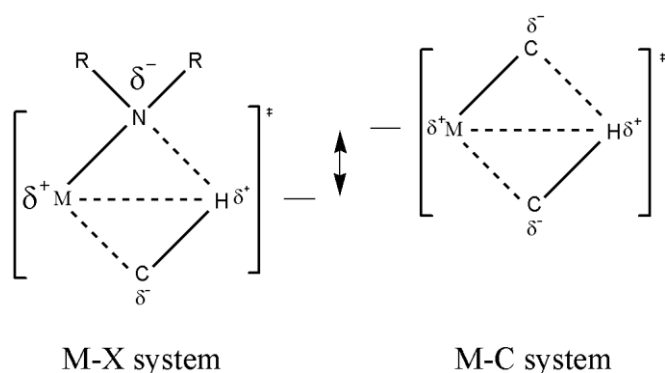


Figure 1.8. Energy differences at transition state between C-H activation with M-X vs. M-C.

1.4.3.b Regeneration of metal non-dative ligand system

In terms of designing the ideal system for efficient C-H bond activation, alkyl and aryl C-H activation by transition metals with non-dative ligands has been studied or shown. The next important challenge is find a way to regenerate M-X complex after C-H activation step to complete catalytic cycles.

Conversion of M-R bond to M-OR is required to catalyze functionalization of hydrocarbon C-H bond. In the past, focus on this topic has been the migration of a transition metal alkyl or aryl ligand to a terminal oxo ligand. The main problem in this transformation is strength of metal-oxo bond, and it provides kinetic and thermodynamic inhibit. There is no example has present metal oxo-to-migration from isolable oxo-alkyl or -aryl in thermal reaction but photolytical has done.⁸⁸ Also, the typical polarity of the two bonds involved results in two "nucleophile" reacting (Figure 1.9). For example, oxo-alkyl or oxo-aryl complexes show remarkable stability.⁸⁹⁻⁹¹

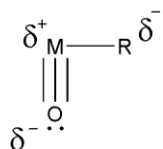
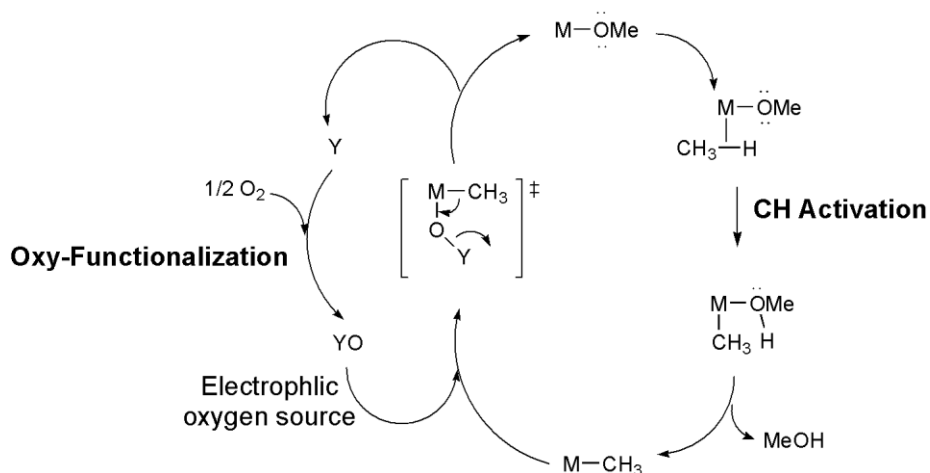


Figure 1.9. Stability of metal oxo-aryl or alkyl complexes.

In 2006, Periana et al. reported net oxygen atom insertion into a M-C bond through a proposed Baeyer-Villiger-type pathway, which could provide a general low energy pathway for formation of M-OR.⁹² Using various oxygen sources such as H₂O₂, PyO, IO₄⁻ and PhIO, oxygen was inserted into a Re^{VII}-Me bond, and the resulting methoxo species was hydrolyzed in water to produce methanol. This chemistry *may* require high oxidation state metal

complexes and has only been observed with Re(VII). In Scheme 1.16, the right side of the cycle is C-H activation, which requires lower oxidation state of metal systems. On the other hand, oxy-functionalization steps may prefer to proceed with highly electrophilic metal center (Scheme 1.16). Thus, way to find the balance between the two cycles is important for this catalytic cycle to achieve C-H activation and simultaneous oxy-functionalization.



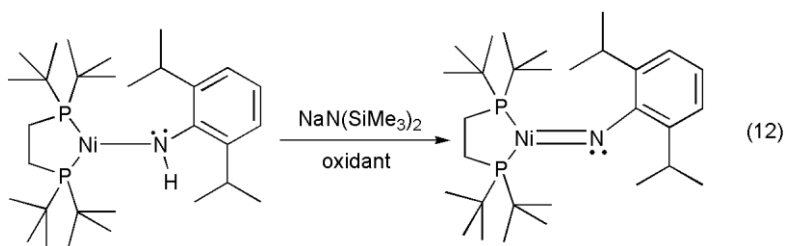
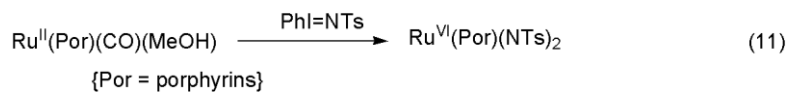
Scheme 1.16. Proposed mechanism for "oxy" functionalization of C-H bonds.

1.5 Late transition metal imido and oxo complexes

Imido and oxo ligands are formally -2 ligands that can donate up to 6 electrons. A variety of early and middle transition metal imido/oxo complexes have been synthesized, and the reactivity of those complexes are dependent on metal, oxidation state and sterics from ancillary ligands.⁹³⁻⁹⁷ Late transition metal imido or oxo complexes can initiate metal-mediated nitrogen or oxygen atom transfer reactions, including aziridination of olefins, amination of alkanes and epoxidation of olefins.

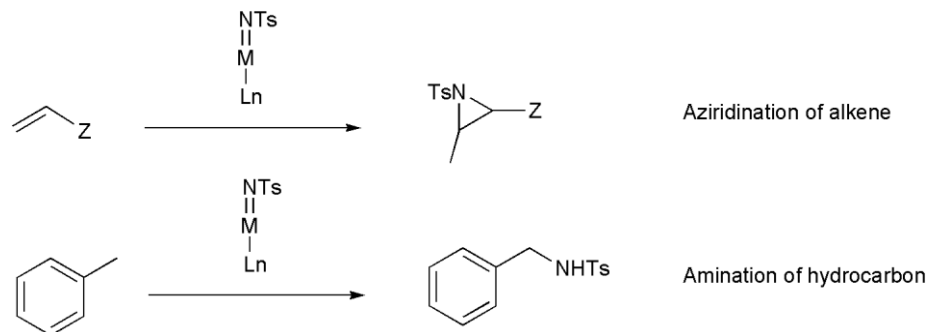
1.5.1 Examples of late transition metal imido and oxo species

There are a few known synthetic routes to form imido and oxo species. The most commonly used route for late transition metals is reaction with nitrene or oxo sources such as azides (ArN_3), tosylimino phenyliodinane (TsN=IPh) and iodosyl benzene (PhI=O) (eq 11).⁹⁸⁻¹⁰³ Net hydrogen atom abstraction from amido complexes is another way to synthesize a metal imido complex. For example, Hillhouse et al. isolated three coordinate nickel imido complexes from proton/electron abstraction of Ni-amido species (eq 12).¹⁰⁴ Hill et al. discovered formation of the oxo complex $\text{K}_7\text{Na}_9[\text{O=Pt}^{\text{IV}}(\text{H}_2\text{O})\text{L}_2]$, ($\text{L} = \text{PW}_9\text{O}_{34}^{9-}$) from $[\text{Pt}^{\text{II}}(\text{PW}_9\text{O}_{34})]^{16-}$.¹⁰⁵ Peters et al. synthesized Fe(III) imide complex from Fe(I) through reaction with *p*-tolyl azide.¹⁰⁶⁻¹⁰⁸ Warren et al. synthesized doubly bridged $[\text{Co}]_2(\mu\text{-NR})_2$, singly bridged $[\text{M}]_2(\mu\text{-NR})$ ($\text{M} = \text{Ni}$ or Cu) using β -diketiminato ligand by addition of phenyl azide or PhI=NTs .⁹⁹ A terminal TpCo imido has been synthesized from trimethylsilyl azide by Theopold et al.¹⁰⁹



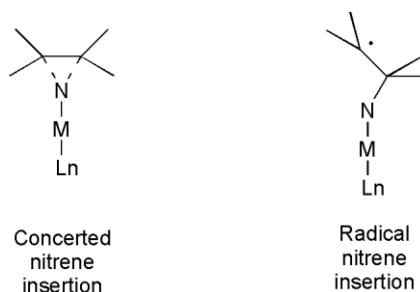
1.5.2 Reactivity of late transition metal imido and oxo species

Metal-mediated nitrogen atom transfer provides a route for the construction of N-C bonds. But, understanding of mechanisms of aziridination of alkenes and amination of alkanes is still developing (Scheme 1.17).



Scheme 1.17. Aziridination and amination catalyzed by metal-imido complex.

This is in part due to the instability of the intermediates of these reactions between $M=NTs$ and alkenes and alkanes, which prevents their isolation. Therefore, a direct study of mechanisms is not typically feasible. In general, the two types of proposed intermediate for reaction with alkenes such as concerted nitrene insertion ($2 e^-$) or N-C formation by radical pathway (Scheme 1.18).¹⁰⁰



Scheme 1.18. Intermediates of aziridination: two-electron insertion and one electron insertion.

$\text{Fe}^{\text{IV}}=\text{NTs}$ species have been shown to insert in to an alkene double bond and the reaction apparently proceeds through a carboradical intermediate with $\text{Fe}^{\text{V}}=\text{NTs}$ or a four-membered Fe-C-C-N metallocycle. However, the putative $\text{Fe}(\text{V})=\text{NTs}$ species is not isolable so direct observation of any intermediate species is not possible, nor are conventional kinetic methods.¹⁰¹

The aziridination of alkenes by $\text{PhI}=\text{NTs}$ catalyzed by copper has given the best regio- and stereoselectivity. Again, $\text{Cu}=\text{NTs}$ intermediate species were not observable. Overall, all the active catalysts are highly reactive with alkenes, and the relative energy level of intermediates is too high for isolation and characterization. On the other hand, observable metal imido complexes do not have any reactivity towards alkenes.¹¹⁰ The balance between stability and reactivity of metal imido is required in order to understand the aziridination of alkenes and amination of alkanes mechanisms and make progress toward a viable catalyst.

1.6 Summary

Late transition metals possessing a non-dative ligand (non-dative ligand = amido, oxide and alkoxide) have been shown to activate aryl and alkyl C-H bonds. The system consists of a highly basic heteroatomic ligand and an electrophilic metal center, which is the source of the reactivity to break an inert C-H bond. Subsequent regeneration of the M-X system is the next key step to succeed the complete catalytic cycle for a 1,2-addition path. Using an oxidant to insert into a M-C bond after the C-H activation is low energy route to regenerate the catalyst. Thus, two key steps are required for catalytic cycle; C-H activation and oxy-functionalization. Thus, electrophilicity of metal center and basicity of nondative heteroatomic ligand seem to play important role for the transformation of C-H activation and oxy-functionalization. This research project is directing towards understanding and finding way to maximize electrophilicity of metal center without attenuating basicity of X.

In addition, late transition metal imido and oxo species have been shown to be reactive towards nucleophilic alkene C=C bonds and less nucleophilic alkane C-H bonds. The isolation of intermediate species has proven difficult but important to gain further understanding of metal mediated aziridination of alkenes and amination of alkanes to produce more active catalysts.

My research is focused on attempting synthesis and study of new pseudo-octahedral ruthenium^{IV} imido/oxo complexes, which have a lot of potential utilities to understand late transition metal non-dative heteroatomic ligand systems including basicity/nucleophilicity of non-dative heteroatomic ligand related to oxidation state of metal center. For example, we are not aware one metal complex can activate C-H bond through 1,2-addition pathway and

reductively eliminate products. If Ru(IV) with non-dative heteroatomic ligand complex can activate C-H bond, reductive elimination of product should be more favorable than using Ru(II) complexes. Also, reactivity of Ru(IV) imido/oxo species toward alkane and alkene has been interest to understand furthermore about metal mediated aziridination of alkenes and amination of alkanes reactions.

Platinum^{IV}, isoelectronic metal with Ru^{II}, -amido synthesis were attempted to study what dominates electrophilicity of metal center and basicity/nucleophilicity of non-dative heteroatomic ligand. Metal identity and oxidation state should impact on those factors as well as ancillary ligand affect. Also, oxygen atom insertion to Pt^{IV}-CH₃ bond has been studied using various oxidants. We are expecting this reaction undergo Baeyer-Villiger-type pathway similar to Re^{VII}-CH₃ (MTO) system demonstrated. We believe this is low energy pathway to regenerate metal non-dative heteroatomic ligand complex.

REFERENCES

1. Ohkuma, T.; Sandoval, C. A.; Srinivasan, R.; Lin, Q.; Wei, Y.; Muniz, K.; Noyori, R. *J. Am. Chem. Soc.* **2005**, 127, (23), 8288-8289.
2. Sanford, M. S.; Love, J. A.; Grubbs, R. H. *J. Am. Chem. Soc.* **2001**, 123, 6543-6554.
3. Blackwell, H. E.; O'Leary, D. J.; Chatterjee, A. K.; Washenfelder, R. A.; Busmann, D. A.; Grubbs, R. H. *J. Am. Chem. Soc.* **2000**, 122, 58-71.
4. Nelson, M. J.; Seitz, S. P.; Cowling, R. A. *Biochemistry* **1990**, 29, (29), 6897-6903.
5. Ogo, S.; Wada, S.; Watanabe, Y.; Iwase, M.; Wada, A.; Harata, M.; Jitsukawa, K.; Masuda, H.; Einaga, H. *Angew. Chem. Int. Ed.* **1998**, 37, (15), 2102-2104.
6. Tsuji, J. *New J. Chem.* **2000**, 24, (3), 127-135.
7. Müller, T. E.; Beller, M. *Chem. Rev.* **1998**, 98, 675-703.
8. Backvall, J. E.; Akermark, B.; Ljunggren, S. O. *J. Am. Chem. Soc.* **1979**, 101, (9), 2411-2416.
9. Senn, H. M.; Blöchl, P. E.; Tongi, A. *J. Am. Chem. Soc.* **2000**, 122, 4098-4107.
10. Alonso, D. A.; Brandt, P.; Nordin, S. J. M.; Andersson, P. G. *J. Am. Chem. Soc.* **1999**, 121, (41), 9580-9588.
11. Yamakawa, M.; Ito, H.; Noyori, R. *J. Am. Chem. Soc.* **2000**, 122, (7), 1466-1478.
12. Noyori, R.; Hashiguchi, S. *Acc. Chem. Res.* **1997**, 30, (2), 97-102.
13. Shekhar, S. R.; Hartwig, J. F.; Mathew, J. S.; Blackmond, D. G.; Strieter, E. R.; Buchwald, S. L. *Org. Lett.* **2006**, 128, 3584-3591.
14. Wolfe, J. P.; Tomori, H.; Sadighi, J. P.; Yin, J. J.; Buchwald, S. L. *J. Org. Chem.* **2000**, 65, (4), 1158-1174.
15. Torraca, K. E.; Huang, X. H.; Parrish, C. A.; Buchwald, S. L. *J. Am. Chem. Soc.* **2001**, 123, (43), 10770-10771.
16. Tzschucke, C. C.; Murphy, J. M.; Hartwig, J. F. *Org. Lett.* **2007**, 9, (5), 761-764.
17. Lee, S.; Jorgensen, M.; Hartwig, J. F. *Org. Lett.* **2001**, 3, (17), 2729-2732.

18. Bryndza, H. E.; Calabrese, J. C.; Marsi, M.; Roe, D. C.; Tam, W.; Bercaw, J. E. *J. Am. Chem. Soc.* **1986**, 108, (16), 4805-4813.
19. Bryndza, H. E.; Domaille, P. J.; Tam, W.; Fong, L. K.; Paciello, R. A.; Bercaw, J. E. *Polyhedron* **1988**, 7, 1441-1452.
20. Fulton, J. R.; Holland, A. W.; Fox, D. J.; Bergman, R. G. *Acc. Chem. Res.* **2002**, 35, 44-56.
21. Bryndza, H. E.; Tam, W. *Chem. Rev.* **1988**, 88, 1163-1188.
22. Fryzuk, M. D.; Montgomery, C. D. *Coord. Chem. Rev.* **1989**, 95, 1-40.
23. Glueck, D. S.; Bergman, R. G. *Organometallics* **1991**, 10, 1479-1486.
24. Glueck, D. S.; Winslow, L. J. N.; Bergman, R. G. *Organometallics* **1991**, 10, 1462-1479.
25. Simpson, R. D.; Bergman, R. G. *Organometallics* **1992**, 11, 3980-3993.
26. Kaplan, A. W.; Bergman, R. G. *Organometallics* **1998**, 17, 5072-5085.
27. Woerpel, K. A.; Bergman, R. G. *J. Am. Chem. Soc.* **1993**, 115, 7888-7889.
28. Feng, Y.; Lail, M.; Barakat, K. A.; Cundari, T. R.; Gunnoe, T. B.; Petersen, J. L. *J. Am. Chem. Soc.* **2005**, 127, 14174-14175.
29. Conner, D.; Jayaprakash, K. N.; Wells, M. B.; Manzer, S.; Gunnoe, T. B.; Boyle, P. D. *Inorg. Chem.* **2003**, 42, 4759-4772.
30. Conner, D.; Jayaprakash, K. N.; Cundari, T. R.; Gunnoe, T. B. *Organometallics* **2004**, 23, 2724-2733.
31. Zhao, J.; Goldman, A. S.; Hartwig, J. F. *Science* **2005**, 307, 1080-1082.
32. Soper, J. D.; Bennett, B. K.; Lovell, S.; Mayer, J. M. *Inorg. Chem.* **2001**, 40, 1888-1893.
33. Goj, L. A.; Blue, E. D.; Delp, S. A.; Gunnoe, T. B.; Cundari, T. R.; Pierpont, A. W.; Petersen, J. L.; Boyle, P. D. *Inorg. Chem.* **2006**, 45.
34. Zhang, J.; Gunnoe, T. B.; Petersen, J. L. *Inorg. Chem.* **2005**, 44, 2895-2907.
35. Fox, D. J.; Bergman, R. G. *J. Am. Chem. Soc.* **2003**, 125, 8984-8985.

36. Fulton, J. R.; Sklenak, S.; Bouwkamp, M. W.; Bergman, R. G. *J. Am. Chem. Soc.* **2002**, 124, 4722-4737.
37. Zhang, X.-X.; Sadighi, J. P.; Mackewitz, T. W.; Buchwald, S. L. *J. Am. Chem. Soc.* **2000**, 122, 7606-7607.
38. Mayer, J. M. *Acc. Chem. Res.* **1998**, 31, 441-450.
39. Caulton, K. G. *New J. Chem.* **1994**, 18, 25-41.
40. Bergman, R. G. *Polyhedron* **1995**, 14, 3227-3237.
41. Hartwig, J. F., Palladium-Catalyzed Amination of Aryl Halides and Sulfonates. In *Modern Amination Methods*, Ricci, A., Ed. Wiley-VCH: Weinheim, 2000; pp 195-262.
42. Hartwig, J. F. *Pure Appl. Chem.* **2004**, 76, 507-516.
43. Utsunomiya, M.; Hartwig, J. F. *J. Am. Chem. Soc.* **2004**, 126, 2702-2703.
44. Nettekoven, U.; Hartwig, J. F. *J. Am. Chem. Soc.* **2002**, 124, 1166-1167.
45. Kawatsura, M.; Hartwig, J. F. *J. Am. Chem. Soc.* **2000**, 122, 9546-9547.
46. Kwong, F. Y.; Buchwald, S. L. *Org. Lett.* **2002**, 4, 3517-3520.
47. Utsunomiya, M.; Kawatsura, M.; Hartwig, J. F. *Angew. Chem. Int. Ed.* **2003**, 42, 5865-5868.
48. Utsunomiya, M.; Kuwano, R.; Kawatsura, M.; Hartwig, J. F. *J. Am. Chem. Soc.* **2003**, 125, 5608-5609.
49. Kranenburg, M.; Vanderburgt, Y. E. M.; Kamer, P. C. J.; Vanleeuwen, P. W. N. M.; Goubitz, K.; Fraanje, J. *Organometallics* **1995**, 14, (6), 3081-3089.
50. Shekhar, S.; Ryberg, P.; Hartwig, J. F.; Mathew, J. S.; Blackmond, D. G.; Strieter, E. R.; Buchwald, S. L. *J. Am. Chem. Soc.* **2006**, 128, (11), 3584-3591.
51. Hartwig, J. F., Palladium-Catalyzed Amination of Aryl Halides and Sulfonates. In *Modern Amination Methods*, Ricci, A., Ed. Wiley-VCH: Weinheim, 2000.
52. Hartwig, J. F. *Angew. Chem. Int. Ed.* **1998**, 37, 2046-2067.
53. Yang, B. H.; Buchwald, S. L. *J. Organomet. Chem.* **1999**, 576, 125-146.

54. Wolfe, J. P.; Wagaw, S.; Marcoux, J.-F.; Buchwald, S. L. *Acc. Chem. Res.* **1998**, 31, 805-818.
55. Munro-Leighton, C.; Blue, E. D.; Gunnoe, T. B. *J. Am. Chem. Soc.* **2006**, 128, (5), 1446-1447.
56. Munro-Leighton, C.; Delp, S. A.; Blue, E. D.; Gunnoe, T. B. *Organometallics* **2007**, 26, (6), 1483-1493.
57. Delp, S. A.; Munro-Leighton, C.; Goj, L. A.; Gunnoe, T. B.; Petersen, J. L.; Boyle, P. D. *Inorg. Chem.* **2007**, 46, (7), 2365.
58. Goldberg, K. I.; Goldman, A. S., *Activation and Functionalization of C-H Bonds*. American Chemical Society: Washington, DC, 2004; Vol. 885.
59. Stahl, S. S.; Labinger, J. A.; Bercaw, J. E. *Angew. Chem. Int. Ed.* **1998**, 37, 2180-2192.
60. Shilov, A. E.; Shul'pin, G. B., *Activation and Catalytic Reactions of Saturated Hydrocarbons in the Presence of Metal Complexes*. Kluwer Academic Publishers: Dordrecht, 2000; Vol. 21.
61. Labinger, J. A.; Bercaw, J. E. *Nature* **2002**, 417, 507-514.
62. Bergman, R. G. *Science* **1984**, 223, 902-908.
63. Arndtsen, B. A.; Bergman, R. G.; Mobley, T. A.; Peterson, T. H. *Acc. Chem. Res.* **1995**, 28, 154-162.
64. Jones, W. D.; Feher, F. J. *Acc. Chem. Res.* **1989**, 22, 91-100.
65. Ritleng, V.; Sirlin, C.; Pfeffer, M. *Chem. Rev.* **2002**, 102, 1731-1769.
66. Dyker, G. *Angew. Chem. Int. Ed.* **1999**, 38, 1698-1712.
67. Crabtree, R. H. *Chem. Rev.* **1985**, 85, 245-269.
68. Shilov, A. E.; Shul'pin, G. B. *Chem. Rev.* **1997**, 97, 2879-2932.
69. Guari, Y.; Sbao-Etienne, S.; Chaudret, B. *Eur. J. Inorg. Chem.* **1999**, 1047-1055.
70. Kakiuchi, F.; Murai, S. *Acc. Chem. Res.* **2002**, 35, 826-834.

71. Murai, S.; Kakiuchi, F.; Sekine, S.; Tanaka, Y.; Kamatani, A.; Sonoda, M.; Chatani, N. *Pure App. Chem.* **1994**, 66, 1527-1534.
72. Jia, C.; Kitamura, T.; Fujiwara, Y. *Acc. Chem. Res.* **2001**, 34, 633-639.
73. Kakiuchi, F.; Chatani, N. *Adv. Synth. Catal.* **2003**, 345, 1077-1101.
74. Fekl, U.; Goldberg, K. I. *Adv. Inorg. Chem.* **2003**, 54, 259-320.
75. Trost, B. M.; Toste, F. D.; Pinkerton, A. B. *Chem. Rev.* **2001**, 101, (7), 2067-2096.
76. Cummins, C. C.; Baxter, S. M.; Wolczanski, P. T. *J. Am. Chem. Soc.* **1988**, 110, 8731-8733.
77. Feng, Y.; Lail, M.; Foley, N. A.; Gunnoe, T. B.; Barakat, K. A.; Cundari, T. R.; Petersen, J. L. *J. Am. Chem. Soc.* **2006**, 128, 7982-7994.
78. Wong-Foy, A. G.; Bhalla, G.; Liu, X. Y.; Periana, R. A. *J. Am. Chem. Soc.* **2003**, 125, 14292-14293.
79. Tenn, I. W. J.; Young, K. J. H.; Bhalla, G.; Oxgaard, J.; Goddard III, W. A.; Periana, R. A. *J. Am. Chem. Soc.* **2005**, 127, 14172-14173.
80. Bhalla, G.; Liu, X. Y.; Oxgaard, J.; Goddard, W. A.; Periana, R. A. *J. Am. Chem. Soc.* **2005**, 127, (32), 11372-11389.
81. Sandoval, C. A.; Ohkuma, T.; Muniz, K.; Noyori, R. *J. Am. Chem. Soc.* **2003**, 125, (44), 13490-13503.
82. Murata, K.; Konishi, H.; Ito, M.; Ikariya, T. *Organometallics* **2002**, 21, 253-255.
83. Guo, R. W.; Morris, R. H.; Song, D. *J. Am. Chem. Soc.* **2005**, 127, (2), 516-517.
84. Clapham, S. E.; Hadzovic, A.; Morris, R. H. *Coord. Chem. Rev.* **2004**, 248, (21-24), 2201-2237.
85. Abdur-Rashid, K.; Clapham, S. E.; Hadzovic, A.; Harvey, J. N.; Lough, A. J.; Morris, R. H. *J. Am. Chem. Soc.* **2002**, 124, (50), 15104-15118.
86. Wolfe, J. P.; Wagaw, S.; Buchwald, S. L. *J. Am. Chem. Soc.* **1996**, 118, (30), 7215-7216.
87. Widenhoefer, R. A.; Buchwald, S. L. *Organometallics* **1996**, 15, (16), 3534-3542.

88. Brown, S. N.; Mayer, J. M. *Organometallics* **1995**, 14, 2951-2960.
89. Spaltenstein, E.; Erikson, T. K. G.; Critchlow, S. C.; Mayer, J. M. *J. Am. Chem. Soc.* **1989**, 111, (2), 617-623.
90. Herrmann, W. A. *Angew. Chem. Int. Ed. Engl.* **1988**, 27, (10), 1297-1313.
91. Bottomley, F.; Sutin, L. *Adv. Organomet. Chem.* **1988**, 28, 339-396.
92. Conley, B. L.; Ganesh, S. K.; Gonzales, J. M.; Tenn, W. J.; Young, K. J. H.; Oxgaard, J.; Goddard, W. A.; Periana, R. A. *J. Am. Chem. Soc.* **2006**, 128, (28), 9018-9019.
93. Walsh, P. J.; Hollander, F. J.; Bergman, R. G. *J. Am. Chem. Soc.* **1988**, 110, 8729-8731.
94. Harlan, E. W.; Holm, R. H. *J. Am. Chem. Soc.* **1990**, 112, 186-193.
95. Guiducci, A. E.; Boyd, C. L.; Mountford, P. *Organometallics* **2006**, 25, (5), 1167-1187.
96. Formentin, P.; Alvaro, M.; Garcia, H.; Palomares, E.; Sabater, M. J. *New J. Chem.* **2002**, 26, (11), 1646-1650.
97. Pérez, P. J.; White, P. S.; Brookhart, M.; Templeton, J. L. *Inorg. Chem.* **1994**, 33, 6050-6056.
98. Müller, P.; Fruit, C. *Chem. Rev.* **2003**, 103, 2905-2919.
99. Badiei, Y. M.; Krishnaswamy, A.; Melzer, M. M.; Warren, T. H. *J. Amer. Chem. Soc.* **2006**, 128, (47), 15056-15057.
100. Au, S.-M.; Huang, J.-S.; Yu, W.-Y.; Fung, W.-H.; Che, C.-M. *J. Am. Chem. Soc.* **1999**, 121, 9120-9132.
101. Mahy, J.-P.; Bedi, G.; Battioni, P.; Mansuy, D. *J. Chem. Soc., Perkin Trans. II* **1988**, 1517-1524.
102. Li, Z.; Quan, R. W.; Jacobsen, E. N. *J. Am. Chem. Soc.* **1995**, 117, 5889-5890.
103. Evans, D. A.; Faul, M. M.; Bilodeau, M. T.; Anderson, B. A.; Barnes, D. M. *J. Am. Chem. Soc.* **1993**, 115, 5328-5329.
104. Mindiola, D. J.; Hillhouse, G. L. *J. Am. Chem. Soc.* **2001**, 123, 4623-4624.

105. Anderson, T. M.; Neiwert, W. A.; Kirk, M. L.; Piccoli, P. M. B.; Schultz, A. J.; Koetzle, T. F.; Musaev, D. G.; Morokuma, K.; Cao, R.; Hill, C. L. *Science* **2004**, 306, (5704), 2074-2077.
106. Brown, S. D.; Peters, J. C. *J. Am. Chem. Soc.* **2004**, 126, (14), 4538-4539.
107. Lu, C. C.; Saouma, C. T.; Day, M. W.; Peters, J. C. *J. Am. Chem. Soc.* **2007**, 129, (1), 4-5.
108. Brown, S. D.; Mehn, M. P.; Peters, J. C. *J. Am. Chem. Soc.* **2005**, 127, (38), 13146-13147.
109. Thyagarajan, S.; Shay, D. T.; Incarvito, C. D.; Rheingold, A. L.; Theopold, K. H. *J. Am. Chem. Soc.* **2003**, 125, 4440-4441.
110. Wigley, D. E. *Prog. Inorg. Chem.* **1994**, 42, 239-482.

CHAPTER 2

2.1 Introduction

2.1.1 Background of metal imido and oxo species

Oxo and imido ligands are highly prevalent in metal-mediated chemistry.¹⁻⁶ Such moieties have been used with inert ancillary ligands to support catalysts^{2, 7-9} as well as reactive sites for atom (O) or group (NR) transfer and other reactions.^{2, 4, 5, 8-13} The majority of oxo or imido complexes are systems in which the metal is formally in a high oxidation state. For such systems, the presence of at least two empty d orbitals that are of π -symmetry with respect to the M-oxo or M-imido bond axis maximizes ligand-metal bonding (Figure 2.1). In contrast, if metal $d\pi$ atomic orbitals are occupied, ligand-metal π -bonding is disrupted, which can enhance reactivity at the heteroatomic ligand. There are only a few examples of oxo or imido ligands coordinated to metals which do *not* possess formal triple bonds ($1\sigma + 2\pi$).^{7, 14-16} Similar to our chemistry with d^6 complexes that possess amido, hydroxo and related ligands,¹⁷ we are interested in disrupting ligand-to-metal π -donation for formally dianionic oxo and imido ligands in order to access highly reactive hetero-ligands.

It is challenging to find a balance that affords highly reactive, yet isolable, complexes. Herein, our strategies were to disrupt ligand-metal π -bonding with a d^4 electron count (Figure 2.1), but to enhance ionic bonding via incorporation of the electronegative O-based ancillary ligand acac (acac = acetylacetonate). To complete the coordination sphere, we selected an η^6 -arene system. Thus, our template for attempted construction of new oxo/imido systems is $[(\eta^6\text{-arene})\text{Ru}^{\text{II}}(\kappa^2\text{-O, O-acac})]^+$ (Chart 1).

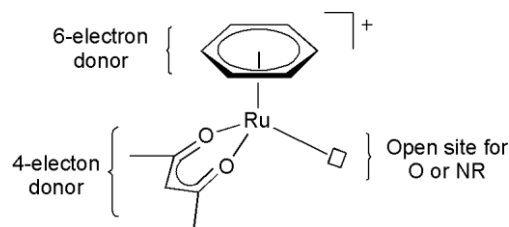


Chart 2.1. Template of $[(\eta^6\text{-arene})\text{Ru}^{\text{II}}(\kappa^2\text{-O,O-acac})]^+$.

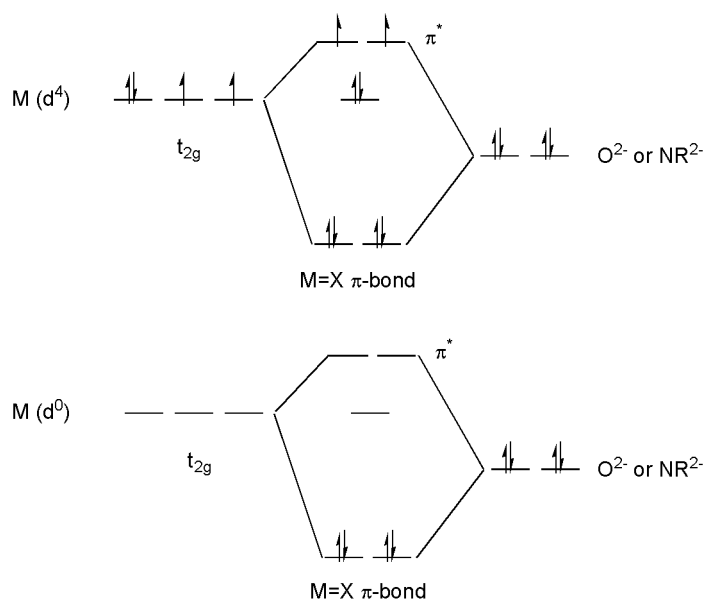


Figure 2.1. Molecular orbital diagram of π -bonding on d^4 and d^0 formally octahedral metal imido or oxo complex.

2.1.2 Various metal complexes with *p*-cymene and acetylacetonate ligands

The coordination chemistry of mono-metallic half-sandwich compounds has been of significant interest in inorganic and organometallic chemistry.¹⁸⁻²² Formally charge-neutral η^6 -arene ligands have played a prominent role in this field and can serve as ancillary ligands as well as intermediates for arene functionalization.^{15, 23-31} Hexa-hapto aromatic Ru(II) complexes provide a flexible template upon which to build diverse coordination

environments and to develop metal-mediated catalysis,³²⁻⁴⁶ with the η^6 -arene ligand providing a site to potentially vary sterics and electronics. In addition, the use of Ru(II)- η^6 -arene complexes in medicinal applications has been explored.⁴⁷⁻⁵⁴

The acetylacetonate ligand, often abbreviated acac, typically occupies two coordination sites by O-metal bonding.⁵⁵⁻⁵⁷ Alternatively, to a more limited extent η^1 -C binding has also been observed (Figure 2.2).^{58, 59} The donating ability of acac type ligands can be tuned by substituting the "back-bone" methyl group with electron-donating or electron-withdrawing groups.^{60, 61}

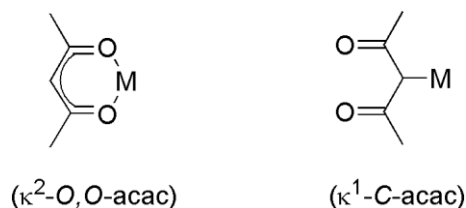


Figure 2.2. Two potential coordination modes for acetylacetonate are $\kappa^2\text{-O,O}$ and $\kappa^1\text{-C}$.

The combination of an η^6 -arene ligand and a formally anionic oxygen-based acac ligand provides a coordination sphere with both "soft" and "hard" donors (Chart 2.1). The η^6 -arene ligand and ruthenium likely form bonds with substantial covalent character. When $\kappa^2\text{-O,O-acac}$ coordinates to ruthenium, the electron deficient (relative to carbon) O-donor ligand donates less electron density to the metal center and results in more polar bonds. We sought to access $(\eta^6\text{-}p\text{-cymene})\text{Ru}(\kappa^2\text{-O,O-acac})\text{X}$ and formally exchange monoanionic X with O or NR to form $[(\eta^6\text{-}p\text{-cymene})(\kappa^2\text{-O,O-acac})\text{Ru}=\text{O}]^+$ or $[(\eta^6\text{-}p\text{-cymene})(\kappa^2\text{-O,O-acac})\text{Ru}=\text{NR}]^+$ (Chart 2.2).

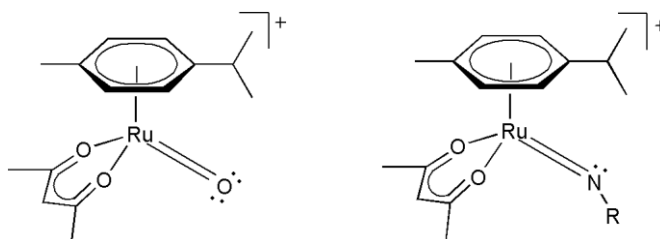
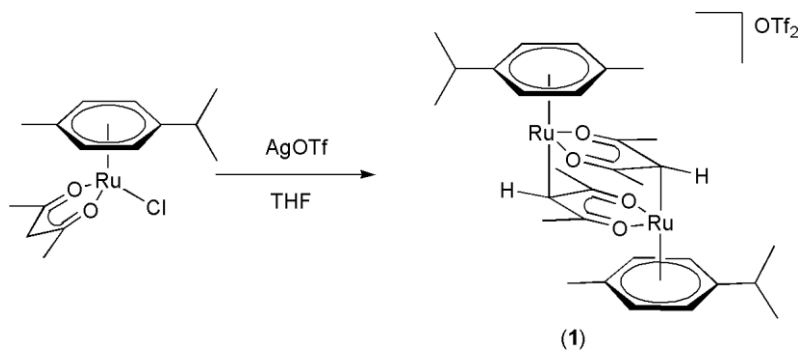


Chart 2.2. Possible $[(\eta^6\text{-}p\text{-cymene})(\kappa^2\text{-}O,O\text{-acac})\text{Ru}^{\text{IV}}]$ oxo and imido complexes.

2.2 Synthesis and characterization of $[(\eta^6\text{-}p\text{-cymene})\text{Ru}(\kappa^2\text{-}O,O\text{-acac-}\mu\text{-CH})_2][\text{OTf}]_2$

The reaction of previously reported $(\eta^6\text{-}p\text{-cymene})\text{Ru}(\text{acac})\text{Cl}$ ^{19, 21} with AgOTf results in chloride/triflate metathesis to produce $[(\eta^6\text{-}p\text{-cymene})\text{Ru}(\kappa^2\text{-}O,O\text{-acac-}\mu\text{-CH})_2][\text{OTf}]_2$ (**1**) (Scheme 2.1). Consistent with chloride/triflate exchange, the ¹⁹F NMR spectrum of **1** reveals a singlet at -78.0 ppm. Also, ¹H NMR and ¹³C NMR spectra are consistent with the metathesis product **1** (Figure 2.3 and Figure 2.4). We anticipated that this reaction would produce the monomeric product of simple chloride/triflate exchange, $(\eta^6\text{-}p\text{-cymene})\text{Ru}(\kappa^2\text{-}O,O\text{-acac-}\mu\text{-CH})(\text{OTf})$ (**1-OTf**); however, a single crystal X-ray diffraction reveals that **1** does not have a Ru-OTf linkage, rather, the C-H moiety of two acac ligands serves to bridge two Ru centers to form the bimetallic complex $[(\eta^6\text{-}p\text{-cymene})\text{Ru}(O,O\text{-acac-}\mu\text{-CH})_2][\text{OTf}]_2$ (**1**) (Figure 2.5, Tables 2.1 and Table 2.2). Thus, in the solid state, the acac π -system apparently forms a stronger bond with Ru than does the weakly coordinating triflate ligand.



Scheme 2.1. Metathesis reaction to yield $[(\eta^6\text{-}p\text{-cymene})\text{Ru}(\kappa^2\text{-}O,O\text{-acac-}\mu\text{-CH})_2][\text{OTf}]_2$ (**1**).

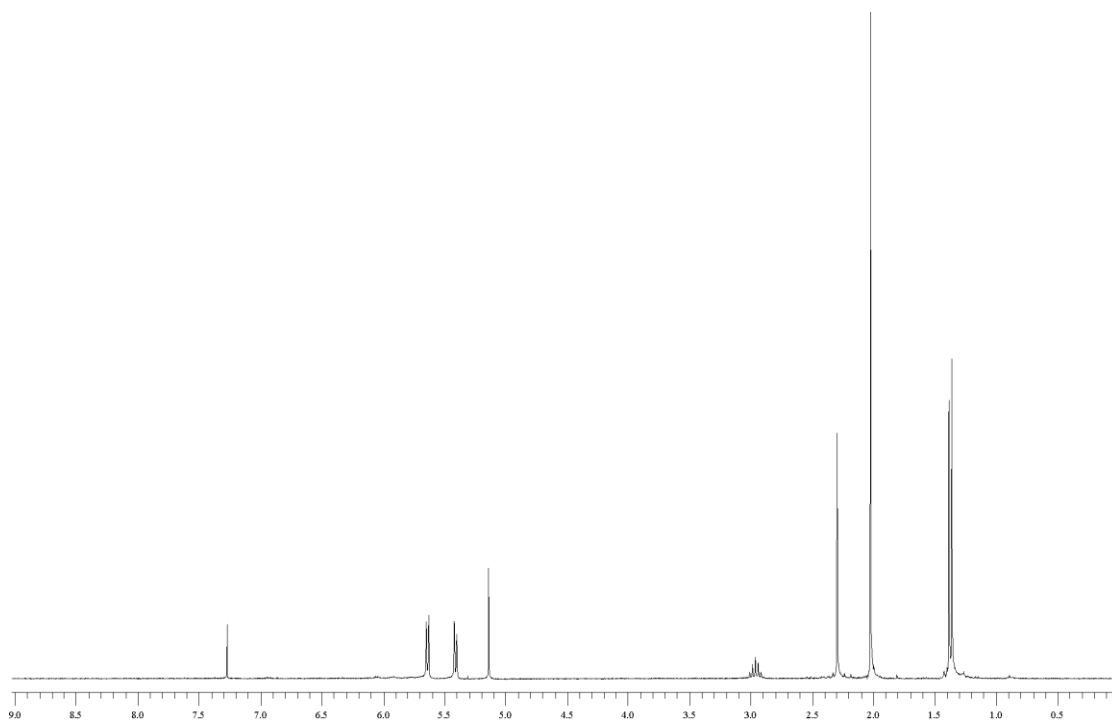


Figure 2.3. ^1H NMR spectrum of $[(\eta^6\text{-}p\text{-cymene})\text{Ru}(\kappa^2\text{-}O,O\text{-acac-}\mu\text{-CH})_2][\text{OTf}]_2$ (**1**) in CDCl_3 .

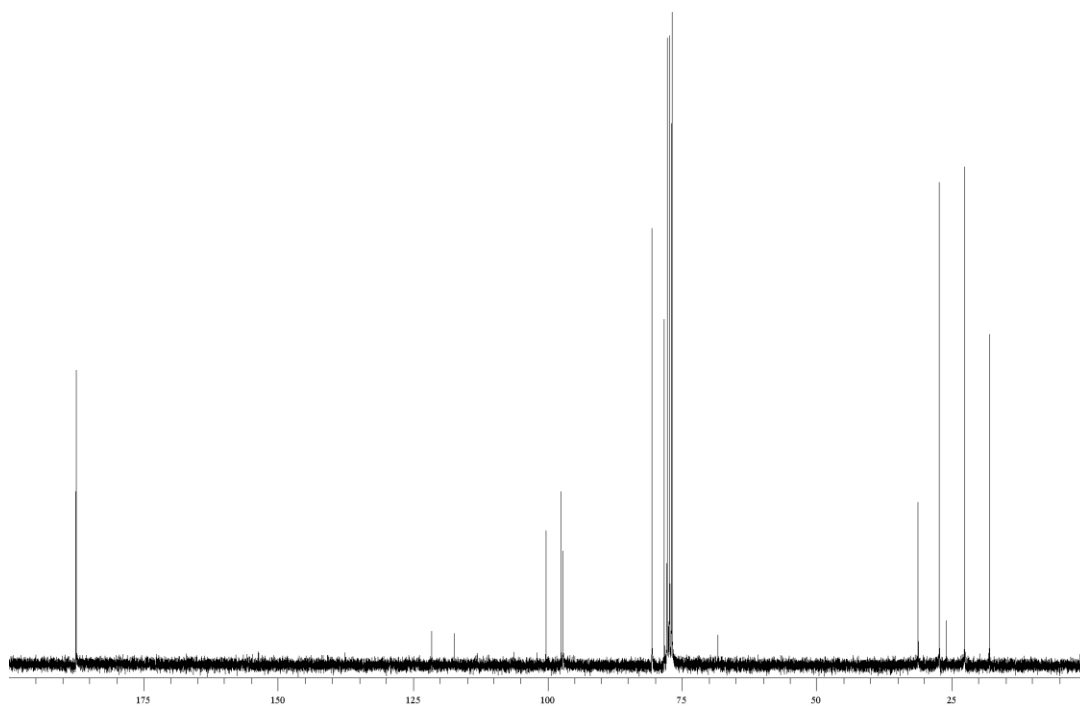


Figure 2.4. ^{13}C NMR spectrum of $[(\eta^6\text{-}p\text{-cymene})\text{Ru}(\kappa^2\text{-}O,O\text{-acac-}\mu\text{-CH})_2][\text{OTf}]_2$ (**1**) in CDCl_3 .

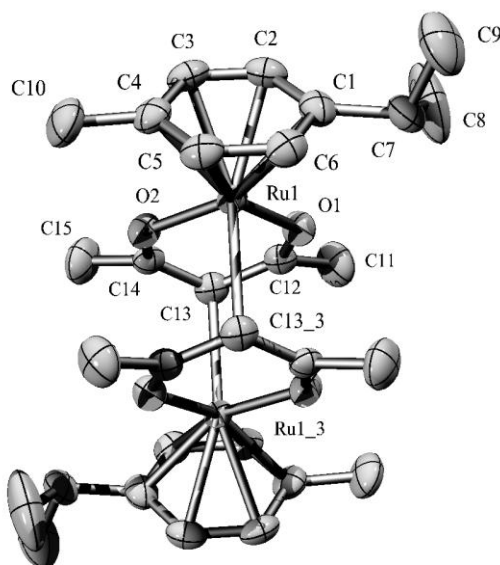


Figure 2.5. ORTEP (scaled to enclose 30% probability) of $[(\eta^6\text{-}p\text{-cymene})\text{Ru}(\kappa^2\text{-}O,O\text{-acac-}\mu\text{-CH})_2][\text{OTf}]_2$ (**1**).

Table 2.1. Selected bond distances (Å) and angles (°) for $[(\eta^6\text{-}p\text{-cymene})\text{Ru}(\kappa^2\text{-}O,O\text{-acac-}\mu\text{-CH})_2[\text{OTf}]_2$ (**1**).

<i>Bond lengths</i> (Å)			
Ru(1)-Cent ^a	1.671	Ru(1)-C(4)	2.189(3)
Ru(1)-O(1)	2.085(2)	Ru(1)-C(5)	2.179(3)
Ru(1)-O(2)	2.081(2)	Ru(1)-C(6)	2.188(3)
Ru(1)-C(1)	2.208(3)	Ru(1)-C(13) ^b	2.315(3)
Ru(1)-C(2)	2.190(3)	O(1)-C(12)	1.242(3)
Ru(1)-C(3)	2.179(3)	O(2)-C(14)	1.246(3)
<i>Bond angles</i> (°)			
O(2)-Ru(1)-O(1)	86.4(1)	O(1)-C(12)-C(11)	115.9(3)
C(12)-O(1)-Ru(1)	128.3(2)	C(13)-C(12)-C(11)	118.1(3)
C(14)-O(2)-Ru(1)	128.3(2)	C(12)-C(13)-C(14)	120.0(2)
C(3)-C(4)-C(10)	120.3(3)	O(2)-C(14)-C(13)	125.6(2)
O(1)-C(12)-C(13)	126.0(2)	O(2)-C(14)-C(15)	116.1(3)

^aCent corresponds to the centroid of the central six-membered ring of the *p*-cymene ligand. ^bSymmetry transformations used to generate equivalent atoms: -x+2,-y+2,-z+2.

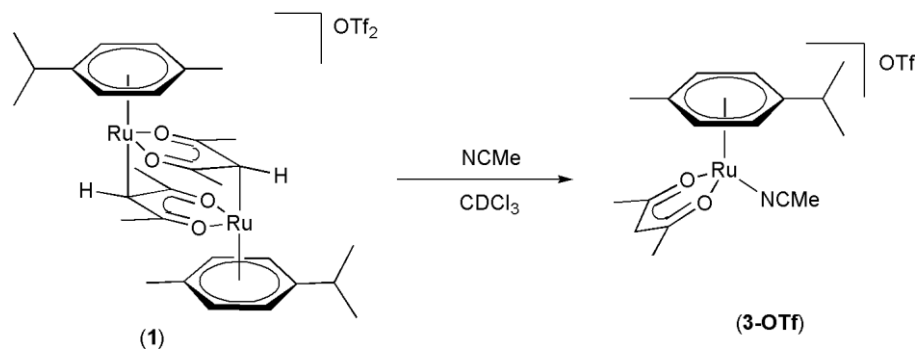
Table 2.2. Crystal data and structure refinement for complexes **1**, **5** and **7**.

	Complex 1	Complex 5	Complex 7
Empirical formula	C ₁₆ H ₂₁ F ₃ O ₅ RuS	C ₅₆ H ₄₆ B ₂ F ₂₄ N ₆ Ru	C ₅₂ H ₄₀ BCl ₃ F ₂₄ Ru ₂
Formula weight	483.47	1381.68	1440.14
T (K)	223(2)	293(2)	110
λ (Å)	0.71073	0.71073	0.71070
Crystal system	monoclinic	monoclinic	triclinic
Space group	P2 ₁ /n	P2 ₁ /c	P $\bar{1}$
<i>a</i> (Å)	10.1067(8)	12.9695(8)	12.6470(3)
<i>b</i> (Å)	16.674(1)	18.945(1)	14.174(4)
<i>c</i> (Å)	11.752(1)	24.865(2)	16.992(5)
α (°)	90	90	72.119(2)
β (°)	108.291(2)	98.393(1)	73.622(1)
γ (°)	90	90	86.217(1)
<i>V</i> (Å ³)	1880.4(3)	6044.2(6)	2780.51(1)
<i>Z</i>	4	4	2
ρ_{calc} (g/cm ³)	1.708	1.518	1.720
Crystal size (mm)	0.26 x 0.32 x 0.34	0.12 x 0.28 x 0.54	0.20 × 0.18 × 0.16
GOF	1.049	0.963	1.034
R1, wR2 {I>2 σ (I)}	0.0332, 0.0912	0.0534, 0.1407	0.0331, 0.0775

Examples of complexes with μ -CH bridging β -diketonate ligands are known.⁶² For complex **1**, the bond distance between Ru and the bridging acac carbon is 2.315(3) Å. This bond distance is longer than typical Ru^{II}-C bond distances of Ru-alkyl linkages,^{17, 63-66} which are in the range of 2.16(2) Å to 2.21(2) Å, as well as Ru-C bond distances of η^2 -olefins {Ru-(η^2 -C₂H₄) 2.151, 2.148 Å (2),⁶⁷} and vinyl ligands {Ru-(η^1 -C₂R₃) 2.111 Å (4),⁶⁸}. The average bond distance for Ru-C_{arene} interactions for complex **1** is 2.189(3) Å. There are several examples of structurally characterized Ru(II) systems with η^6 -*p*-cymene ligands. For instance, [(η^6 -*p*-cymene)Ru(1,2,3,4-Me₄-1,3-butadiene)Cl][ClO₄]⁶⁹ system has an average

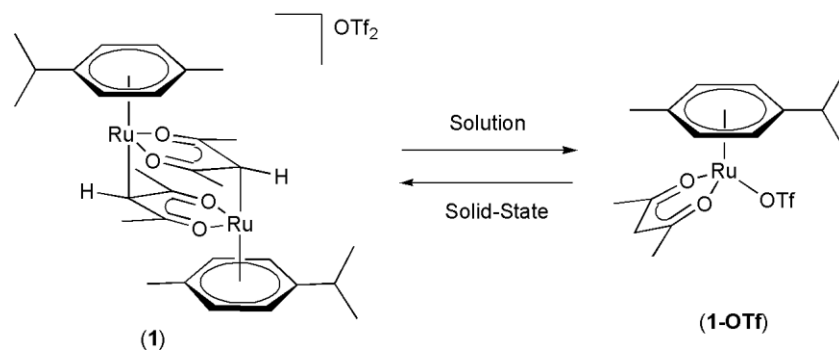
Ru-C_{arene} bond distance of 2.280(4) Å, the average Ru-C_{arene} distance of [(η⁶-*p*-cymene)Ru(PPh₃)₂Cl]²² is 2.278(2) Å while those of [(η⁶-*p*-cymene)Ru(1,2-S₂C₂B₁₀C₁₀-S,S')(arylamine)]⁷⁰ and [(η⁶-*p*-cymene)Ru[S₂C₂(B₁₀H₁₀)](PPh₃)]⁷¹ are 2.227(8) Å and 2.263(4) Å, respectively.

It is likely that the μ-CH bridging acac structure of **1** does not persist in solution. The chemical shift of the acac-CH moiety of **1** in CDCl₃ is 5.17 ppm. This value is quite similar to the analogous chemical shift of other acac complexes reported herein (the range is 6.04 ppm to 5.21 ppm), which is suggestive of a simple κ²-*O,O* coordination mode. Other evidence suggests that (η⁶-*p*-cymene)Ru(κ²-*O,O*-acac)OTf is present in solution (see below). In addition, if the μ-CH bridging acac structure persists in solution, it is easily displaced. For example, placing **1** in CDCl₃ with acetonitrile produces [(η⁶-*p*-cymene)Ru(κ²-*O,O*-acac)(NCMe)][OTf] (**3-OTf**) within 5 minutes at room temperature (Scheme 2.2). The production of **3-OTf** has been observed by ¹H NMR spectroscopy while [(η⁶-*p*-cymene)Ru(κ²-*O,O*-acac)(NCMe)][BAR'₄] (**3**) has been isolated.

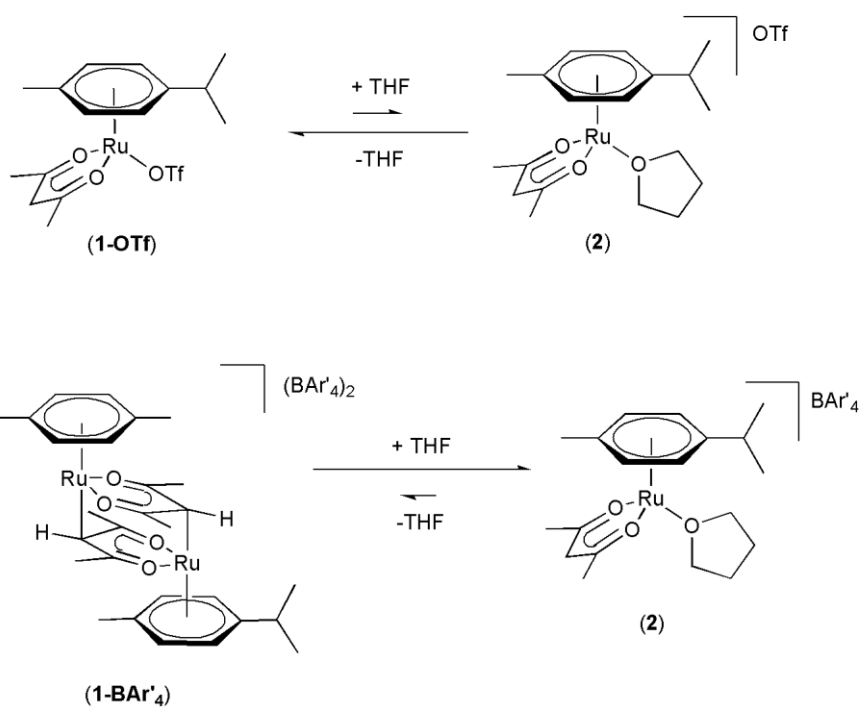


Scheme 2.2. Ligand exchange of [(η⁶-*p*-cymene)Ru(κ²-*O,O*-acac-μ-CH)]₂[OTf]₂ (**1**) with acetonitrile.

In THF solution, **1** does not coordinate THF, which is consistent with a monomeric form of $(\eta^6\text{-}p\text{-cymene})\text{Ru}(\kappa^2\text{-}O,O\text{-acac})\text{OTf}$ in solution (Scheme 2.3). In contrast, the reaction of **1** and NaBAR'_4 ($\text{Ar}' = 3,5\text{-}(\text{CF}_3)_2\text{C}_6\text{H}_3$) in THF produces $[(\eta^6\text{-}p\text{-cymene})\text{Ru}(\kappa^2\text{-}O,O\text{-acac})(\text{THF})][\text{BAR}'_4]$ (**2**) (Scheme 2.9). Hence, THF does not compete with OTf for coordination to Ru but does displace the $\mu\text{-CH}$ linkage (Scheme 2.4).



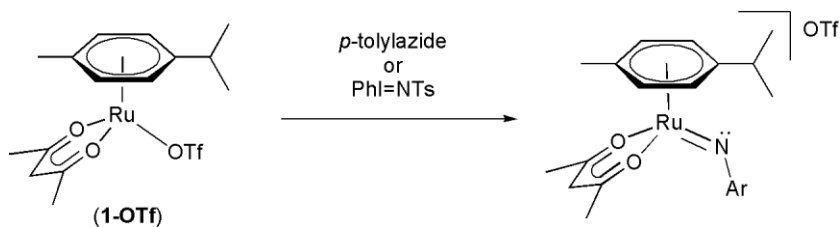
Scheme 2.3. Competition between coordination of acac-CH and OTf.



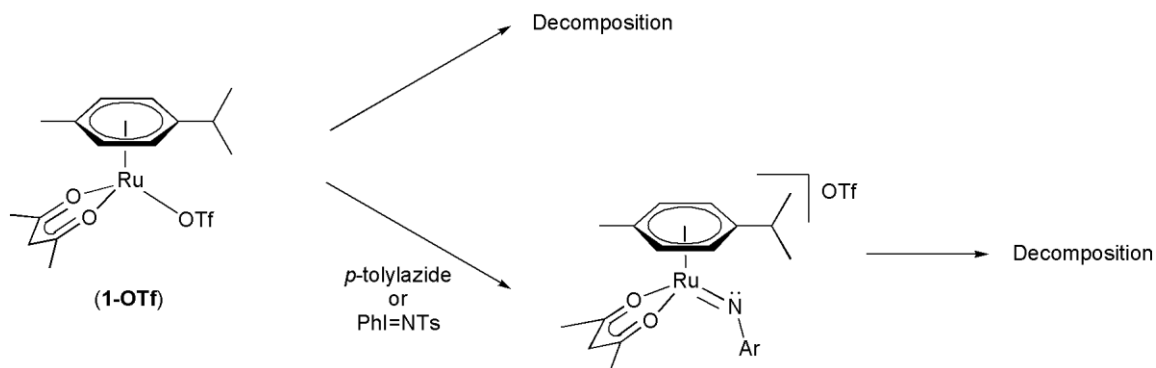
Scheme 2.4. Equilibria for coordination of THF as a function of counterion.

2.2.1 Reaction of $[(\eta^6\text{-}p\text{-cymene})\text{Ru}(\kappa^2\text{-}O,O\text{-acac-}\mu\text{-CH})_2][\text{OTf}]_2$ with $p\text{-tolylazide}$ and PhI=NTs

Nitrene sources such as $p\text{-tolylazide}$ and PhI=NTs ($\text{Ts} = p\text{-tolylsulfonyl}$) were used in attempts to oxidize the Ru(II) center by two electrons and form monomeric imido complexes of the type $[(\eta^6\text{-}p\text{-cymene})(\kappa^2\text{-}O,O\text{-acac})\text{Ru}=\text{N}(\text{Ar})]^+$ ($\text{Ar} = \text{Ts}$ or $p\text{-tolyl}$). The possible formation of Ru imido complexes are shown in Scheme 2.5. There are four likely outcomes for these reactions: 1) formation of a stable $[(\eta^6\text{-}p\text{-cymene})(\kappa^2\text{-}O,O\text{-acac})\text{Ru}=\text{N}(\text{Ar})]^+$, 2) formation of an unstable $[(\eta^6\text{-}p\text{-cymene})(\kappa^2\text{-}O,O\text{-acac})\text{Ru}=\text{N}(\text{Ar})]^+$ which undergoes to decomposition, 3) no reaction, or 4) decomposition of starting materials. An octahedral d^4 imido complex is expected to be paramagnetic (Figure 2.1), which would likely be NMR inactive or give broad resonances.

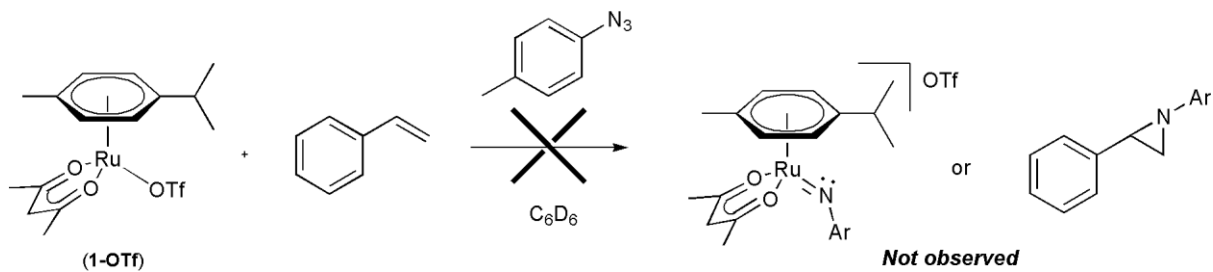


Scheme 2.5. Potential reaction to yield $[(\eta^6\text{-}p\text{-cymene})(\kappa^2\text{-}O,O\text{-acac})\text{Ru}=\text{N}(\text{Ar})]^+$.



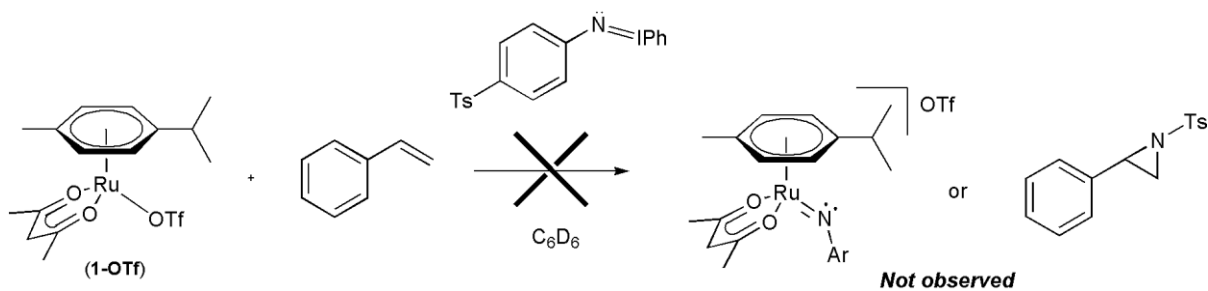
Scheme 2.6. Possible decomposition pathways.

Transition metal imido complexes often react with olefins to produce aziridine via net nitrene transfer. Thus, in an effort to gain indirect evidence for the transient formation of $[(\eta^6\text{-}p\text{-cymene})(\kappa^2\text{-}O,O\text{-acac})\text{Ru}=\text{N}(\text{Ar})]^+$, in separate experiments, we reacted complex **1** with $\text{N}_3(p\text{-tolyl})$ and PhINTs in the presence of styrene. The reaction of **1** and *p*-tolyl-azide in the presence of styrene did not yield an aziridination product (Scheme 2.7). After 60 hours, **1** remained in solution without decomposition. There is no observation of reaction with $\text{N}_3(p\text{-tolyl})$. For example, there is no observation of $\text{N}_3(p\text{-tolyl})$ consumption or $\text{NH}_2(p\text{-tolyl})$ formation.



Scheme 2.7. Reaction of **1** with *p*-tolylazide.

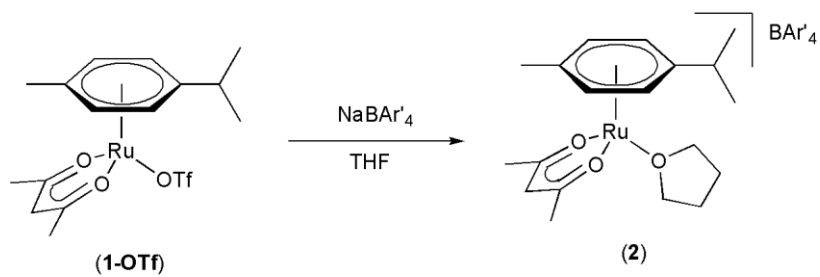
Similarly, reaction of **1**, PhI=NTs and styrene did not produce *N*-(*p*-tolylsulfonyl)-2-phenyl aziridine (Scheme 2.8). Starting material **1** decomposes into unknown compounds while giving off free *p*-cymene. During this reaction, the formation of TsNH₂ and iodobenzene was observed by ¹H NMR spectroscopy. Although the hydrogen atom sources for TsNH₂ formation were not determined, it is almost certain the hydrogen atoms are not from C₆D₆ since no observation of TsND₂ was made.



Scheme 2.8. Reaction of **1** with PhI=NTs.

2.3 Synthesis and characterization of [(η⁶-*p*-cymene)Ru(κ²-*O,O*-acac)(THF)][BAR'₄]

The combination of **1** and NaBAR'₄ (Ar' = 3,5-(CF₃)₂C₆H₃) in THF produces [(η⁶-*p*-cymene)Ru(κ²-*O,O*-acac)(THF)][BAR'₄] (**2**) (Scheme 2.9). The ¹H NMR spectrum of **2** reveals resonances of 3.49 and 1.74 ppm, and the carbon resonances at 70.9 and 25.5 ppm in the ¹³C NMR spectrum correspond to the α- and β- positions, respectively, of the coordinated THF. In comparison, free THF peaks resonate at 3.76 and 1.85 ppm in ¹H NMR spectrum and at 68.0 and 25.6 ppm in ¹³C NMR spectrum. Thus, coordination of THF to the cationic Ru(II) results in a slight upfield shift of resonances of the THF ligand (Figure 2.6 and Figure 2.7).



Scheme 2.9. Synthesis of $[(\eta^6\text{-}p\text{-cymene})\text{Ru}(\kappa^2\text{-}O,O\text{-acac})(\text{THF})][\text{BAR}'_4]$ (**2**).

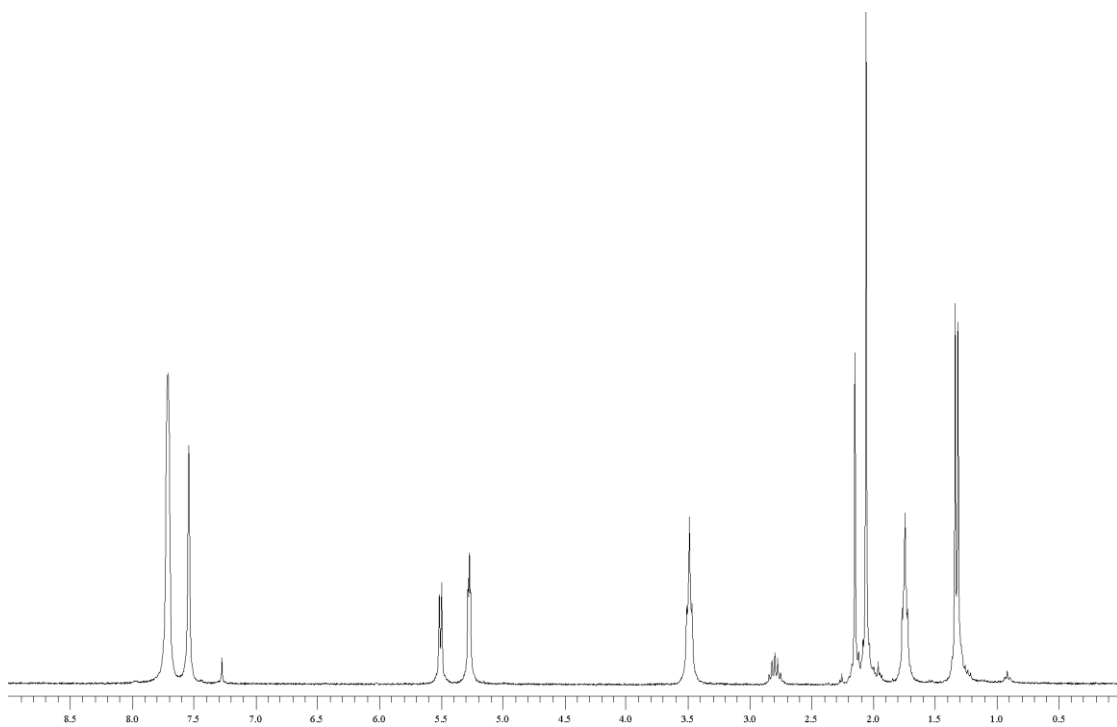


Figure 2.6. ¹H NMR spectrum of $[(\eta^6\text{-}p\text{-cymene})\text{Ru}(\kappa^2\text{-}O,O\text{-acac})(\text{THF})][\text{BAR}'_4]$ (**2**) in CDCl₃.

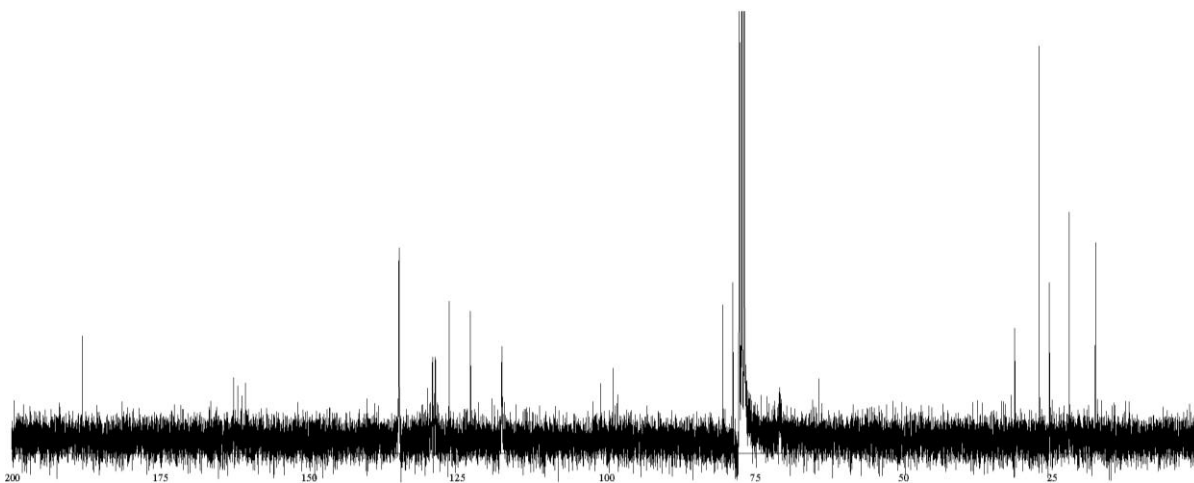
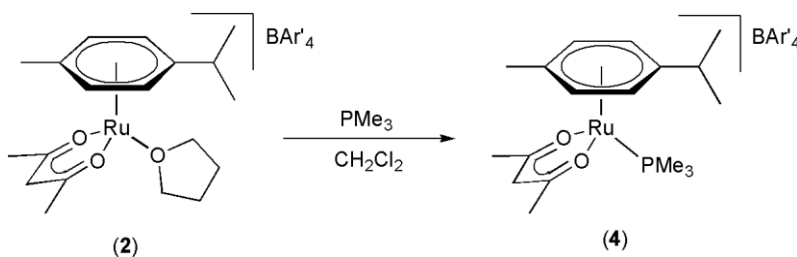


Figure 2.7. ^{13}C NMR spectrum of $[(\eta^6\text{-}p\text{-cymene})\text{Ru}(\kappa^2\text{-}O,O\text{-acac})(\text{THF})][\text{BAr}'_4]$ (**2**) in CDCl_3 .

The THF ligand of **2** is quite labile. For example, the combination of **2** and PMe_3 in CH_2Cl_2 produces $[(\eta^6\text{-}p\text{-cymene})\text{Ru}(\kappa^2\text{-}O,O\text{-acac})(\text{PMe}_3)][\text{BAr}'_4]$ (**4**) (Scheme 2.10). Consistent with THF/ PMe_3 exchange, the ^{19}F NMR spectrum of **1** reveals a singlet at -58.8 ppm. Performing this reaction in an NMR tube in CDCl_3 reveals the formation of free THF (Figure 2.8). Coordinated PMe_3 shows up at 1.28 ppm while free PMe_3 reveals at 1.04 ppm. At room temperature, ^1H NMR and ^{13}C NMR spectra define the structure with mirror symmetry due to *p*-cymene and acac resonances.



Scheme 2.10. Ligand exchange reaction of **2** with PMe_3 .

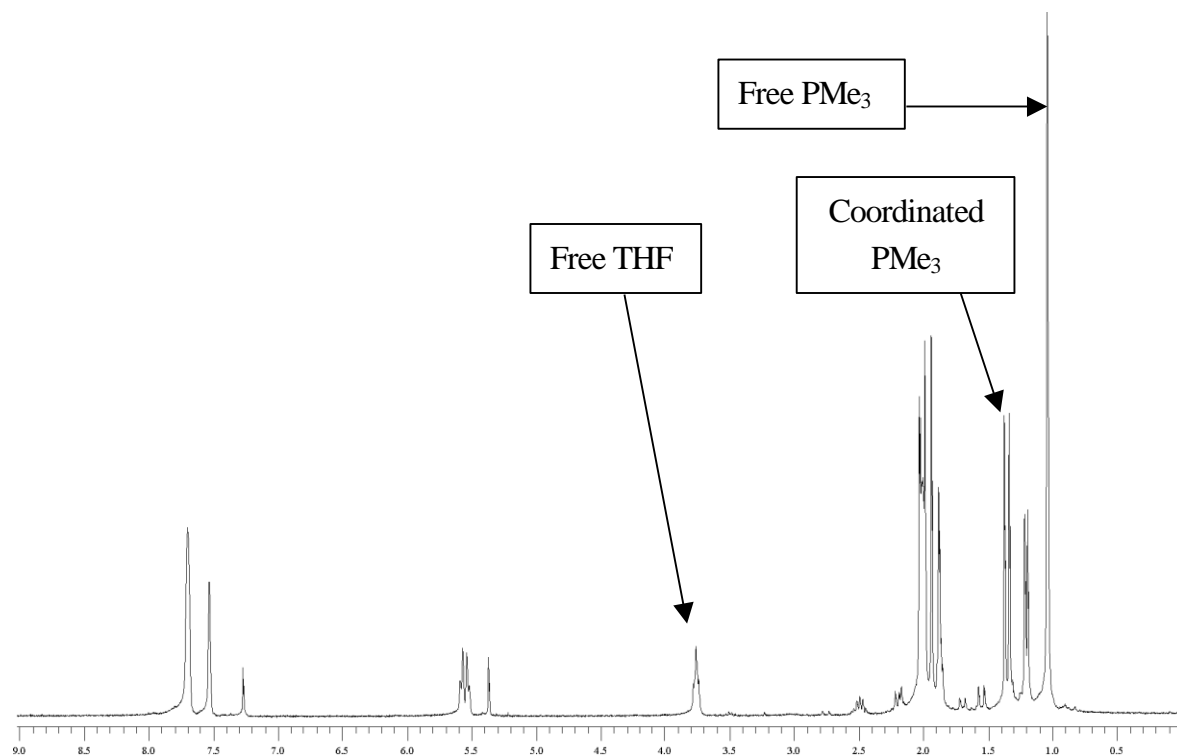
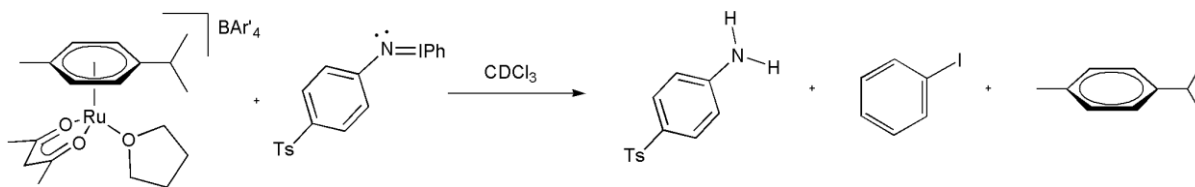


Figure 2.8. ¹H NMR spectrum of reaction product from the addition of PMe₃ to **2** in CDCl₃.

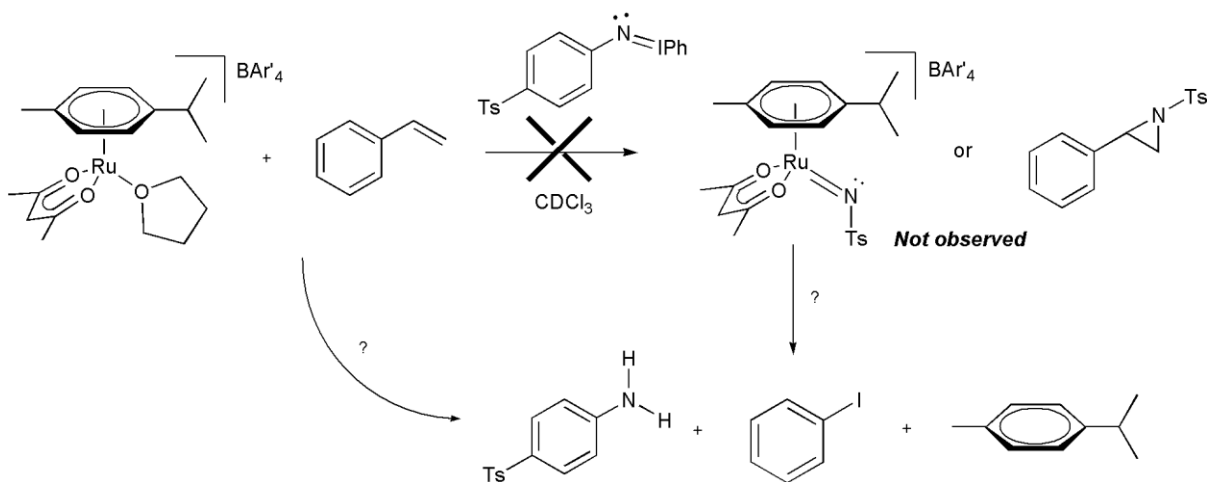
Complex **2** reacts with 10 equivalents of NCMe to produce [(η⁶-*p*-cymene)Ru(κ²-*O,O*-acac)(NCMe)][BAR'₄] (**3**) (Scheme 2.11). Performing the reaction in NCCD₃ reveals complete conversion to **3** within 5 minutes with concomitant formation of free THF (Figure 2.9). Consistent with THF/NCMe exchange, the ¹⁹F NMR spectrum of **1** reveals a singlet at –58.8 ppm. Coordinated NCMe shows up at 1.98 ppm as a singlet while free NCMe reveals at 2.1 ppm. At room temperature, ¹H NMR and ¹³C NMR spectra define the structure with mirror symmetry due to methyl of *p*-cymene and acac resonances.

access to a single open coordination site, thus **2** may be more reactive than $[(\eta^6\text{-}p\text{-cymene})\text{Ru}(\text{O},\text{O}\text{-acac}\text{-}\mu\text{-CH})_2][\text{OTf}]_2$ (**1**) since the BAR'_4 anion does not compete for the open coordination site but OTf does (Scheme 2.3). Therefore, **2** has more of a chance to successfully react with nitrene and oxo sources to produce ruthenium imido and oxo complexes, respectively.

The combination of **2** and $\text{PhI}=\text{NTs}$ results in the observation of free *p*-cymene, iodobenzene and *p*-tolylsulfonyl amine (Scheme 2.12). During this transformation, **2** decomposes to multiple products. Furthermore, no production of *N*-(*p*-tolylsulfonyl)-2-phenyl aziridine was observed in the ^1H NMR spectrum when **2**, PhINTs and styrene were reacted (Figure 2.10 and Scheme 2.13). The reactions with and without styrene give the same pattern of decomposition. It is not determined how complex **2** decomposes to free *p*-cymene, iodobenzene and *p*-tolylsulfonyl amine. Importantly, there are hydrogen atom sources ($\text{H}\cdot$) involved in these reactions since tosylamine is produced. Che et al. observed a mass balance of aziridine and TsNH_2 products is close to 100% in stoichiometric reaction of bis(tosylimido)ruthenium^{VI} (porphyrins) with alkenes,⁹ which suggests that for Ru system hydrogen atom abstraction reactions can compete with aziridination reaction.



Scheme 2.12. Reaction of **2** with $\text{PhI}=\text{NTs}$.



Scheme 2.13. Reaction of **2** and PhI=NTs in the presence of styrene.

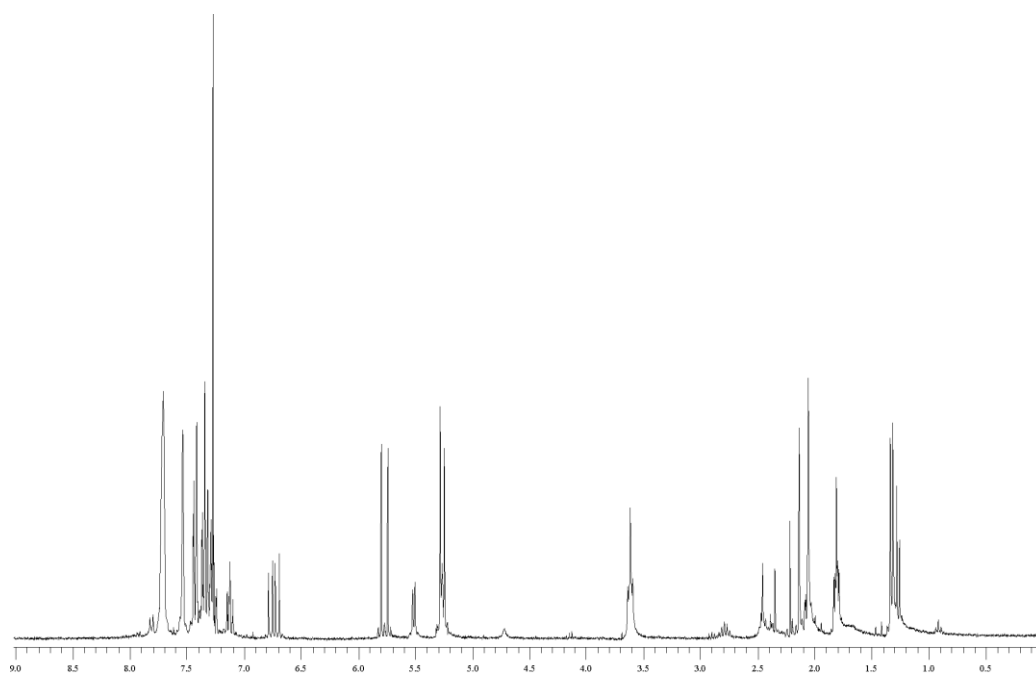
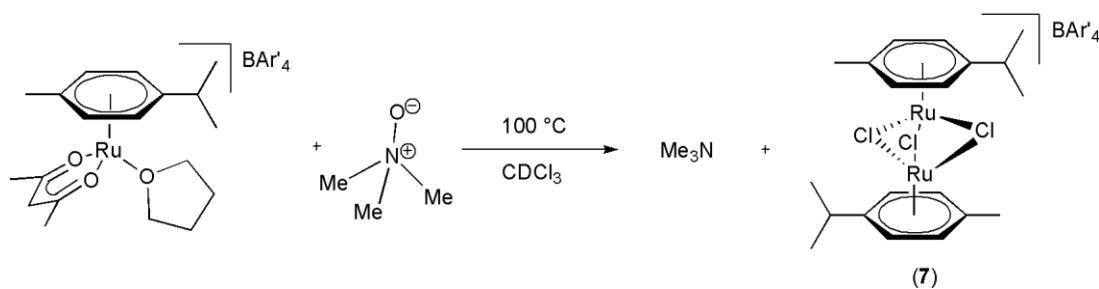


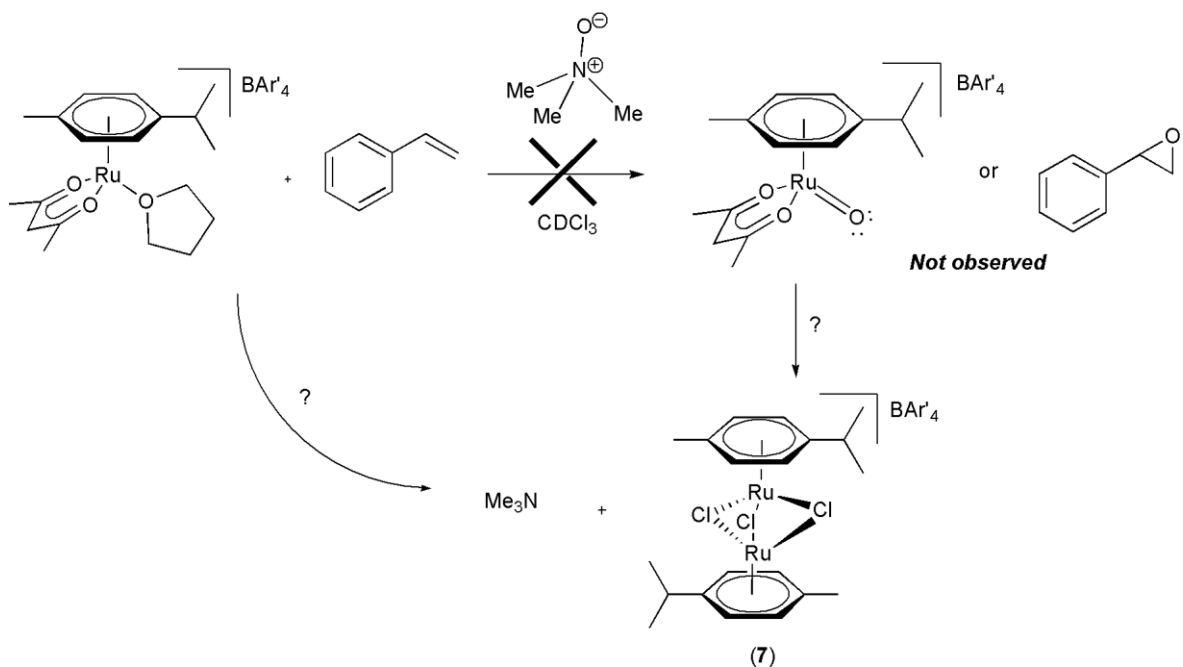
Figure 2.10. ¹H NMR spectrum of reaction of **2** and PhI=NTs in the presence of styrene.

When reacting complex **2** and trimethylamine-*N*-oxide, no evidence of a Ru(IV) oxo species was observed. Although trimethylamine was released at room temperature, the ¹H

NMR spectrum does not reveal conversion of complex **2**. As the reaction is heated at 80 °C, the production of trimethylamine increases, and complex **2** is converted to binuclear complex **7** (Scheme 2.14). Complex **7** is also formed in the absence of Me₃NO (see below), which suggests that trimethylamine-*N*-oxide does not likely react with complex **2** (Scheme 2.15). Furthermore, attempted reaction of **2** with Me₃NO in the presence of styrene does not produce styrene oxide.



Scheme 2.14. Reaction of **2** with trimethylamine-*N*-oxide.



Scheme 2.15. Reaction of **2** and trimethylamine-*N*-oxide with presence of styrene.

2.3.2 Reactivity of $[(\eta^6\text{-}p\text{-cymene})\text{Ru}(\kappa^2\text{-}O,O\text{-acac})(\text{THF})][\text{BAr}'_4]$ with *p*-tolyl-azide

Upon addition of *p*-tolylazide to a CH_2Cl_2 solution of $[(\eta^6\text{-}p\text{-cymene})\text{Ru}(\kappa^2\text{-}O,O\text{-acac})(\text{THF})][\text{BAr}'_4]$ (**2**), a new set of resonances appear along with the disappearance of resonances due to starting material. This new complex is likely the ligand exchange product $[(\eta^6\text{-}p\text{-cymene})\text{Ru}(\kappa^2\text{-}O,O\text{-acac})(\text{N}_3\text{Ar})][\text{BAr}'_4]$ (**6**) ($\text{Ar} = p\text{-tolyl}$) (Scheme 2.11). Interestingly, new $\eta^6\text{-arene}$ C-H peaks appear 1:2:1 ratio at 5.82, 5.51 and 5.13 ppm, which presents an asymmetric character in chloroform solution while every the other peak shows mirror symmetry. The chemical shift of the acac-C-H moiety of **6** in CDCl_3 is 6.04 ppm, which is the most deshielded among complexes **1**, **2**, **3**, **4** and **6**. Also, The ^{19}F NMR spectrum of **6** reveals a singlet at -62.8 ppm. The ^1H NMR spectrum is consistent with **6** as shown in Figure 2.11. After addition of styrene to **6**, there is no observation of *N*-(4-*N*-methylphenyl)-2-phenylaziridine resonances in the ^1H NMR spectrum. Also, **6** decomposes to **7** (the same decomposition product of **2** in CDCl_3 at 100°C) upon heating at 80°C in CDCl_3 with and without styrene.

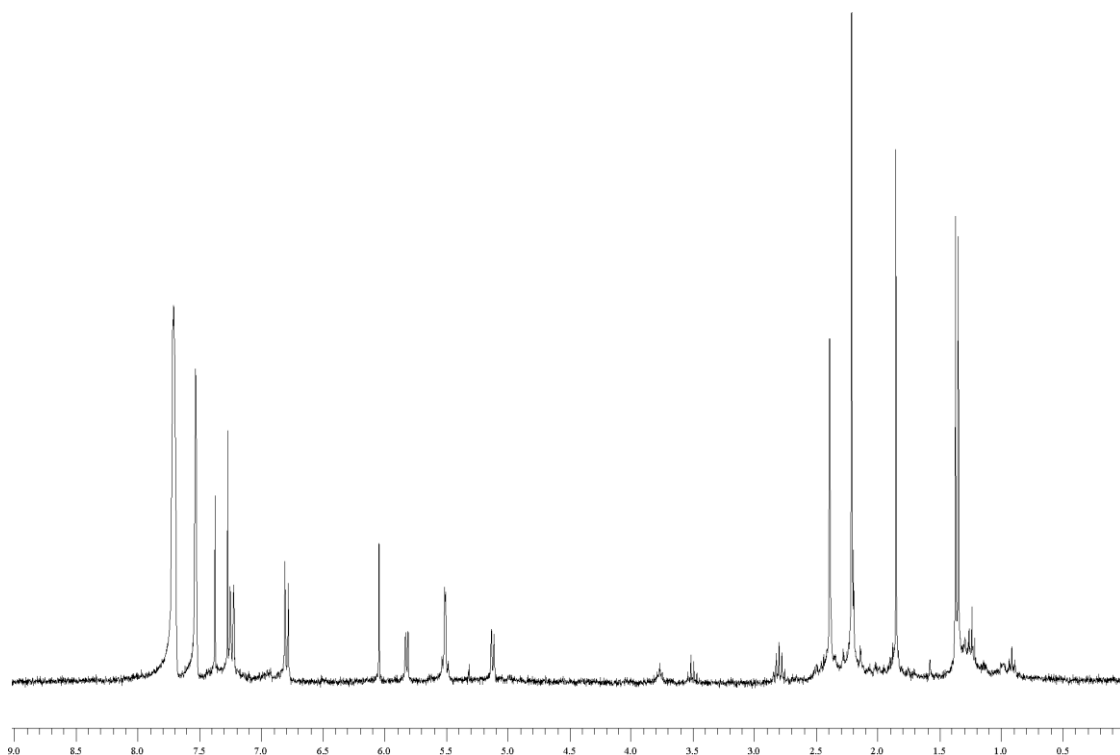
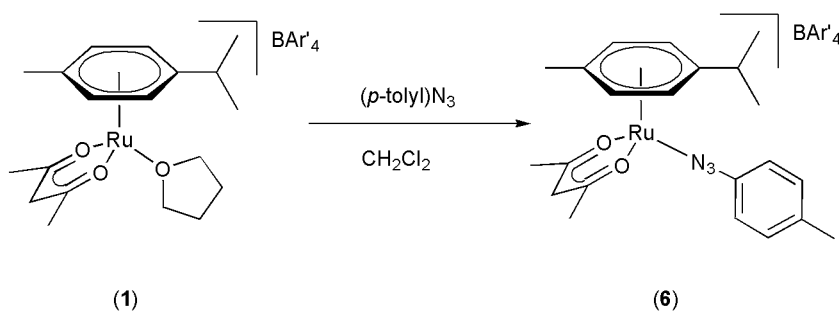


Figure 2.11. ^1H NMR spectrum of $[(\eta^6\text{-}p\text{-cymene})\text{Ru}(\kappa^2\text{-}O,O\text{-acac})(\text{N}_3\text{Ar})][\text{BAR}'_4]$ (**6**) in CDCl_3 .



Scheme 2.16. Ligand exchange of THF with *p*-tolyl-azide.

2.3.3 Hydrogenation Catalysis

Since the THF ligand of $[(\eta^6\text{-}p\text{-cymene})\text{Ru}(\kappa^2\text{-}O,O\text{-acac})(\text{THF})][\text{BAR}'_4]$ (**2**) is labile, we suspected that complex **2** might serve as a catalyst precursor. In order to test the ability

of **2** to coordinate and activate substrates, we chose two reactions with substantial precedent: olefin aziridination and olefin hydrogenation. For the former, complex **2** shows no activity. For example, a CDCl₃ solution of PhINTs, styrene and 5 mol % of **2** results in no production of aziridine reaction after 48 hours at room temperature. At this time, complex **2** is observed to decompose to multiple uncharacterized complexes. In contrast, a solution of styrene and 5 mol % **2** in CDCl₃ under 30 psi of dihydrogen results in the formation of ethylbenzene (eq 9). Monitoring the reaction at 60 °C reveals 31% yield of ethylbenzene after 36 hours. At this time, ¹H NMR spectroscopy reveals decomposition of **2** into multiple products, and prolonged reaction times do not result in additional production of ethylbenzene.

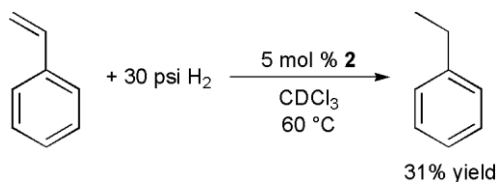
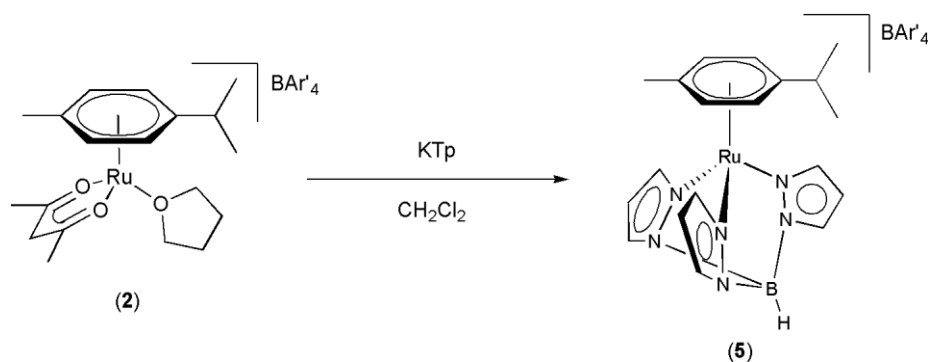


Chart 3. Hydrogenation of ethyl benzene catalyzed by complex **2**.

2.4 Synthesis and characterization of [TpRu(η⁶-*p*-cymene)][BAR'₄]

Thinking that the formally anionic and six-electron donating ligand Tp {Tp = hydridotris(pyrazolyl)borate} might displace the *p*-cymene ligand to form charge neutral TpRu(κ²-*O,O*-acac)L systems, we reacted **2** with KTp. Instead of Tp/*p*-cymene exchange, the reaction of [(η⁶-*p*-cymene)Ru(κ²-*O,O*-acac)(THF)][BAR'₄] (**2**) with KTp results in the displacement of the anionic acac ligand and THF to produce [TpRu(η⁶-*p*-cymene)][BAR'₄] (**5**) (Scheme 2.17). In the downfield region of the ¹H NMR spectrum of **5**, there are three resonances due to the Tp ligand, which is consistent with the presence of a molecular C₃ axis

of rotation (Figure 2.12). The ^{13}C NMR spectrum is also consistent with the complex **5** due to presence of only three resonances corresponding to Tp carbons (Figure 2.13). A single crystal X-ray diffraction study of **5** confirmed its identity (Figure 2.14). Bond distances and angles are presented in Table 2.3 with data collection and structure solution parameters given in Table 2.2. The *p*-cymene ligand is asymmetrically coordinated to Ru with Ru-C_{arene} bond lengths of the C-substituted aromatic positions {2.236(3) and 2.236(4) Å} that are longer than the Ru-C_{arene} bond distances of unsubstituted positions (average Ru-C_{arene} bond distance of unsubstituted positions = 2.181(3) Å), which likely reflects a steric influence.



Scheme 2.17. Reaction of **2** with KTp.

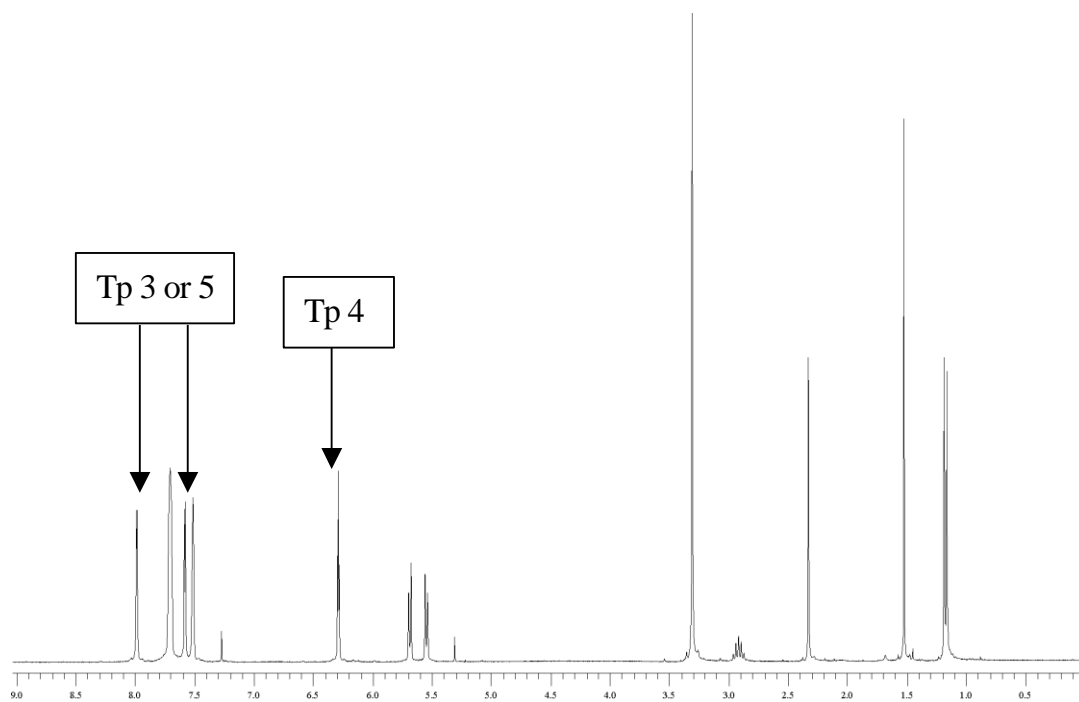


Figure 2.12. ^1H NMR of $[\text{TpRu}(\eta^6\text{-}p\text{-cymene})][\text{BAR}'_4]$ (**5**).

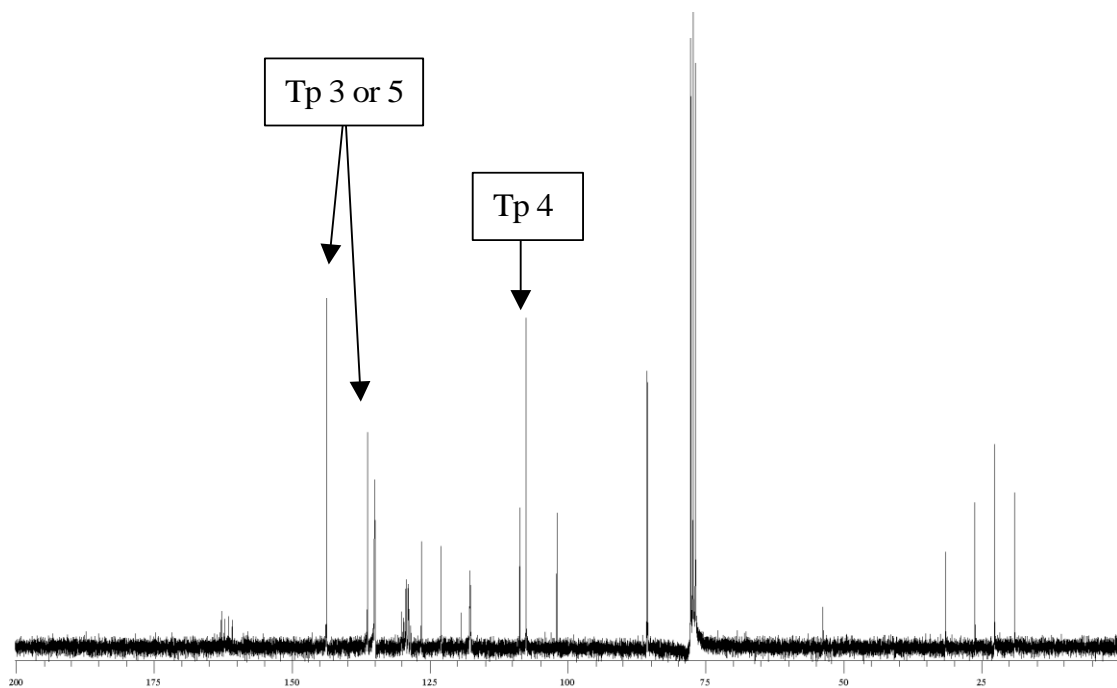


Figure 2.13. ^{13}C NMR of $[\text{TpRu}(\eta^6\text{-}p\text{-cymene})][\text{BAR}'_4]$ (**5**).

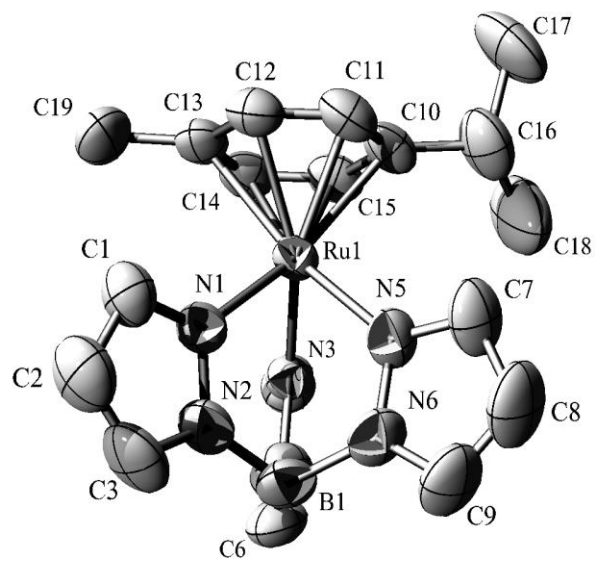


Figure 2.14. ORTEP (30% probability) of [TpRu(η⁶-p-cymene)][BAr'₄] (5).

Table 2.3. Selected bond distances (Å) and angles (°) for [TpRu(η^6 -*p*-cymene)][BAR'₄] (**5**).

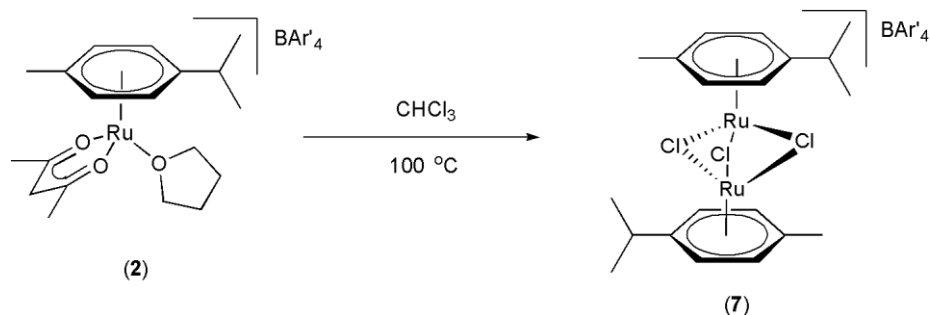
<i>Bond length</i> (Å)			
Ru(1)-N(3)	2.096(3)	Ru(1)-C(13)	2.236(4)
Ru(1)-N(1)	2.103(2)	C(10)-C(15)	1.397(5)
Ru(1)-N(5)	2.106(3)	C(10)-C(11)	1.429(5)
Ru(1)-Cent ^a	1.694	C(10)-C(16)	1.494(6)
Ru(1)-C(15)	2.174(3)	C(11)-C(12)	1.371(5)
Ru(1)-C(14)	2.182(3)	C(12)-C(13)	1.416(5)
Ru(1)-C(12)	2.183(3)	C(13)-C(14)	1.408(5)
Ru(1)-C(11)	2.185(3)	C(13)-C(19)	1.491(5)
Ru(1)-C(10)	2.236(3)	C(14)-C(15)	1.398(5)
<i>Bond angles</i> (°)			
N(1)-Ru(1)-Cent ^a	129.0	N(1)-Ru(1)-N(5)	81.9(1)
N(3)-Ru(1)-Cent ^a	127.1	N(2)-N(1)-Ru(1)	120.9(2)
N(5)-Ru(1)-Cent ^a	131.5	N(2)-B(1)-N(4)	108.6(3)
N(3)-Ru(1)-N(1)	86.7(1)	N(2)-B(1)-N(6)	107.1(3)
N(3)-Ru(1)-N(5)	84.3(1)	N(6)-B(1)-N(4)	106.8(3)

^aCent corresponds to the centroid of the six-membered ring of the *p*-cymene molecule.

2.5 Reaction of [(η^6 -*p*-cymene)Ru(κ^2 -*O,O*-acac)(THF)][BAR'₄] in Chloroform and Methylene Chloride

Heating (100 °C) complex **2** in CHCl₃ or CH₂Cl₂ forms the binuclear complex {[(η^6 -*p*-cymene)₂Ru]₂(μ -Cl)₃}[BAR'₄] (**7**) (Scheme 2.18). Qualitatively, the rate of the formation of **7** is faster in CHCl₃ than CH₂Cl₂. According to the integration of the ¹H NMR spectrum, a tri-bridged binuclear complex with one BAR'₄ anion is most consistent with the spectrum (Figure 2.15). In addition, a single crystal X-ray diffraction study of **7** confirmed its identity (Figure 2.16). Bond distances and angles are presented in Table 2.4 with data collection and structure solution parameters given in Table 2.2. The average bond distance from Ru to arene carbon is 2.167(2) Å, which is the closest contact among the complexes **1**, **5** and **7**. The steric

effect can be expected due to the less sterically bulky chloride ligand. Although the Ru-C_{arene} bond distance of the C-substituted positions, are noticeably longer than the average distance of Ru-C_{arene} of unsubstituted positions {2.160(2) Å}, those bond differences are not as large as in **1** or **5**. This observation supports the steric argument for such a close interaction of Ru and arene ligand.



Scheme 2.18. Product of **2** in CHCl₃ in at 100 °C.

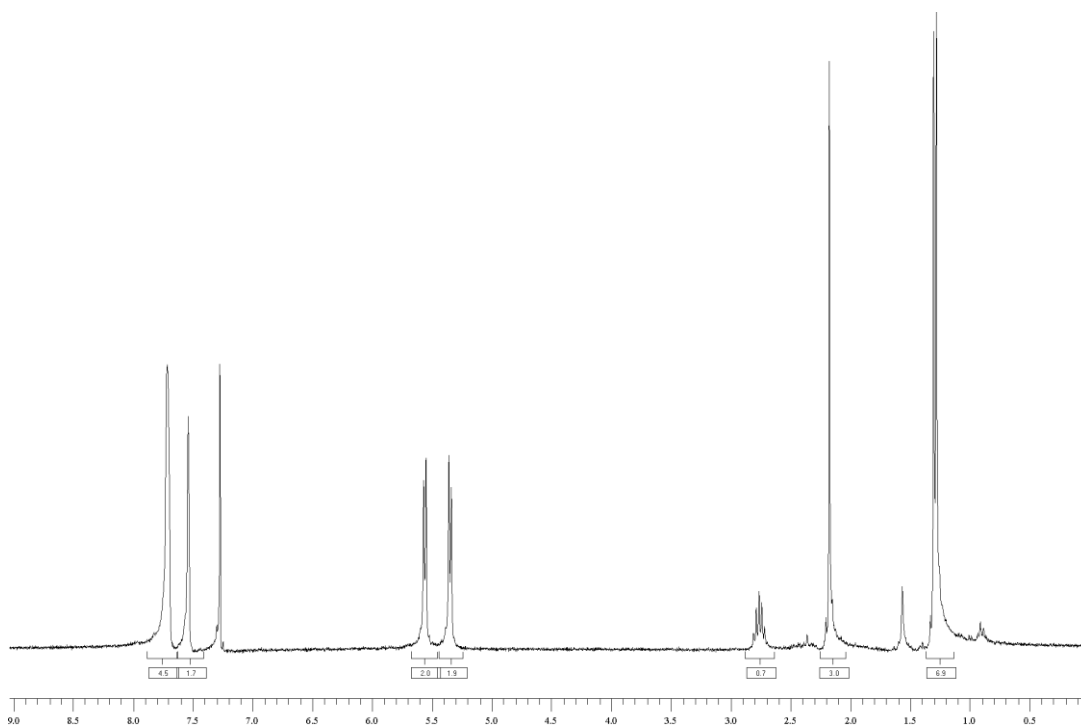


Figure 2.15. ¹H NMR of {[(η⁶-*p*-cymene)₂Ru]₂(μ-Cl)₃}[BAR'₄] (**7**).

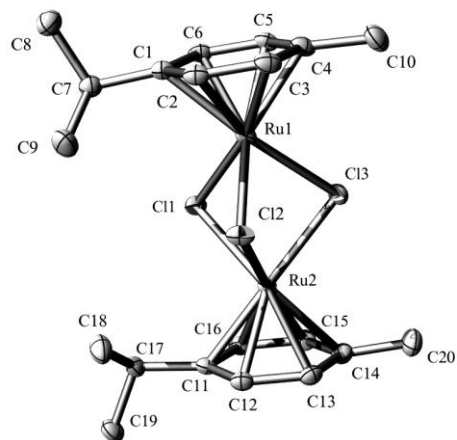


Figure 2.16. ORTEP (50% probability) of $[(\eta^6\text{-}p\text{-cymene})_2\text{Ru}]_2(\mu\text{-Cl})_3[\text{BAr}'_4]$ (**7**).

Table 2.4. Selected bond distances (Å) and angles (°) for $\{[(\eta^6\text{-}p\text{-cymene})_2\text{Ru}]_2(\mu\text{-Cl})_3\}[\text{BAR}'_4]$ (**7**).

<i>Bond length (Å)</i>			
Ru(1)-C(1)	2.178(2)	Ru(2)-C(11)	2.172(2)
Ru(1)-C(2)	2.153(2)	Ru(2)-C(12)	2.152(2)
Ru(1)-C(3)	2.160(2)	Ru(2)-C(13)	2.162(2)
Ru(1)-C(4)	2.181(2)	Ru(2)-C(14)	2.186(2)
Ru(1)-C(5)	2.170(2)	Ru(2)-C(15)	2.169(2)
Ru(1)-C(6)	2.159(2)	Ru(2)-C(16)	2.151(2)
Ru(1)-C(11)	2.4320(4)	Ru(1)-C(11)	2.4380(4)
Ru(1)-C(12)	2.4185(4)	Ru(1)-C(12)	2.4217(4)
Ru(1)-C(13)	2.4502(4)	Ru(1)-C(13)	2.4497(4)
<i>Bond angles (°)</i>			
C(1)-Ru(1)-Cl(1)	96.94(4)	C(9)-C(7)-C(8)	111.0(2)
C(1)-Ru(1)-Cl(2)	112.64(4)	C(1)-C(7)-C(9)	113.6(2)
C(1)-Ru(1)-Cl(3)	166.70(4)	C(1)-C(7)-C(8)	108.9(1)
C(4)-Ru(1)-Cl(3)	93.71(5)	C(3)-C(4)-C(10)	120.9(2)
C(4)-Ru(1)-Cl(2)	126.60(5)	C(11)-Ru(2)-Cl(1)	96.98(4)
C(4)-Ru(1)-Cl(1)	150.20(5)	C(12)-Ru(2)-Cl(1)	127.15(5)
C(7)-C(1)-Ru(1)	128.5(1)	C(13)-Ru(2)-Cl(1)	165.56(5)
C(10)-C(4)-Ru(1)	128.1(1)	C(14)-Ru(2)-Cl(1)	149.30(5)
Ru(1)-Cl(1)-Ru(2)	84.12(1)	C(15)-Ru(2)-Cl(2)	165.98(5)
Ru(1)-Cl(2)-Ru(2)	84.76(1)	C(16)-Ru(2)-Cl(1)	91.70(5)
Ru(2)-Cl(3)-Ru(1)	83.49(1)	Cl(2)-Ru(2)-Cl(3)	79.60(1)

2.6 Electrochemistry

The combination of the "soft" donor (η^6 -arene) and "hard" oxygen donor acac ligands sets up an interesting electronic mix. In order to probe the electron density of the new Ru systems, we performed cyclic voltammetry experiments. Table 5 displays a list of complexes and observed redox potentials.

Table 2.5. The redox potentials for the various Ru(II) complexes

<u>Complex</u>	<u>Ru(II/I)^{a,b}</u>
$[(\eta^6\text{-}p\text{-cymene})\text{Ru}(\kappa^2\text{-}O, O\text{-acac})\{\text{N}_3(p\text{-tolyl})\}][\text{BAr}'_4]$ (6)	-0.50 V
$[(\eta^6\text{-}p\text{-cymene})\text{Ru}(\kappa^2\text{-}O, O\text{-acac})(\text{THF})][\text{BAr}'_4]$ (2)	-0.78 V
$\{[(\eta^6\text{-}p\text{-cymene})_2\text{Ru}]_2(\mu\text{-Cl})_3\}[\text{BAr}'_4]$ (7)	-0.92 V
$[(\eta^6\text{-}p\text{-cymene})\text{Ru}(\kappa^2\text{-}O, O\text{-acac})\text{OTf}]$ (1-OTf)	-1.13 V
$[(\eta^6\text{-}p\text{-cymene})\text{Ru}(\kappa^2\text{-}O, O\text{-acac})(\text{NCMe})][\text{BAr}'_4]$ (3)	-1.24 V
$[\text{TpRu}(\eta^6\text{-}p\text{-cymene})][\text{BAr}'_4]$ (5)	-1.45 V
$[(\eta^6\text{-}p\text{-cymene})\text{Ru}(\kappa^2\text{-}O, O\text{-acac})(\text{PMe}_3)][\text{BAr}'_4]$ (4)	-1.63 V

^a Reported versus NHE. ^b All potentials are irreversible ($E_{p,a}$) except for complex **2**, which is reversible ($E_{1/2}$).

For all complexes, scans to positive potentials (2.0 V versus NHE) revealed no redox activity. Thus, the combination of the η^6 -arene and acac or Tp ligands and overall cationic charge results in electron-deficient Ru(II) systems, which suggests that such complexes might be strongly Lewis acidic. In contrast, scans at negative potentials (vs. NHE) result in reduction of the Ru complexes, which is consistent with Ru(II) to Ru(I) transformations. With the exception of complex **2**, the reductions are irreversible. The order of the absolute value of the reduction potentials for complexes of the general formula $[(\eta^6\text{-}p\text{-cymene})\text{Ru}(\kappa^2\text{-}O, O\text{-acac})(\text{L})][\text{BAr}'_4]$, **6** < **2** < **1** < **3** < **4**, suggests that the relative donating ability of the ligands (from most donating to least donating) is: $\text{PMe}_3 > \text{NCMe} > \mu\text{-CH/OTf} > \text{THF} > \text{N}_3(p\text{-tolyl})$. The more negative reduction potential of complex **1** relative to **2** is consistent with the lack of coordination of THF upon dissolution of **1** in THF. The Ru(II/I) reduction potentials suggest that the $\mu\text{-Cl}_3$ moiety is more strongly donating than the combination of

the κ^2 -acac ligand and THF, but more weakly donating than the κ^2 -acac ligand in combination with NCMe or PMe₃.

2.7 Summary

Synthesis, characterization and some structural studies for various complexes consisting of η^6 -*p*-cymene and κ^2 -acac ligands were done, and the complexes $[(\eta^6$ -*p*-cymene)Ru(κ^2 -*O,O*-acac- μ -CH)]₂[OTf]₂ (**1**) and $[(\eta^6$ -*p*-cymene)Ru(κ^2 -*O,O*-acac)(THF)][BAR'₄] (**2**) allow access to the cationic fragment $[(\eta^6$ -*p*-cymene)Ru(κ^2 -*O,O*-acac)]⁺. However, electrochemistry experiments suggest that the η^6 -*p*-cymene/ κ^2 -*O,O*-acac fragment is overall poorly donating, which results in relatively electron-deficient complexes that might possess substantial Lewis acidity. Hence, neither complex **1** nor **2** undergo formation of Ru(IV) imido or oxo complexes, which are more electron deficient systems.

The a few nitrene and oxo sources such as N₃(*p*-tolyl), PhI=NTs and trimethylamine-*N*-oxide were reacted with complex **1** and **2** to attempt synthesis of ruthenium^{IV} imido or oxo complexes. However, we could not observe direct or indirect evidences for formation of those complexes. For example, there are no observations of aziridination or epoxidation products as indirect evidence when complex **1** or **2** combine with nitrene or oxo source in CDCl₃ with presence of styrene.

2.8 Experimental procedures

Unless otherwise noted, all synthetic procedures were performed under anaerobic conditions in a nitrogen-filled glovebox or using standard Schlenk techniques. Glovebox

purity was maintained by periodic nitrogen purges and was monitored by an oxygen analyzer ($O_2 < 15$ ppm for all reactions in glovebox). Benzene, tetrahydrofuran and diethyl ether (stored over 4 Å molecular sieves) were dried by distillation from sodium/benzophenone. Pentane was distilled over sodium. Acetonitrile and methanol were dried by distillation from CaH_2 . Hexanes, toluene (stored over 4 Å molecular sieves) and methylene chloride were purified by passage through a column of activated alumina. Benzene- d_6 , acetonitrile- d_3 , and chloroform- d_1 were degassed using three freeze-pump-thaw cycles and stored under a nitrogen atmosphere over 4 Å molecular sieves. 1H NMR spectra were recorded on a Varian Mercury 300 or 400 MHz spectrometer, and ^{13}C NMR spectra (operating frequency 75 MHz) were recorded on a Varian Mercury 300 MHz spectrometer. All 1H and ^{13}C NMR spectra are referenced against residual proton signals (1H NMR) or the ^{13}C resonances of the deuterated solvent (^{13}C NMR). ^{19}F NMR spectra were obtained on a Varian 300 MHz spectrometer (operating frequency 282 MHz) and referenced against an external standard of hexafluorobenzene ($\delta = -164.9$). Electrochemical experiments were performed under a nitrogen atmosphere using a BAS Epsilon Potentiostat. Cyclic voltammograms were recorded in a standard three-electrode cell from -2.00 V to +2.00 V with a glassy carbon working electrode and tetrabutylammonium hexafluorophosphate (TBAH) as electrolyte. Tetrabutylammonium hexafluorophosphate was dried under dynamic vacuum at 140 °C for 48 hours prior to use. All potentials are reported versus NHE (normal hydrogen electrode) using cobaltocenium hexafluorophosphate as an internal standard. The preparation, isolation and characterization of KTp, $(\eta^6\text{-}p\text{-cymene})Ru(\kappa^2\text{-}O,O\text{-acac})Cl$ and $NaBAr'_4$ $\{Ar' = 3,5\text{-}$

(CF₃)-C₆H₃} have been previously reported.^{19, 21, 72, 73} Elemental analyses were performed by Atlantic Microlabs, Inc.

Synthesis of $[(\eta^6\text{-}p\text{-cymene})\text{Ru}(\text{O},\text{O}\text{-acac}\text{-}\mu\text{-CH})_2][\text{OTf}]_2$ (1). ($\eta^6\text{-}p\text{-cymene})\text{Ru}(\text{acac})\text{Cl}$ (0.765 g, 2.07 mmol) was dissolved in 40 mL of THF. Upon addition of AgOTf (0.584 g, 2.27 mmol) a white precipitate (presumably AgCl) formed. The solution was stirred for 30 minutes at room temperature, after which time it was filtered through a plug of Celite. The filtrate was concentrated to approximately 10 mL in vacuo, and hexanes (approximately 40 mL) were added to yield a precipitate. The product was collected via vacuum filtration through a fine porosity frit to give an orange solid (0.919 g, 92% yield). ¹H NMR (CDCl₃, δ): 5.64 (2H, d, ³J_{HH} = 6 Hz, *p*-cymene aromatic CH), 5.42 (2H, d, ³J_{HH} = 6 Hz, *p*-cymene aromatic CH), 5.17 (1H, s, acac- μ -CH), 2.97 (1H, sept, ³J_{HH} = 7 Hz, CH(CH₃)₂), 2.31 (3H, s, *p*-cymene Ar-CH₃), 2.05 (6H, s, acac-CH₃), 1.39 (6H, d, ³J_{HH} = 7 Hz, CH(CH₃)₂). ¹³C{¹H} NMR (CDCl₃, δ): 187.5 (s, acac C-O), 119.4 (q, ¹J_{CF} = 319 Hz, SO₃CF₃), 100.3 (s, acac C-H), 97.5 and 97.1 (each a s, *p*-cymene 1,4-positions), 80.5 and 78.3 (each a s, *p*-cymene 2,3-positions), 31.2 (s, *p*-cymene CH(Me)₂), 27.2 (s, *p*-cymene methyl), 22.5 (s, acac CH₃), 17.9 (s, *p*-cymene CH(CH₃)₂). ¹⁹F{¹H} NMR (CDCl₃, δ): -78.0 (s, SO₃CF₃). CV (THF, 100 mV/s, TBAH): E_{p,a} = -1.13 V, Ru(II/I). Anal. Calc. for C₃₂H₄₂Ru₂F₆O₁₀S₂: C, 39.67; H, 4.37, O; 16.52. Found: C, 39.10; H, 4.50, O; 16.58.

Synthesis of $[(\eta^6\text{-}p\text{-cymene})\text{Ru}(\kappa^2\text{-O},\text{O}\text{-acac})(\text{THF})][\text{BAr}'_4]$ (2). ($\eta^6\text{-}p\text{-cymene})\text{Ru}(\text{O},\text{O}\text{-acac}\text{-}\mu\text{-CH})_2[\text{OTf}]_2$ (1) (1.30 g, 2.7 mmol) was dissolved in 40 mL of THF. NaBAr'₄ (4.79 g, 5.4 mmol) was added to the solution, and the resulting mixture was stirred for 12 hours. The volatiles were removed in vacuo, the residual material was dissolved in

approximately 20 mL of CH₂Cl₂, and the solution was filtered through a plug of Celite. The filtrate volume was reduced to approximately 10 mL in vacuo, and hexanes (approximately 40 mL) were added to form a precipitate. The product was collected via vacuum filtration through a fine porosity frit to give an orange solid (2.26 g, 66% yield). ¹H NMR (CDCl₃, δ): 7.71 (8H, br s, ortho BAr'₄), 7.54 (4H, br s, para BAr'₄), 5.50 (2H, d, ³J_{HH} = 6 Hz, *p*-cymene aromatic CH), 5.27 (2H, d, ³J_{HH} = 6 Hz, *p*-cymene aromatic CH), 5.27 (1H, s, acac-CH), 3.49 (4H, m, α-THF), 2.79 (1H, sept, ³J_{HH} = 7 Hz, CH(CH₃)₂), 2.15 (3H, s, *p*-cymene CH₃), 2.06 (6H, s, acac CH₃), 1.74 (4H, m, β-THF), 1.32 (6H, d, ³J_{HH} = 7 Hz, *p*-cymene CH(CH₃)₂). ¹³C{¹H} NMR (CDCl₃, δ): 188.3 (s, acac C-O), 161.8 (1,1,1,1 quartet, ¹J_{CB} = 51 Hz, ipso C of BAr'₄), 134.9 (s, para-C of BAr'₄), 129.1 (q, ²J_{CF} = 29 Hz, meta-C of BAr'₄), 127.5 (q, ¹J_{CF} = 272 Hz, CF₃ of BAr'₄), 117.6 (s, ortho-C of BAr'₄), 101.0, 98.9, 98.2, 80.4, 78.7 (all s, *p*-cymene aromatic and acac C-O), 70.9 (s, α-C of THF), 31.3 (s, CH(CH₃)₂), 27.2 (s, acac methyl), 25.5 (s, β-C of THF), 22.2 (s, *p*-cymene CH₃), 17.7 (s, *p*-cymene CH(CH₃)₂). ¹⁹F{¹H} NMR (CDCl₃, δ): -62.8 (s, BAr'₄). CV (THF, TBAH, 100 mV/s): E_{1/2} = -0.78 V, Ru(II/I). Anal. Calc. for C₅₁H₄₁RuF₂₄BO₃: C, 48.24; H, 3.25. Found: C, 47.87; H, 3.29.

Synthesis of [(η⁶-*p*-cymene)Ru(κ²-*O,O*-acac)(NCMe)][BAr'₄] (3). [(η⁶-*p*-cymene)Ru(κ²-*O,O*-acac)(THF)][BAr'₄] (2) (0.53 g, 0.42 mmol) was dissolved in 40 mL of NCMe, and the solution was stirred for approximately 10 minutes. The volatiles were removed in vacuo, and the residual material was dissolved in approximately 5 mL of CH₂Cl₂. The addition of hexanes (approximately 40 mL) afforded a precipitate. The solid was collected via vacuum filtration through a fine porosity frit to give an orange solid (0.46 g, 88% yield). ¹H NMR (CDCl₃, δ): 7.71 (8H, br s, ortho BAr'₄), 7.54 (4H, br s, para BAr'₄),

5.52 (2H, d, $^3J_{\text{HH}} = 6$ Hz, *p*-cymene Ar-CH), 5.21 (1H, s, acac-CH), 5.21 (2H, d, $^3J_{\text{HH}} = 5$ Hz, *p*-cymene Ar-CH), 2.75 (1H, sept, $^3J_{\text{HH}} = 7$ Hz, $\text{CH}(\text{CH}_3)_2$), 2.18 (3H, s, NCCH_3), 2.11 (3H, s, *p*-cymene CH_3), 1.98 (6H, s, acac CH_3), 1.28 (6H, d, $^3J_{\text{HH}} = 7$ Hz, *p*-cymene $\text{CH}(\text{CH}_3)_2$). $^{13}\text{C}\{^1\text{H}\}$ NMR (CDCl_3 , δ): 188.1 (s, acac C-O), 161.9 (1,1,1,1 quartet, $^1J_{\text{CB}} = 50$ Hz, ipso C of BAr'_4), 135.0 (s, para-C of BAr'_4), 129.1 (q, $^2J_{\text{CF}} = 34$ Hz, meta-C of BAr'_4), 124.8 (q, $^1J_{\text{CF}} = 273$ Hz, CF_3 of BAr'_4), 122.7 (s, NCCH_3), 117.7 (s, ortho-C of BAr'_4), 103.0, 100.7, 99.2, 84.4, 80.4 (all s, *p*-cymene aromatic and acac C-O), 31.1 (s, $\text{CH}(\text{CH}_3)_2$), 27.1 (s, acac methyl), 22.1 (s, *p*-cymene CH_3), 17.6 (s, *p*-cymene $\text{CH}(\text{CH}_3)_2$), 3.0 (s, NCCH_3). $^{19}\text{F}\{^1\text{H}\}$ NMR (CDCl_3 , δ): -58.8 (s, BAr'_4). CV (NCMe, TBAH, 100mV/s): $E_{\text{p,a}} = -1.24$ V, Ru(II/I). Anal. Calc. for $\text{C}_{49}\text{H}_{36}\text{BF}_2\text{NO}_3\text{Ru}$: C, 47.45; H, 2.93; N, 1.13. Found: C, 47.44; H, 2.92; N, 1.12.

Synthesis of $[(\eta^6\text{-}i\text{-p-cymene})\text{Ru}(\kappa^2\text{-}O,O\text{-acac})(\text{PMe}_3)][\text{BAr}'_4]$ (4). $[(\eta^6\text{-}i\text{-p-cymene})\text{Ru}(\kappa^2\text{-}O,O\text{-acac})(\text{THF})][\text{BAr}'_4]$ (2) (0.52 g, 0.41 mmol) was dissolved in 40 mL of dichloromethane. Trimethylphosphine (0.03 g, 0.45 mmol) was added to the solution, and the resulting mixture was stirred for 5 minutes. The solution volume was reduced to approximately 5 mL in vacuo, and hexanes (approximately 40 mL) were added to form a precipitate. The product was collected via vacuum filtration through a fine porosity frit to give a yellow solid (0.46 g, 88% yield). ^1H NMR (CDCl_3 , δ): 7.71 (8H, br s, ortho BAr'_4), 7.54 (4H, br s, para BAr'_4), 5.50 (2H, d, $^3J_{\text{HH}} = 6$ Hz, *p*-cymene aromatic C-H), 5.38 (2H, d, $^3J_{\text{HH}} = 5$ Hz, *p*-cymene aromatic C-H), 5.38 (1H, s, acac-CH), 2.47 (1H, sept, $^3J_{\text{HH}} = 7$ Hz, $\text{CH}(\text{CH}_3)_2$), 1.93 (6H, s, acac CH_3), 1.84 (3H, s, *p*-cymene CH_3), 1.28 (9H, d, $^2J_{\text{PH}} = 12$ Hz, $\text{P}(\text{CH}_3)_3$), 1.18 (6H, d, $^3J_{\text{HH}} = 7$ Hz, *p*-cymene $\text{CH}(\text{CH}_3)_2$). $^{13}\text{C}\{^1\text{H}\}$ NMR (CDCl_3 , δ): 189.8

(s, acac C-O), 161.9 (1,1,1,1 quartet, $^1J_{CB} = 50$ Hz, ipso C of BAr'₄), 135.0 (s, para-C of BAr'₄), 129.1 (q, $^2J_{CF} = 31$ Hz, meta-C of BAr'₄), 124.8 (q, $^1J_{CF} = 273$ Hz, CF₃ of BAr'₄), 117.7 (s, ortho-C of BAr'₄), 105.0, 101.8, 96.6, 89.2, 87.8 (all s, *p*-cymene aromatic and acac C-O), 30.7 (s, CH(CH₃)₂), 27.2 (s, acac methyl), 21.8 (s, *p*-cymene CH₃), 16.7 (s, *p*-cymene CH(CH₃)₂), 14.3 (d, $^1J_{CP} = 31$ Hz, P(CH₃)₃). $^{19}\text{F}\{^1\text{H}\}$ NMR (CDCl₃, δ): -58.8 (s, BAr'₄). CV (THF, TBAH, 100 mV/s): E_{p,a} = -1.63 V, Ru(II/I). Anal. Calc. for C₅₀H₄₂BF₂₄O₂PRu: C, 47.09; H, 3.32; O, 2.51. Found: C, 46.79; H, 3.29; O, 2.70.

Synthesis of [TpRu(η^6 -*p*-cymene)][BAr'₄] (5). [(η^6 -*p*-cymene)Ru(κ^2 -*O,O*-acac)(THF)][BAr'₄] (2) (0.130 g, 0.102 mmol) was dissolved in 40 mL of dichloromethane, and KTp (0.0373 g, 0.153 mmol) was added to the solution. The mixture was stirred for approximately 12 hours. The solution was filtered through a plug of Celite, and the filtrate was concentrated to approximately 10 mL under reduced pressure. Upon addition of hexanes (approximately 40 mL), a red precipitate formed. The solid was collected via vacuum filtration through a fine porosity frit to give red solid (0.53 g, 45% yield). ^1H NMR (CDCl₃, δ): 7.99 (3H, d, $^3J_{\text{HH}} = 2$ Hz, Tp 3 or 5 position), 7.70 (8H, br s, BAr'₄ ortho), 7.56 (3H, d, $^3J_{\text{HH}} = 2$ Hz, Tp 3 or 5 position), 7.51 (4H, br s, BAr'₄ para), 6.29 (3H, t, $^3J_{\text{HH}} = 2$ Hz, Tp 4 position), 5.68 (2H, d, $^3J_{\text{HH}} = 6$ Hz, *p*-cymene aromatic C-H), 5.55 (2H, d, $^3J_{\text{HH}} = 6$ Hz, *p*-cymene aromatic C-H), 2.92 (1H, sept, $^3J_{\text{HH}} = 7$ Hz, CH(CH₃)₂), 2.33 (3H, s, *p*-cymene CH₃), 1.17 (6H, d, $^3J_{\text{HH}} = 7$ Hz, *p*-cymene CH(CH₃)₂). $^{13}\text{C}\{^1\text{H}\}$ NMR (CDCl₃, δ): 161.8 (1,1,1,1 quartet, $^1J_{CB} = 50$ Hz, ipso C of BAr'₄), 143.7 and 136.3 (each a s, Tp 3,5-position), 135.0 (s, para-C of BAr'₄), 129.0 (q, $^2J_{CF} = 42$ Hz, meta-C of BAr'₄), 124.7 (q, $^1J_{CF} = 272$ Hz, CF₃ of BAr'₄), 117.7 (ortho-C of BAr'₄), 108.7, 107.5, 102.0, 85.7, 85.5 (all s, *p*-cymene aromatic

and Tp 4 position), 31.5 (s, CH(CH₃)₂), 22.7 (s, *p*-cymene CH₃), 19.0 (s, *p*-cymene CH(CH₃)₂). ¹⁹F{¹H} NMR (CDCl₃, δ): -58.8 (s, BAr'₄). CV (THF, TBAH, 100 mV/s): E_{p,a} = -1.45 V, Ru(II/I). Anal. Calc. for C₅₁H₃₆RuB₂F₂₄N₆: C, 46.70; H, 2.77, N, 6.41. Found: C, 46.85; H, 2.94, N, 6.18.

Synthesis of [(η⁶-*p*-cymene)Ru(κ²-*O,O*-acac)(N₃Ar)][BAr'₄] (6). [(η⁶-*p*-cymene)Ru(κ²-*O,O*-acac)(THF)][BAr'₄] (2) (0.334 g, 0.263 mmol) was dissolved in 40 mL of dichloromethane, and *p*-tolylazide (0.052 g, 0.394 mmol) was added to the solution. The mixture was stirred for approximately 1 hour. The solution was filtered through a plug of Celite, and the filtrate was concentrated to approximately 10 mL under reduced pressure. Upon addition of hexanes (approximately 40 mL), a black precipitate formed. The solid was collected via vacuum filtration through a fine porosity frit to give red solid (0.17 g, 49% yield). ¹H NMR (CDCl₃, δ): 7.71 (8H, br s, ortho BAr'₄), 7.53 (4H, br s, para BAr'₄), 7.24 (2H, d, ³J_{HH} = 9 Hz, azide aromatic CH), 6.79 (2H, d, ³J_{HH} = 9 Hz, azide aromatic CH), 6.04 (1H, s, acac-CH), 5.82, 5.51, 5.13 (4H total, 1:2:1 integration, each a each, *p*-cymene aromatic CH), 2.79 (1H, sept, ³J_{HH} = 7 Hz, CH(CH₃)₂), 2.20 (3H, s, *p*-cymene CH₃), 2.18 (3H, s, azide CH₃), 1.85 (6H, s, acac CH₃), 1.35 (6H, d, ³J_{HH} = 7 Hz, *p*-cymene CH(CH₃)₂). ¹³C{¹H} NMR (CDCl₃, δ): 188.1 (s, acac C-O), 161.9 (1:1:1:1 quartet, ¹J_{CB} = 50 Hz, ipso C of BAr'₄), 137.1 (s, ipso C of azide), 135.0 (s, para-C of BAr'₄), 131.5 (s, para C of azide), 129.2 (q, ²J_{CF} = 34 Hz, meta-C of BAr'₄), 128.6 (s, ortho C of azide), 125.0 (s, meta C of azide), 124.8 (q, ¹J_{CF} = 273 Hz, CF₃ of BAr'₄), 117.7 (s, ortho-C of BAr'₄), 86.5, 86.4, 86.2, 83.8, 83.6 (all s, *p*-cymene aromatic and acac C-H), 32.0 (s, CH(CH₃)₂), 24.2 (s, azide CH₃), 23.2 (s, acac CH₃), 22.3 (s, *p*-cymene C-CH₃), 19.2 (s, *p*-cymene CH(CH₃)₂), 3.0 (s,

NCCH₃). ¹⁹F{¹H} NMR (CDCl₃, δ): -62.8 (s, BAr'₄). CV (THF, TBAH, 100 mV/s): E_{p,a} = -0.50 V, Ru(II/I).

Synthesis of $[(\eta^6\text{-}p\text{-cymene})_2\text{Ru}]_2(\mu\text{-Cl})_3[\text{BAr}'_4]$ (7). A thick-walled glass tube was charged with $[(\eta^6\text{-}p\text{-cymene})\text{Ru}(\kappa^2\text{-}O,O\text{-acac})(\text{THF})][\text{BAr}'_4]$ (2) (0.20 g, 0.157 mmol) and 30 mL of CHCl₃. The solution was heated at 100 °C for three weeks. After filtration through a fine porosity frit, the solution was concentrated to approximately 10 mL. Hexanes (approximately 40 mL) were added to form a dark red precipitate. The solid was collected via vacuum filtration through a fine porosity frit to give a dark red solid (0.09 g, 45% yield). ¹H NMR (CDCl₃, δ): 7.71 (8H, br s, BAr'₄ ortho), 7.53 (4H, br s, BAr'₄ para), 5.56 (2H, d, ³J_{HH} = 6 Hz, *p*-cymene aromatic CH), 5.36 (2H, d, ³J_{HH} = 6 Hz, *p*-cymene aromatic CH), 2.76 (1H, sept, ³J_{HH} = 7 Hz, CH(CH₃)₂), 2.18 (3H, s, *p*-cymene CH₃), 1.29 (6H, d, ³J_{HH} = 7 Hz, *p*-cymene CH(CH₃)₂). ¹³C{¹H} NMR (CDCl₃, δ): 161.8 (1,1,1,1 quartet, ¹J_{CB} = 50 Hz, ipso C of BAr'₄), 135.0 (s, para-C of BAr'₄), 129.1 (q, ²J_{CF} = 34 Hz, meta-C of BAr'₄), 124.7 (q, ¹J_{CF} = 272 Hz, CF₃ of BAr'₄), 117.7 (ortho-C of BAr'₄), 102.5, 97.3, 78.9 and 78.2 (all s, *p*-cymene aromatic), 31.7 (s, CH(CH₃)₂), 22.3 (s, *p*-cymene CH₃), 19.0 (s, *p*-cymene CH(CH₃)₂). ¹⁹F{¹H} NMR (CDCl₃, δ): -59.1 (s, BAr'₄). CV (THF, TBAH, 100 mV/s): E_{p,a} = -0.92 V, Ru(II/I). Anal. Calc. for C₅₂H₄₀Ru₂BF₂₄Cl₃: C, 43.37; H, 2.80. Found: C, 42.86; H, 2.89.

Attempted catalytic aziridination reaction of $[(\eta^6\text{-}p\text{-cymene})\text{Ru}(O,O\text{-acac-}\mu\text{-CH})_2][\text{OTf}]_2$ (1) with *p*-tolyl-azide. $[(\eta^6\text{-}p\text{-cymene})\text{Ru}(O,O\text{-acac-}\mu\text{-CH})_2][\text{OTf}]_2$ (1) (0.01 g, 0.0203 mmole), styrene (0.012 g, 0.103 mmole) and *p*-tolyl-azide (0.0027 g, 0.203 mmole) were combined in a screw cap NMR tube in C₆D₆ (0.5 ml). The reaction was followed by ¹H

NMR until no further decomposition of the metal complex was noted. No aziridine production was confirmed by ^1H NMR of aziridine products in C_6D_6 and comparison to published data.⁷⁴ Initial ^1H NMR spectra taken of $[(\eta^6\text{-}p\text{-cymene})\text{Ru}(\text{O},\text{O}\text{-acac}\text{-}\mu\text{-CH})_2][\text{OTf}]_2$ in the presence of styrene before addition of *p*-tolyl-azide.

Attempted catalytic aziridination reaction of $[(\eta^6\text{-}p\text{-cymene})\text{Ru}(\text{O},\text{O}\text{-acac}\text{-}\mu\text{-CH})_2][\text{OTf}]_2$ (1) with PhI=NTs. $[(\eta^6\text{-}p\text{-cymene})\text{Ru}(\text{O},\text{O}\text{-acac}\text{-}\mu\text{-CH})_2][\text{OTf}]_2$ (1) (0.01 g, 0.0203 mmole), styrene (0.012 g, 0.103 mmole) and PhINTs (0.035 g, 0.103 mmole) were combined in a screw cap NMR tube in CDCl_3 (0.5 ml). The reaction was followed by ^1H NMR until no further decomposition of the metal complex was noted. No aziridine production was confirmed by ^1H NMR in CDCl_3 and comparison to published data.⁷⁵ Initial ^1H NMR spectra taken of $[(\eta^6\text{-}p\text{-cymene})\text{Ru}(\text{O},\text{O}\text{-acac}\text{-}\mu\text{-CH})_2][\text{OTf}]_2$ in the presence of styrene before addition of PhINTs.

Attempted catalytic aziridination reaction of $[(\eta^6\text{-}p\text{-cymene})\text{Ru}(\text{O},\text{O}\text{-acac}\text{-}\mu\text{-CH})_2][\text{OTf}]_2$ (1) with PhI=NTs. $[(\eta^6\text{-}p\text{-cymene})\text{Ru}(\kappa^2\text{-O},\text{O}\text{-acac})(\text{THF})][\text{BAr}'_4]$ (0.01 g, 0.008 mmole), styrene (0.002 g, 0.156 mmole) and PhINTs (0.054 g, 0.156 mmole) were combined in a screw cap NMR tube in CDCl_3 (0.5 ml). The reaction was followed by ^1H NMR until no further decomposition of the metal complex was noted. No aziridine production was confirmed by ^1H NMR in CDCl_3 and comparison to published data.⁷⁵ Initial ^1H NMR spectra taken of $[(\eta^6\text{-}p\text{-cymene})\text{Ru}(\kappa^2\text{-O},\text{O}\text{-acac})(\text{THF})][\text{BAr}'_4]$ in the presence of styrene before addition of PhINTs.

Attempted catalytic epoxidation reaction of $[(\eta^6\text{-}p\text{-cymene})\text{Ru}(\kappa^2\text{-O},\text{O}\text{-acac})(\text{THF})][\text{BAr}'_4]$ (2) with trimethylamine-N-oxide. $[(\eta^6\text{-}p\text{-cymene})\text{Ru}(\kappa^2\text{-O},\text{O}\text{-acac})(\text{THF})][\text{BAr}'_4]$ (2) with trimethylamine-N-oxide.

acac)(THF)][BAr'₄] (0.01 g, 0.008 mmole), styrene (0.002 g, 0.156 mmole) and trimethylamine-N-oxide (0.012 g, 0.156 mmole) were combined in a screw cap NMR tube in CDCl₃ (0.5 ml). The reaction was followed by ¹H NMR until no further decomposition of the metal complex was noted. No epoxide production was confirmed by ¹H NMR in CDCl₃ and comparison to separated free styrene oxide ¹H NMR spectrum in CDCl₃. Initial ¹H NMR spectra taken of [(η⁶-*p*-cymene)Ru(κ²-*O,O*-acac)(THF)][BAr'₄] in the presence of styrene before addition of PhINTs.

Hydrogenation of Styrene. [(η⁶-*p*-cymene)Ru(κ²-*O,O*-acac)(THF)][BAr'₄] (**2**) (0.013 g, 0.010 mmol) and styrene (0.002 g, 0.2 mmol) were combined in a J-Young NMR tube in CDCl₃ (0.5 mL). The reaction was followed by ¹H NMR spectroscopy under 30 psi of dihydrogen pressure at 60 °C for 36 hours. At this time, 31% yield of ethylbenzene was observed. No additional production of ethylbenzene occurred at longer reaction times, and ¹H NMR spectroscopy revealed decomposition of **2** to multiple products.

REFERENCES

- 1.Rechavi, D.; Lemaire, M. *Chem. Rev.* **2002**, 102, (10), 3467-3493.
- 2.Müller, P.; Fruit, C. *Chem. Rev.* **2003**, 103, 2905-2919.
- 3.Watson, I. D. G.; Yu, L. L.; Yudin, A. K. *Acc. Chem. Res.* **2006**, 39, (3), 194-206.
- 4.Harlan, E. W.; Holm, R. H. *J. Am. Chem. Soc.* **1990**, 112, 186-193.
- 5.Groves, J. T.; Takahashi, T. *J. Am. Chem. Soc.* **1983**, 105, 2073-2074.
- 6.Nugent, W. A.; Mayer, J. M., *Metal-Ligand Multiple Bonds*. John Wiley and Sons: New York, 1988.
- 7.Anderson, T. M.; Neiwert, W. A.; Kirk, M. L.; Piccoli, P. M. B.; Schultz, A. J.; Koetzle, T. F.; Musaev, D. G.; Morokuma, K.; Cao, R.; Hill, C. L. *Science* **2004**, 306, (5704), 2074-2077.
- 8.Liang, J. L.; Huang, J. S.; Yu, X. Q.; Zhu, N. Y.; Che, C. M. *Chem. Eur. J.* **2002**, 8, (7), 1563-1572.
- 9.Au, S.-M.; Huang, J.-S.; Yu, W.-Y.; Fung, W.-H.; Che, C.-M. *J. Am. Chem. Soc.* **1999**, 121, 9120-9132.
- 10.Pérez, P. J.; White, P. S.; Brookhart, M.; Templeton, J. L. *Inorg. Chem.* **1994**, 33, 6050-6056.
- 11.Walsh, P. J.; Hollander, F. J.; Bergman, R. G. *J. Am. Chem. Soc.* **1988**, 110, 8729-8731.
- 12.Li, A.-H.; Dai, L.-X.; Aggarwal, V. K. *Chem. Rev.* **1997**, 97, 2341-2372.
- 13.Guiducci, A. E.; Boyd, C. L.; Mountford, P. *Organometallics* **2006**, 25, (5), 1167-1187.
- 14.Mindiola, D. J.; Hillhouse, G. L. *J. Am. Chem. Soc.* **2001**, 123, 4623-4624.
- 15.Gallagher, L. A.; Meyer, T. J. *J. Am. Chem. Soc.* **2001**, 123, 5308-5312.
- 16.Shu, L. J.; Nesheim, J. C.; Kauffmann, K.; Munck, E.; Lipscomb, J. D.; Que, L. *Science* **1997**, 275, (5299), 515-518.
- 17.Feng, Y.; Lail, M.; Foley, N. A.; Gunnoe, T. B.; Barakat, K. A.; Cundari, T. R.; Petersen, J. L. *J. Am. Chem. Soc.* **2006**, 128, 7982-7994.

18. Carmona, D.; Lamata, M. P.; Oro, L. A. *European Journal of Inorganic Chemistry* **2002**, (9), 2239-2251.
19. Govindaswamy, P.; Mobin, S. M.; Thone, C.; Kollipara, M. R. *Journal of Organometallic Chemistry* **2005**, 690, (5), 1218-1225.
20. Ohnishi, T.; Miyaki, Y.; Asano, H.; Kurosawa, H. *Chemistry Letters* **1999**, (8), 809-810.
21. Fernandez, R.; Melchart, M.; Habtemariam, A.; Parsons, S.; Sadler, P. L. *Chemistry-a European Journal* **2004**, 10, (20), 5173-5179.
22. Lalrempuia, R.; Kollipara, M. R. *Polyhedron* **2003**, 22, (23), 3155-3160.
23. Boller, T. M.; Hartwig, J. F.; Ishiyama, T.; Miyaura, N., *Mechanistic studies of aromatic C-H borylation catalyzed by iridium*. 2003; Vol. 226, p U657-U657.
24. Everaere, K.; Mortreux, A.; Bulliard, M.; Brussee, J.; van der Gen, A.; Nowogrocki, G.; Carpentier, J. F. *Eur. J. Org. Chem.* **2001**, (2), 275-291.
25. Netz, A.; Polborn, K.; Noth, H.; Mueller, T. J. J. *Eur. J. Org. Chem.* **2005**, (9), 1823-1833.
26. Ferguson, G.; Gallagher, J. F.; Lough, A. J.; Notti, A.; Pappalardo, S.; Parisi, M. F. *J. Org. Chem.* **2000**, 65, (3), 930-930.
27. Ferguson, G.; Gallagher, J. F.; Li, Y. W.; McKervey, M. A.; Madigan, E.; Malone, J. F.; Moran, M. B.; Walker, A. *Supramol. Chem.* **1996**, 7, (3), 223-228.
28. Molenveld, P.; Engbersen, J. F. J.; Reinhoudt, D. N. *J. Org. Chem.* **1999**, 64, (17), 6337-6341.
29. Molenveld, P.; Stikvoort, W. M. G.; Kooijman, H.; Spek, A. L.; Engbersen, J. F. J.; Reinhoudt, D. N. *J. Org. Chem.* **1999**, 64, (11), 3896-3906.
30. Molenveld, P.; Kapsabelis, S.; Engbersen, J. F. J.; Reinhoudt, D. N. *J. Am. Chem. Soc.* **1997**, 119, (12), 2948-2949.
31. Molenveld, P.; Engbersen, J. F. J.; Kooijman, H.; Spek, A. L.; Reinhoudt, D. N. *J. Am. Chem. Soc.* **1998**, 120, (27), 6726-6737.
32. Joerger, J. M.; Paris, J. M.; Vaultier, M. *Arkivoc* **2006**, 152-160.
33. Brandt, P.; Roth, P.; Andersson, P. G. *J. Org. Chem.* **2004**, 69, (15), 4885-4890.

34. Widegren, J. A.; Bennett, M. A.; Finke, R. G. *J. Am. Chem. Soc.* **2003**, 125, (34), 10301-10310.
35. Geldbach, T. J.; Pregosin, P. S. *Eur. J. Inorg. Chem.* **2002**, (8), 1907-1918.
36. Chen, Y.; Valentini, M.; Pregosin, P. S.; Albinati, A. *Inorg. Chim. Acta* **2002**, 327, 4-14.
37. den Reijer, C. J.; Wörle, M.; Pregosin, P. S. *Organometallics* **2000**, 19, 309-316.
38. Geldbach, T. J.; Pregosin, P. S.; Bassetti, M. *Organometallics* **2001**, 20, (14), 2990-2997.
39. Alonso, D. A.; Brandt, P.; Nordin, S. J. M.; Andersson, P. G. *J. Am. Chem. Soc.* **1999**, 121, (41), 9580-9588.
40. Canivet, J.; Suss-Fink, G. *Green Chem.* **2007**, 9, (4), 391-397.
41. Lu, X. L.; Yu, X. P.; Lou, J. D. *Synth. React. Inorg. Met.-Org. Chem.* **2006**, 36, (10), 733-745.
42. Ghebreyessus, K. Y.; Nelson, J. H. *J. Organomet. Chem.* **2003**, 669, (1-2), 48-56.
43. Shin, R. Y. C.; Bennett, M. A.; Goh, L. Y.; Chen, W.; Hockless, D. C. R.; Leong, W. K.; Mashima, K.; Willis, A. C. *Inorg. Chem.* **2003**, 42, (1), 96-106.
44. Seo, E. T.; Nelson, R. F.; Fritsch, J. M.; Marcoux, L. S.; Leedy, D. W.; Adams, R. N. *J. Am. Chem. Soc.* **1966**, 88, 3498-3503.
45. Jafarpour, L.; Nolan, S. P. *J. Organomet. Chem.* **2001**, 617-618, 17-27.
46. Esteruelas, M. A.; Oliván, M.; Oñate, E.; Ruiz, N.; Tajada, M. A. *Organometallics* **1999**, 18, 2953-2960.
47. Dougan, S. J.; Melchart, M.; Habtemariam, A.; Parsons, S.; Sadler, P. J. *Inorg. Chem.* **2007**, 46, (4), 1508-1508.
48. Melchart, M.; Habtemariam, A.; Parsons, S.; Moggach, S. A.; Sadler, P. J. *Inorganica Chimica Acta* **2006**, 359, (9), 3020-3028.
49. Gossens, C.; Tavernelli, I.; Rothlisberger, U. *Chimia* **2005**, 59, (3), 81-84.
50. Howarth, J.; Hanlon, K.; Fayne, D.; McCormac, P. *Tetrahedron Lett.* **1997**, 38, 3097-3100.

51. Chi, Y. S.; Hwang, S.; Lee, B. S.; Kwak, J.; Choi, I. S.; Lee, S. *Langmuir* **2005**, 21, (10), 4268-4271.
52. Ruminski, R. R.; Freiheit, D.; Serveiss, D.; Snyder, B.; Johnson, J. E. B. *Inorg. Chim. Acta* **1994**, 224, (1-2), 27-34.
53. Chang, H. C.; Mochizuki, K.; Kitagawa, S. *Inorg. Chem.* **2005**, 44, (11), 3810-3817.
54. Yan, Y. K.; Melchart, M.; Habtemariam, A.; Sadler, P. J. *Chem. Commun.* **2005**, (38), 4764-4776.
55. Tovar-Tovar, A.; Ruiz-Ramirez, L.; Campero, A.; Romerosa, A.; Moreno-Esparza, R.; Rosales-Hoz, M. J. *J. Inorg. Biochem.* **2004**, 98, (6), 1045-1053.
56. Mahapatra, S.; Halfen, J. A.; Wilkinson, J. A.; Wilkinson, E. C.; Pan, G.; Wang, X.; Young, J., V. G.; Cramer, C. J.; Que, J., L.; Tolman, W. B. *J. Am. Chem. Soc.* **1996**, 118, 11555-11574.
57. Gupta, H. K.; Rampersad, N.; Stradiotto, M.; McGlinchey, M. J. *Organometallics* **2000**, 19, (2), 184-191.
58. De Pascali, S. A.; Papadia, P.; Ciccarese, A.; Pacifico, C.; Fanizzi, F. P. *Eur. J. Inorg. Chem.* **2005**, (4), 788-796.
59. Bhalla, G.; Oxgaard, J.; Goddard, W. A.; Periana, R. A. *Organometallics* **2005**, 24, (23), 5499-5502.
60. Brooks, S. C.; Vinyard, D. J.; Richter, M. M. *Inorg. Chim. Acta* **2006**, 359, (14), 4635-4638.
61. Arnold, D. I.; Cotton, F. A.; Matonic, J. H.; Murillo, C. A. *Chem. Commun.* **1996**, (18), 2113-2114.
62. Gibson, D. *Coord. Chem. Rev.* **1969**, 4, (2), 225-&.
63. Corrochano, A. E.; Jalon, F. A.; Otero, A.; Kubicki, M. M.; Richard, P. *Organometallics* **1997**, 16, (1), 145-148.
64. Lindsay, C.; Cesarotti, E.; Adams, H.; Bailey, N. A.; White, C. *Organometallics* **1990**, 9, (9), 2594-2602.
65. Fang, X. G.; Watkin, J. G.; Scott, B. L.; John, K. D.; Kubas, G. J. *Organometallics* **2002**, 21, (11), 2336-2339.

- 66.Ooyama, D.; Tomon, T.; Tsuge, K.; Tanaka, K. *J. Organomet. Chem.* **2001**, 619, (1-2), 299-304.
- 67.Bennett, M. A.; Byrnes, M. J.; Chung, G.; Edwards, A. J.; Willis, A. C. *Inorg. Chim. Acta* **2005**, 358, (5), 1692-1708.
- 68.Wilton-Ely, J. D. E. T.; Wang, M.; Benoit, D. M.; Tocher, D. A. *Eur. J. Inorg. Chem.* **2006**, (15), 3068-3078.
- 69.Doherty, S.; Knight, J. G.; Rath, R. K.; Clegg, W.; Harrington, R. W.; Newman, C. R.; Campbell, R.; Amin, H. *Organometallics* **2005**, 24, (11), 2633-2644.
- 70.Won, J. H.; Lim, H. G.; Kim, B. Y.; Lee, J. D.; Lee, C.; Lee, Y. J.; Cho, S.; Ko, J.; Kang, S. O. *Organometallics* **2002**, 21, (26), 5703-5712.
- 71.Herberhold, M.; Yan, H.; Milius, W. *J. Organomet. Chem.* **2000**, 598, (1), 142-149.
- 72.Trofimenko, S. *J. Am. Chem. Soc.* **1967**, 89, 3170-3177.
- 73.Yakelis, N. A.; Bergman, R. G. *Organometallics* **2005**, 24, (14), 3579-3581.
- 74.Sriraghavan, K.; Ramakrishnan, V. T. *Synth. Commun.* **2001**, 31, (7), 1105-1121.
- 75.Evans, D. A.; Faul, M. M.; Bilodeau, M. T. *J. Am. Chem. Soc.* **1994**, 116, 2742-2753.

CHAPTER 3

3.1 Saturated hydrocarbon C-H activation across M-X bonds of late transition metal complexes with non-dative heteroatomic ligands

There are a few important steps to consider for design of late transition metals with nondative heteroatomic ligands systems for C-H activation and functionalization (Figure 3.1). A key step of single site homogeneous catalyst is creating one *open coordination* site in order to coordinate and activate inert C-H bonds. Similar to coordination of H₂,¹ the coordination of C-H bonds to an *electrophilic metal center* can enhance C-H acidity. In the C-H activation step, a *basic heteroatomic ligand* abstracts a proton from the coordinated C-H moiety.

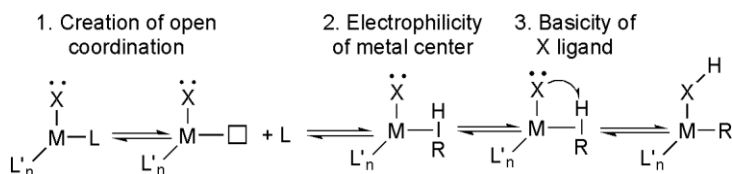
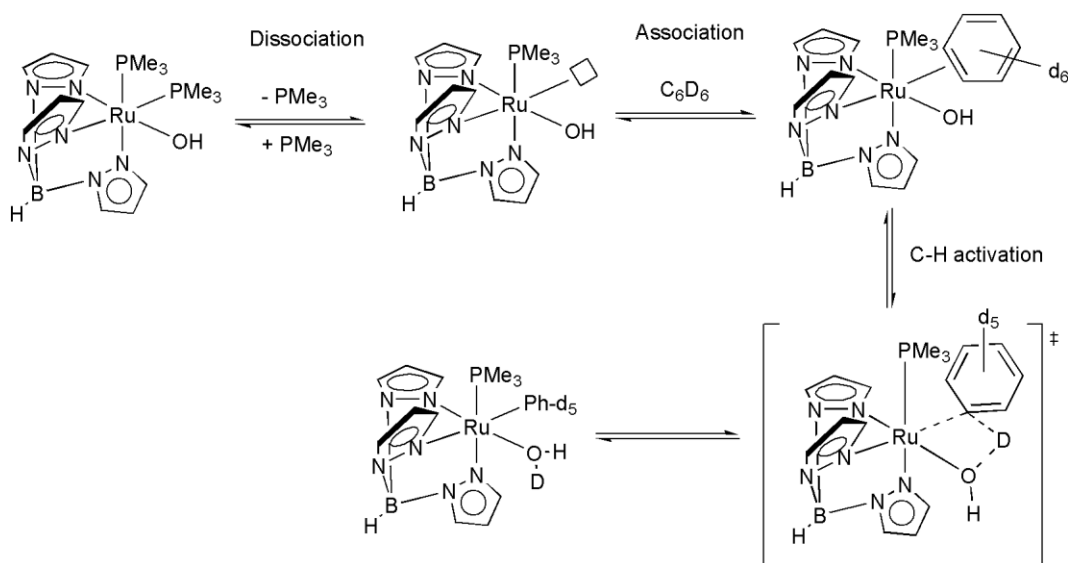


Figure 3.1. Key steps of C-H activation by M-X system (X = OR NR₂, etc.).

3.1.1 C-H activation by Ru(II)-hydroxo/anilido and Ir(III)-methoxo complexes

Activation and selective functionalization of hydrocarbon C-H bonds through metal-mediated transformations have been intensively studied due to the potential improvement on existing synthetic processes.²⁻⁷ One possible catalytic cycle for C-H functionalization involves 1,2-addition of C-H bonds across M-X (X = NHR or OR) bonds (Scheme 1.16).⁸⁻¹³ However, there are few examples of net 1,2-addition of C-H bonds across M-X bonds for low oxidation state late transition metals bearing a heteroatom ligand system.

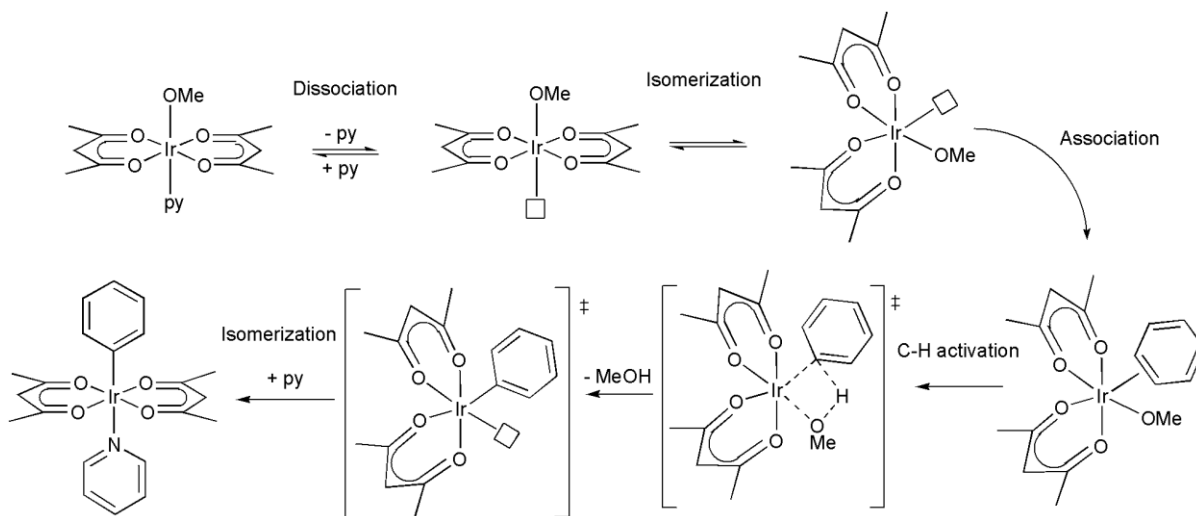
$\text{TpRu}(\text{PMe}_3)_2\text{X}$ ($\text{X} = \text{OH}$ or NHP) systems have been shown to add arene C-H bonds across Ru-OH or Ru-NHR bonds via a 1,2-addition pathway (Scheme 3.1).^{8, 11} However, the addition of benzene C-H bonds across $\text{Ru}^{\text{II}}\text{-OH}$ or $\text{Ru}^{\text{II}}\text{-NHP}$ was found to be thermally disfavored. Hence, the system did not allow the direct observation of metal mediated C-H activation. In order to observe 1,2-addition pathway, isotopically labeling experiments were used. For example, 1,2-addition of C_6D_6 can be monitored via H/D exchange at the heteroatomic ligand and benzene. Extensive kinetic and computational studies have been conducted and support the 1,2-addition mechanism shown in Scheme 3.1.



Scheme 3.1. Proposed mechanism for H/D exchange between $\text{Ru}^{\text{II}}\text{-OH}$ and C_6D_6 .

A related heteroatom-based C-H activation has been observed using $(\kappa^2\text{-acac-}O,O)_2\text{Ir}^{\text{III}}(\text{OMe})(\text{py})$ ($\text{py} = \text{pyridine}$).⁹ Heating $(\kappa^2\text{-acac-}O,O)_2\text{Ir}^{\text{III}}(\text{OMe})(\text{MeOH})$ in C_6H_6 at $160\text{ }^\circ\text{C}$ cleanly yields the product of benzene C-H activation, $(\kappa^2\text{-acac-}O,O)_2\text{Ir}^{\text{III}}(\text{Ph})(\text{py})$, and methanol (Scheme 3.2). When the reaction is carried out in C_6D_6 , CD_3OD and $(\kappa^2\text{-acac-}$

$O,O)_2Ir^{III}(\eta^1-C_6D_5)(py)$ were observed. Significantly, the formation of $(\kappa^2\text{-acac-}O,O)_2Ir^{III}(\text{Ph})(py)$ is thermally favorable, while the formation of $TpRu(PMe_3)(\text{Ph})(\text{XH}_2)$ ($X = \text{O}$ or NPh) from the isoelectronic $TpRu^{II}(PMe_3)_2\text{XH}$ complexes is not (see above).



Scheme 3.2. Proposed mechanism for C-H activation of benzene by $(\kappa^2\text{-acac-}O,O)_2Ir^{III}(\text{OMe})(py)$.

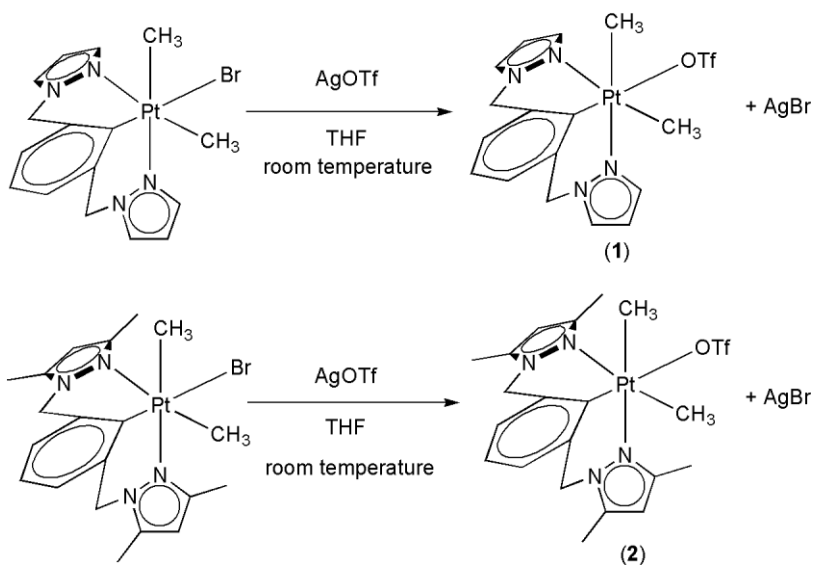
3.1.2 Platinum (IV) complexes

In an effort to further understand the ability of late transition metals with non-dative heteroatomic ligands to affect C-H activation via 1,2-addition reactions, we have attempted to explore reactivity with Pt^{IV} -amido and related complexes, which are isoelectronic with $TpRu(PMe_3)_2X$ ($X = \text{OH}$ or NHPH) and $(\kappa^2\text{-acac-}O,O)_2Ir^{III}(\text{OMe})(\text{MeOH})$. Pt^{IV} is isoelectronic with Ru^{II} and Ir^{III} , but is more electronegative.¹⁴ The comparison suggests the Pt^{IV} center is more electrophilic relative to Ru^{II} , which should positively impact the C-H activation event. When inert C-H bonds coordinate to a metal center, the C-H acidity is enhanced which should facilitate the 1,2-addition. (using the model of 1,2-addition as an intramolecular proton transfer). However, the basicity of the non-dative heteroatomic ligands

also can impact the 1,2-addition, and we expect that increased electrophilicity of metal center might attenuate the basicity of M-X complexes. Thus, comparison of 1,2-addition for Pt^{IV} vs. Ru^{II} and Ir^{III} is of interest. Herein, efforts to prepare six-coordinate Pt^{IV} complexes with non-dative heteroatomic ligands are discussed including the conversion of Pt-Me and oxidant to Pt-OMe systems, which would provide a catalytically viable route to O-C bond formation.

3.1.3 Synthesis of platinum (IV) triflate complexes

(NCN)Pt(Me)₂Br and (NCN')Pt(Me)₂Br {NCN = 2,6-(pzCH₂)₂C₆H₃; NCN' = 2,6-(3,5-Me₂pzCH₂)₂C₆H₃} were synthesized and fully characterized by White et al.¹⁵ The reaction of the above Pt^{IV}-Br complexes with AgOTf immediately results in bromide/triflate metathesis to produce (NCN)Pt(Me)₂OTf (**1**) and (NCN')Pt(Me)₂OTf (**2**) at room temperature (Scheme 3.3). Complex **1** was first made by Dr. Zhang.¹⁶



Scheme 3.3. Synthesis of Pt-OTf complexes.

The ^{19}F NMR spectra of **1** and **2** are consistent with the ligand exchange between the bromide and triflate ligands both revealing a singlet at -74.7 ppm. The ^1H and ^{13}C NMR spectra of **1** and **2** are shown in Figure 3.3 and Figure 3.4. In the ^1H and ^{13}C NMR spectra, the symmetry equivalent Pt-Me groups resonate as a singlet with Pt satellites (^{195}Pt , natural abundance 33.8 %, is $I = 1/2$). The $^2J_{\text{Pt-H}}$ is 70 Hz. The ^1H NMR spectrum is consistent with facial coordination of the NCN and NCN' ligands. For example, resonances due to CH_2 of the NCN/NCN' ligands exhibit two doublets between 4.5 and 6.0 ppm, which is consistent with facial coordination over meridional (Figure 3.2).

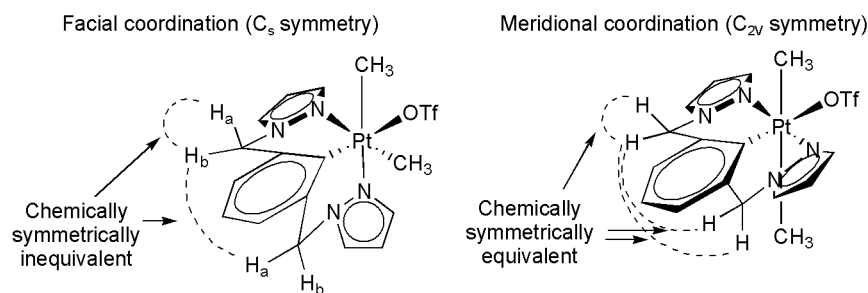


Figure 3.2. Coordination mode of NCN ligand and anticipate ^1H NMR features of CH_2 groups.

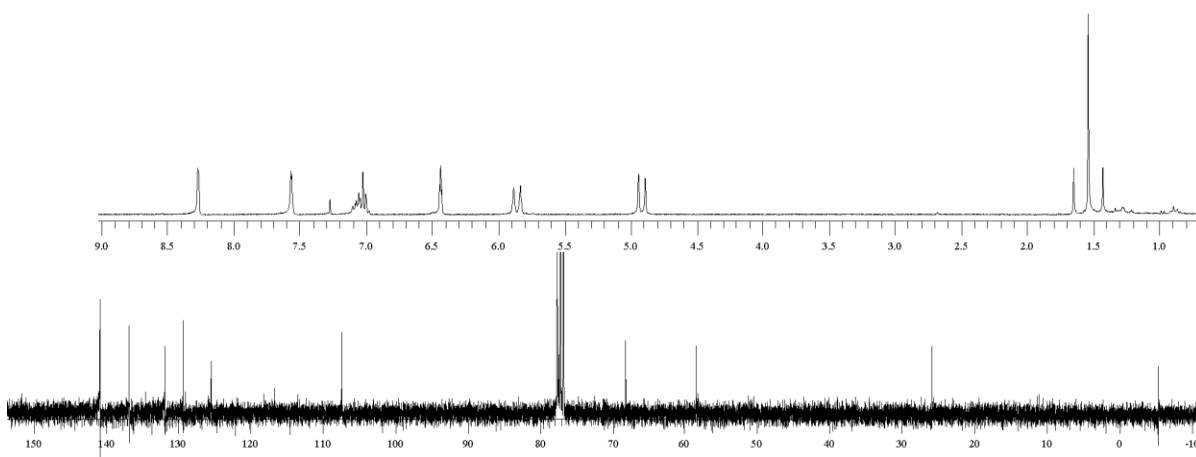


Figure 3.3. ^1H and ^{13}C NMR spectra of $(\text{NCN})\text{Pt}(\text{Me})_2\text{OTf}$ (**1**) in CDCl_3 .

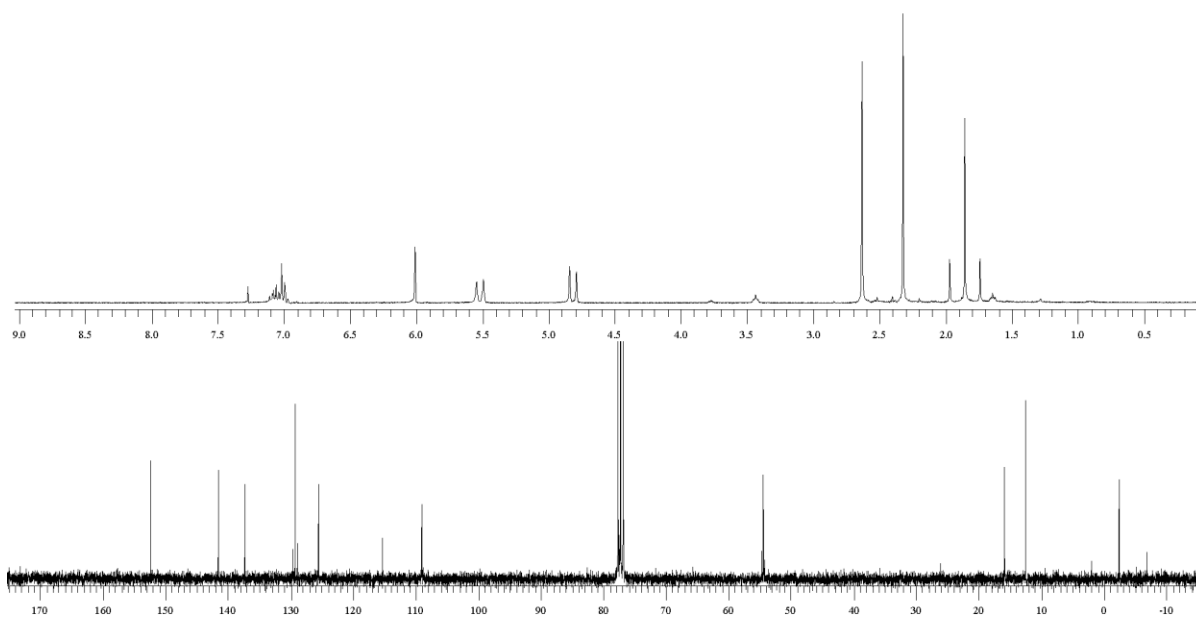


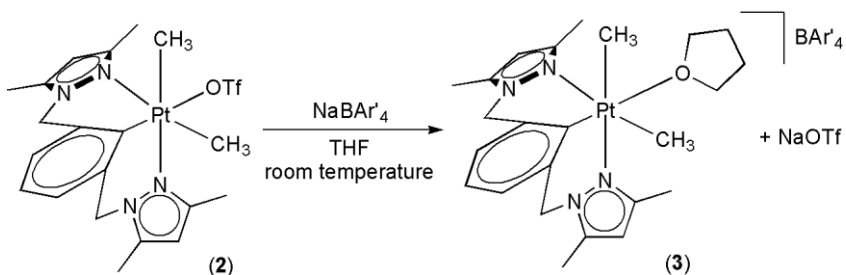
Figure 3.4. ^1H and ^{13}C NMR spectra of $(\text{NCN}')\text{Pt}(\text{Me})_2\text{OTf}$ (**2**) in CDCl_3 .

The synthesis of Pt amido complexes was attempted. Reaction of $(\text{NCN})\text{Pt}(\text{Me})_2\text{OTf}$ and $(\text{NCN}')\text{Pt}(\text{Me})_2\text{OTf}$ with LiNHPH in C_6H_6 did not cleanly yield the corresponding amido complexes, $(\text{NCN})\text{Pt}(\text{Me})_2\text{NHPH}$ / $(\text{NCN}')\text{Pt}(\text{Me})_2\text{NHPH}$. These reactions gave a mixture of products that could not be separated.

3.1.4 Synthesis of platinum (IV) cationic species

The reaction of **2** and NaBAR'_4 $\{\text{Ar}' = 3,5\text{-(CF}_3)_2\text{C}_6\text{H}_3\}$ in THF produces $[(\text{NCN}')\text{Pt}(\text{Me})_2(\text{THF})][\text{BAR}'_4]$ (**3**) (Scheme 3.4). Complex **3** reveals multiplets at 3.83 and 1.94 ppm in the ^1H NMR spectrum, and singlets at 69.6 and 25.2 ppm in the ^{13}C NMR spectrum due to the α - and β -positions of the coordinated THF (Figure 3.5 and Figure 3.6).

Coordination of THF to the cationic Pt^{IV} complex results in a slight downfield shift of resonances compared to free THF peaks, which resonate at 3.76 and 1.85 ppm in ¹H NMR spectrum and at 68.0 and 25.6 ppm in the ¹³C NMR spectrum.



Scheme 3.4. Synthesis of [(NCN')Pt(Me)₂(THF)][BAr'₄] (**3**).

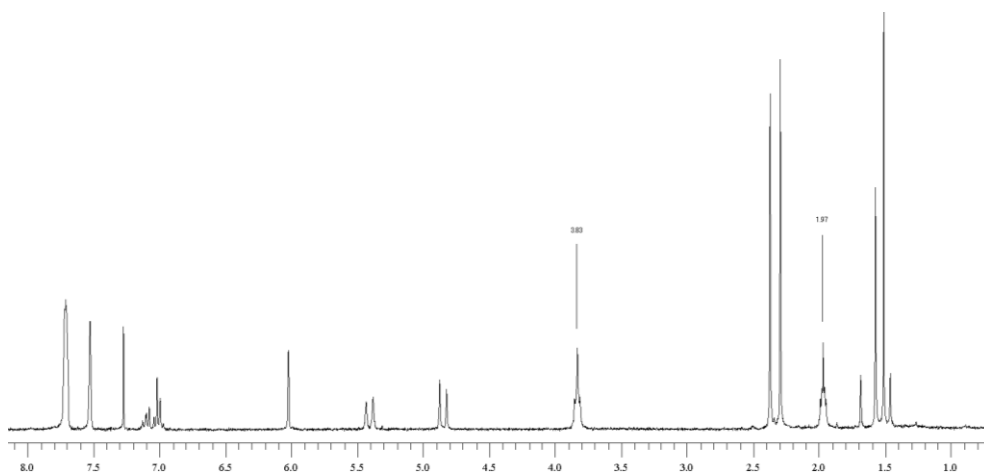


Figure 3.5. ¹H NMR spectra of [(NCN')Pt(Me)₂(THF)][BAr'₄] (**3**) in CDCl₃.

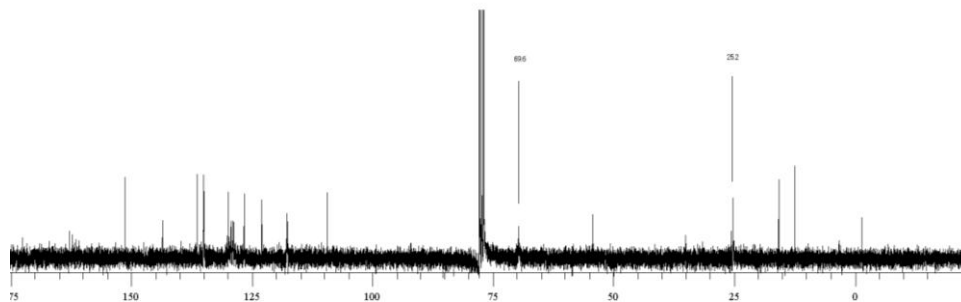


Figure 3.6. ^{13}C NMR spectra of $[(\text{NCN}')\text{Pt}(\text{Me})_2(\text{THF})][\text{BAr}'_4]$ (**3**) in CDCl_3 .

A single X-ray diffraction study of **3** confirmed its identity (Figure 3.7). Bond distances and angles are shown in Table 3.1 with selected crystallographic data given in Table 3.2. As anticipated based on NMR spectroscopy, the NCN' ligand coordinates in a facial mode to the metal center. The N(1)-Pt(1)-N(3) angle is $98.20(9)^\circ$ while the C(1)-Pt(1)-C(2) angle is $82.9(2)^\circ$, consistent with a pseudo-octahedral structure. Examples of solid-state structures of Pt(IV) with coordinated THF are relatively rare. One platinum complex, $[\text{Me}_3\text{Pt}(\text{OSO}_2\text{CF}_3)(\text{THF})_2]$ has been characterized by Dehnicke et al,¹⁷ and the Pt-(κ^1 -O-THF) bond distance is $2.229(4) \text{ \AA}$, which is statically identical to Pt(1)-O(1) ($2.23(2) \text{ \AA}$) of complex **3**. By comparison with platinum(II)-(κ^1 -O-THF) bond distance, the Pt-O bond lengths for $[(\text{P}(\text{iPr}))_2\text{Pt}(\text{H})(\text{THF})][\text{BAr}'_4]$ complex is $2.224(7) \text{ \AA}$ ¹⁸ and for $\{\text{Ph}_2\text{B}(\text{CH}_2\text{-PPh}_2)_2\}\text{Pt}(\text{Me})(\text{THF})\cdot 2(\text{THF})$ complex is $2.170(4) \text{ \AA}$,¹⁹ which are slightly shorter than the Pt(IV) species.

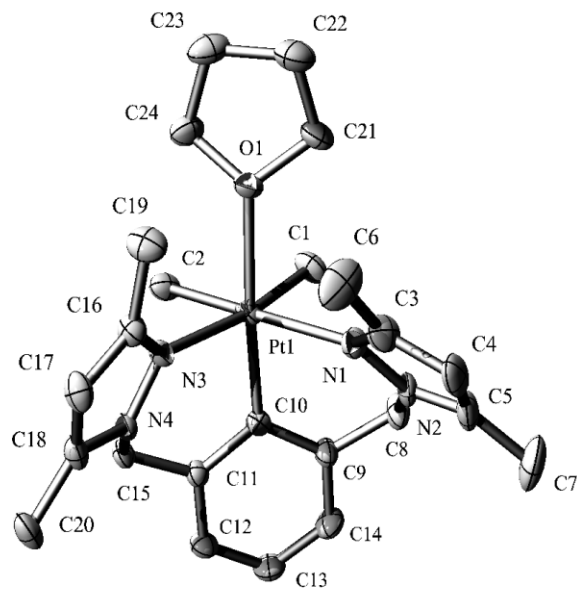


Figure 3.7. ORTEP (scaled to enclose 50% probability) of $[(NCN')Pt(Me)_2(THF)][BAr'_4]$ (**3**) (BAr'_4 anion is not depicted).

Table 3.1. Selected bond distances (Å) and angles (°) for [(NCN')Pt(Me)₂(THF)][BAR'₄] (**3**).

<i>Bond length</i> (Å)			
Pt(1)-O(1)	2.23(2)	C(9)-C(10)	1.407(4)
Pt(1)-N(1)	2.209(2)	C(9)-C(14)	1.390(4)
Pt(1)-N(3)	2.228(2)	C(10)-C(11)	1.407(4)
Pt(1)-C(1)	2.051(3)	C(11)-C(12)	1.395(4)
Pt(1)-C(2)	2.047(3)	C(11)-C(15)	1.491(4)
Pt(1)-C(10)	2.006(3)	C(12)-C(13)	1.384(4)
N(1)-N(2)	1.368(3)	N(3)-N(4)	1.370(3)
N(1)-C(3)	1.350(4)	N(3)-C(16)	1.349(4)
N(2)-C(8)	1.464(4)	N(4)-C(15)	1.469(3)
<i>Bond angles</i> (°)			
O(1)-Pt(1)-N(1)	91.98(8)	N(3)-Pt(1)-C(2)	87.3(1)
O(1)-Pt(1)-N(3)	92.01(8)	N(3)-Pt(1)-C(10)	90.57(9)
O(1)-Pt(1)-C(1)	85.0(1)	C(1)-Pt(1)-C(2)	82.9(1)
O(1)-Pt(1)-C(2)	90.29(9)	C(1)-Pt(1)-C(10)	92.9(1)
O(1)-Pt(1)-C(10)	176.27(9)	C(2)-Pt(1)-C(10)	92.5(1)
N(1)-Pt(1)-N(3)	98.20(9)	Pt(1)-O(1)-C(21)	120.9(2)
N(1)-Pt(1)-C(1)	91.7(1)	Pt(1)-O(1)-C(24)	122.5(2)
N(1)-Pt(1)-C(2)	173.9(1)	C(21)-O(1)-C(24)	104.7(2)
N(1)-Pt(1)-C(10)	84.98(9)	C(10)-C(11)-C(12)	120.7(2)
N(3)-Pt(1)-C(1)	169.8(1)	C(10)-C(11)-C(15)	121.4(2)
N(1)-N(2)-C(8)	122.1(2)	N(4)-C(15)-C(11)	114.0(2)
C(5)-N(2)-C(8)	126.2(3)	N(2)-C(8)-C(9)	111.4(2)

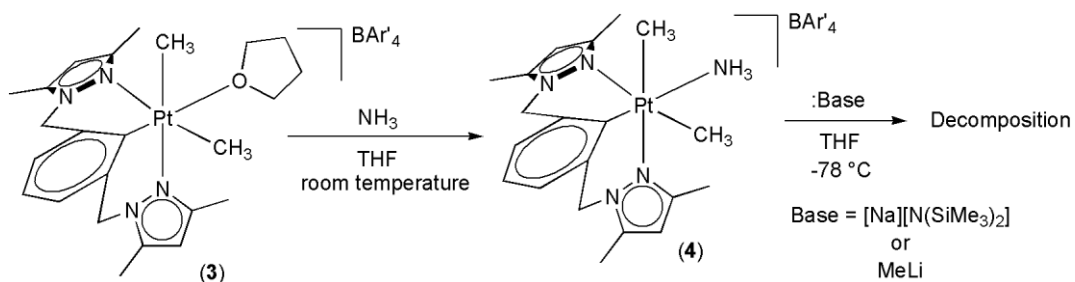
Table 3.2. Selected crystallographic data for complexes **3** and **4**.

Crystal System	Complex 3	Complex 4
Empirical formula	C ₆₁ H ₅₇ BF ₂₄ N ₄ OPt	C ₅₇ H ₅₂ BF ₂₄ N ₅ Pt
Formula Weight	1524.00	1468.94
T (K)	110	293
λ	0.71073	0.71073
Crystal System	monoclinic	monoclinic
Space Group	P 2 ₁ /n	Cc
a (Å)	12.8760(2)	21.6993(13)
b (Å)	13.0399(2)	13.2530(8)
c (Å)	36.8733(6)	22.2267(13)
α (°)	90.0	90
β (°)	95.2340(9)	108.000(1)
γ (°)	90.0	90
V (Å ³)	6165.28(17)	6079.1(6)
Z	4	4
ρ_{calc} (g/cm ³)	1.642	1.605
Crystal Dimensions (mm)	0.30 × 0.24 × 0.16	0.20 x 0.30 x 0.38
GOF	1.21	0.932
R1, wR2 {I>2 σ (I)}	0.057, 0.047	0.0503, 0.0943

The reaction of **2** with NaBAR'₄ in poorly coordinating solvents, such as C₆H₆, results in decomposition to NMR inactive species. Additionally, in the solid-state, complex **3** begins to decompose to uncharacterized Pt complexes in the glove box within 3 weeks.

When complex **3** is dissolved in a THF solution with NH₃, a ligand exchange between THF and NH₃ occurs to yield [(NCN')Pt(Me)₂(NH₃)] [BAR'₄] (**4**), which has been fully characterized (Scheme 3.5). The ¹H NMR and ¹³C NMR spectra of **4** (Figure 3.8) are consistent with the proposed structure. The disappearance of the coordinated THF resonances and the appearance of a broad NH₃ resonance at 2.7 ppm were observed by ¹H NMR spectroscopy, and the NH₃ peak has shoulders on both sides, which are likely due to proton coupling to ¹⁹⁵Pt. Several attempts to deprotonate the NH₃ ligand to yield

$(\text{NCN})\text{Pt}(\text{Me})_2(\text{NH}_2)$ resulted in decomposition into NMR inactive species (Scheme 3.5). For example, addition of $[\text{Na}][\text{N}(\text{SiMe}_3)_2]$ or MeLi into a THF solution with complex **4** at $-78\text{ }^\circ\text{C}$ and addition of $[\text{Na}][\text{N}(\text{SiMe}_3)_2]$ into a C_6H_6 solution with **4** at room temperature all led to decomposition.



Scheme 3.5. Synthesis of $[(\text{NCN}')\text{Pt}(\text{Me})_2(\text{NH}_3)][\text{BAR}'_4]$ (**4**).

A single X-ray diffraction study of **4** confirmed its identity (Figure 3.9). Bond distances and angles are presented in Table 3.3 with selected crystallographic data given in Table 3.2. The angle of $\text{N}(1)\text{-Pt}(1)\text{-N}(3)$ is $101.2(1)^\circ$ wide while $\text{C}(51)\text{-Pt}(1)\text{-C}(52)$ angle is $81.3(2)^\circ$, which is slightly more distorted from the 90° octahedral paradigm than $[(\text{NCN}')\text{Pt}(\text{Me})_2(\text{THF})][\text{BAR}'_4]$ (**3**). Also, the angle of $\text{C}(33)\text{-Pt}(1)\text{-N}(5)$ is $178.0(2)^\circ$, which is closer to 180° than the angle of $\{\text{O}(1)\text{-Pt}(1)\text{-C}(10) = 176.27(9)^\circ\}$ for $[(\text{NCN}')\text{Pt}(\text{Me})_2(\text{THF})][\text{BAR}'_4]$ (**3**) due to less steric influence of NH_3 compared with THF.

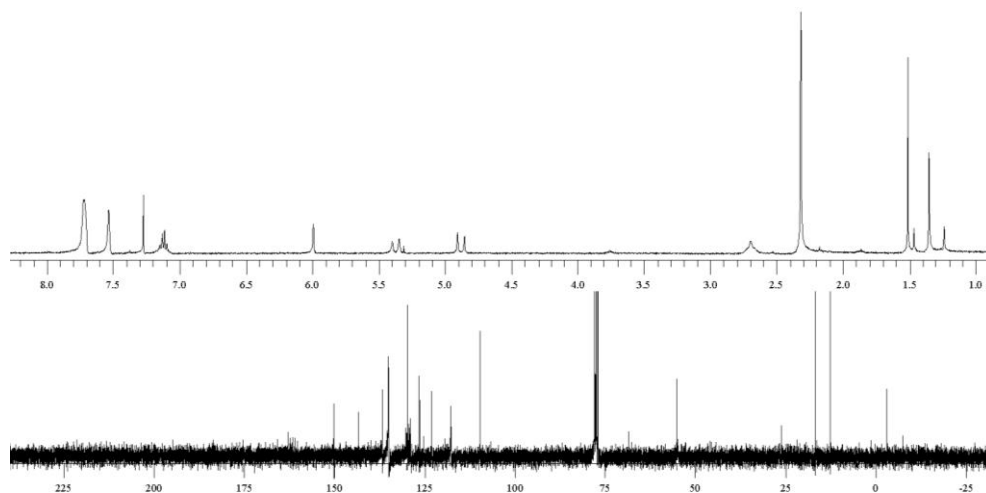


Figure 3.8. ^1H NMR and ^{13}C NMR spectra of $[(\text{NCN}')\text{Pt}(\text{Me})_2(\text{NH}_3)][\text{BAr}'_4]$ (**4**) in CDCl_3 .

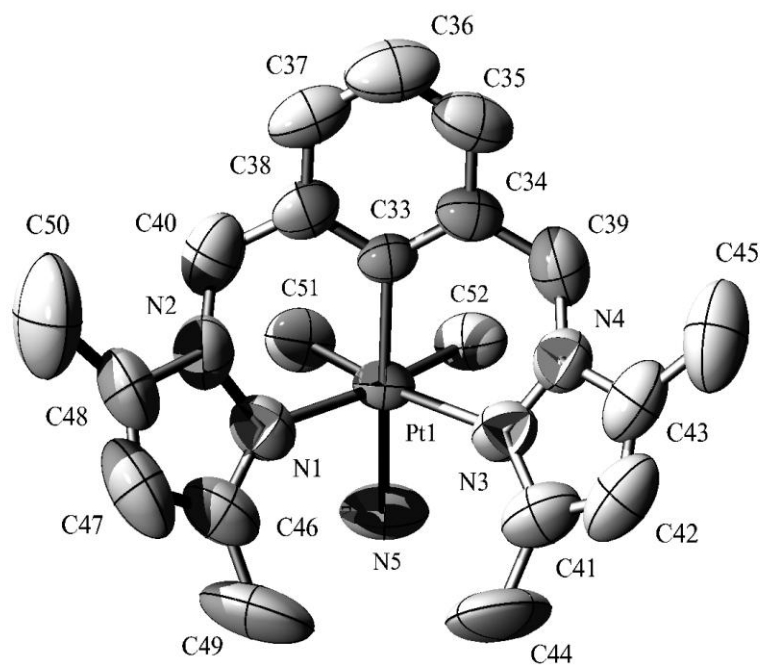


Figure 3.9. ORTEP (scaled to enclose 30% probability) of $[(\text{NCN}')\text{Pt}(\text{Me})_2(\text{NH}_3)][\text{BAr}'_4]$ (**4**) (BAr'_4 anion is not depicted).

Table 3.3. Selected bond distances (Å) and angles (°) for [(NCN')Pt(Me)₂(NH₃)] [BAr'₄] (**4**).

<i>Bond length</i> (Å)			
Pt(1)-C(51)	2.029(4)	N(3)-N(4)	1.332(5)
Pt(1)-C(33)	2.033(3)	N(4)-C(43)	1.367(4)
Pt(1)-C(52)	2.064(4)	N(3)-C(41)	1.341(5)
Pt(1)-N(5)	2.160(4)	C(33)-C(34)	1.389(5)
Pt(1)-N(1)	2.262(3)	C(34)-C(39)	1.511(5)
Pt(1)-N(3)	2.297(3)	C(38)-C(40)	1.50(1)
<i>Bond angles</i> (°)			
C(51)-Pt(1)-C(33)	95.2(2)	C(34)-C(33)-Pt(1)	122.5(2)
C(51)-Pt(1)-C(52)	81.3(2)	C(38)-C(33)-Pt(1)	121.6(2)
N(1)-Pt(1)-N(3)	101.2(1)	C(35)-C(34)-C(33)	121.7(3)
C(51)-Pt(1)-N(5)	85.1(2)	C(35)-C(34)-C(39)	117.8(4)
C(33)-Pt(1)-N(5)	178.0(2)	C(33)-C(38)-C(40)	121.8(4)
N(5)-Pt(1)-N(1)	94.8(2)	N(4)-C(39)-C(34)	112.0(3)
N(5)-Pt(1)-N(3)	94.1(1)	N(2)-C(40)-C(38)	113.1(3)

3.2 Attempted conversion of Pt-R to Pt-OR

Metal-mediated C-O bond formation is equally as challenging as C-H activation of hydrocarbons. Previously substantial efforts have been directed toward conditions necessary to observe the migration of a transition metal alkyl or aryl ligand to a terminal oxo group (Figure 3.10). However, this aryl- or alkyl-to-oxo migration has been found to be an extremely difficult transformation both kinetically and thermodynamically. To our knowledge, there is only a single example of well-defined migration of a hydrocarbyl ligand to a terminal oxo ligand to produce M-OR under thermal conditions.²⁰ Also, the reverse reaction has been published in a handful of cases.²¹⁻²³ First, the strength of metal oxo bonds inhibit this reaction thermodynamically.²⁴⁻²⁶ Also, nucleophilic character of both oxo and alkyl/aryl ligands (Figure 3.11) renders the transformation kinetically challenging. Overall, reaction shown in Figure 3.10 is not facile reaction.

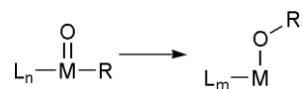


Figure 3.10. The migration of alkyl or aryl groups to terminal oxo ligands in transition metal complexes.

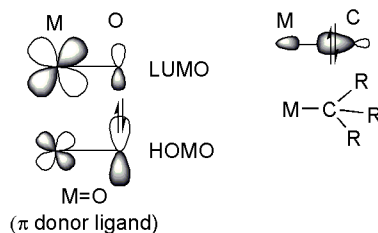
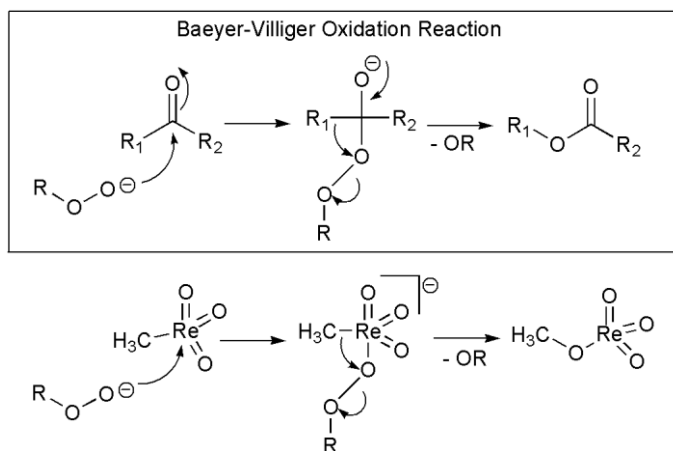


Figure 3.11. Metal oxo complex in orbital occupancy.

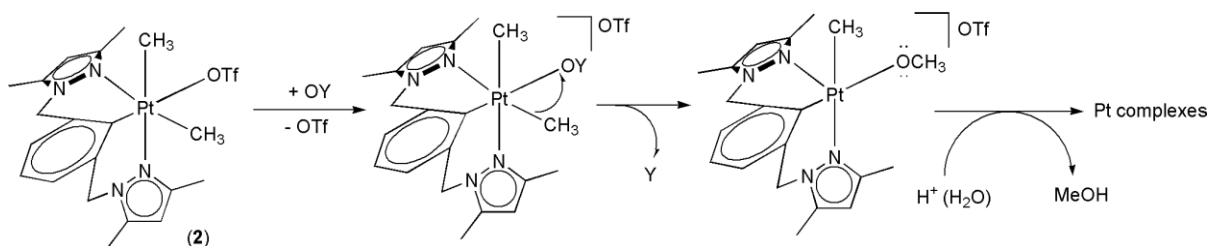
These results conclude that the research should not center on forming metal-oxo bonds, but should focus on insertion using an electrophilic oxygen source. Periana et al. presented a net oxygen atom insertion into the Re-CH₃ bond of MTO (MTO = methyltrioxorhenium).²⁷ The reaction was found to occur with a variety of oxidants (H₂O₂, IO₄⁻ and PhIO), and isotopic-oxygen labeling studies suggest that the inserted oxygen atom does not originate from an oxo ligand. Rather, combined experimental and computational studies suggest the reaction follows a Baeyer-Villiger-type²⁸ mechanism (Scheme 3.6) and possesses a very low activation barrier (13-25 kcal/mol).



Scheme 3.6. Baeyer-Villiger-type reaction for oxygen atom insertion into the Re-CH₃ bond.

3.2.1 Attempted oxygen atom insertion into Pt^{IV}-Me bonds

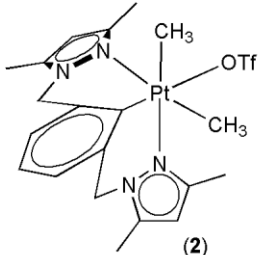
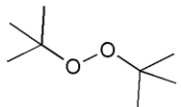
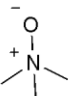
The reaction of (NCN')Pt(Me)₂OTf (**2**) and a variety of oxidants was attempted in effort to insert an oxygen atom into Pt-Me bond in D₂O (Scheme 3.7). If the oxygen atom is inserted into one of the Pt-Me bonds, a Pt methoxo complex should be formed as an intermediate. As the reaction takes place in water, the methoxo ligands can react with water to release methanol. Hence, the production of methanol was used to indicate oxygen insertion into the Pt-Me bond to form Pt-OMe.



Scheme 3.7. Proposed O-atom insertion reaction to (NCN')Pt(Me)₂OTf (**2**).

The reactions of **2** with some oxidants are shown in Table 3.4. The reactions of H₂O₂ and *tert*-butyl peroxide with **2** produce small amounts of methanol. In ¹H NMR spectra, the free methanol resonates at 3.34 ppm.²⁹ The reaction of H₂O₂ and *tert*-butyl peroxide with **2** in D₂O exhibit potential methanol production in ¹H NMR spectra shown in Figure 3.13 and Figure 3.14.

Table 3.4. The results of the reaction of (NCN')Pt(Me)₂OTf (**2**) of various oxidants.

 (2)	H ₂ O ₂		KIO ₄	
Potential MeOH production	Yes	Yes	No	No
Reaction conditions	80 °C	80 °C	80 °C	80 °C
Reaction time	3 days	6 days	12 hours	3 days
Pt complex	Decomposition	Decomposition	Decomposition	No reaction

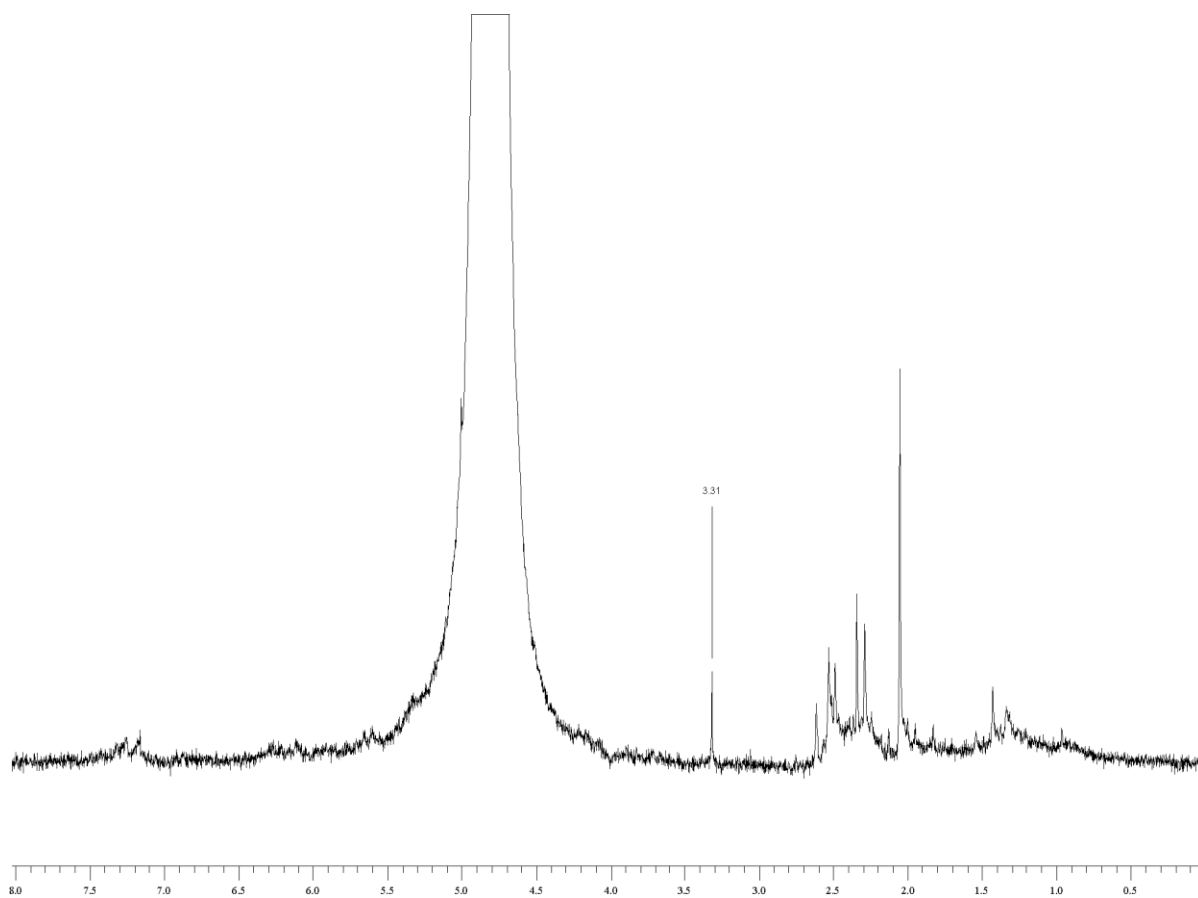


Figure 3.13. The reaction of $(\text{NCN}')\text{Pt}(\text{Me})_2\text{OTf}$ (**2**) with H_2O_2 and the observation of resonance due to methanol.

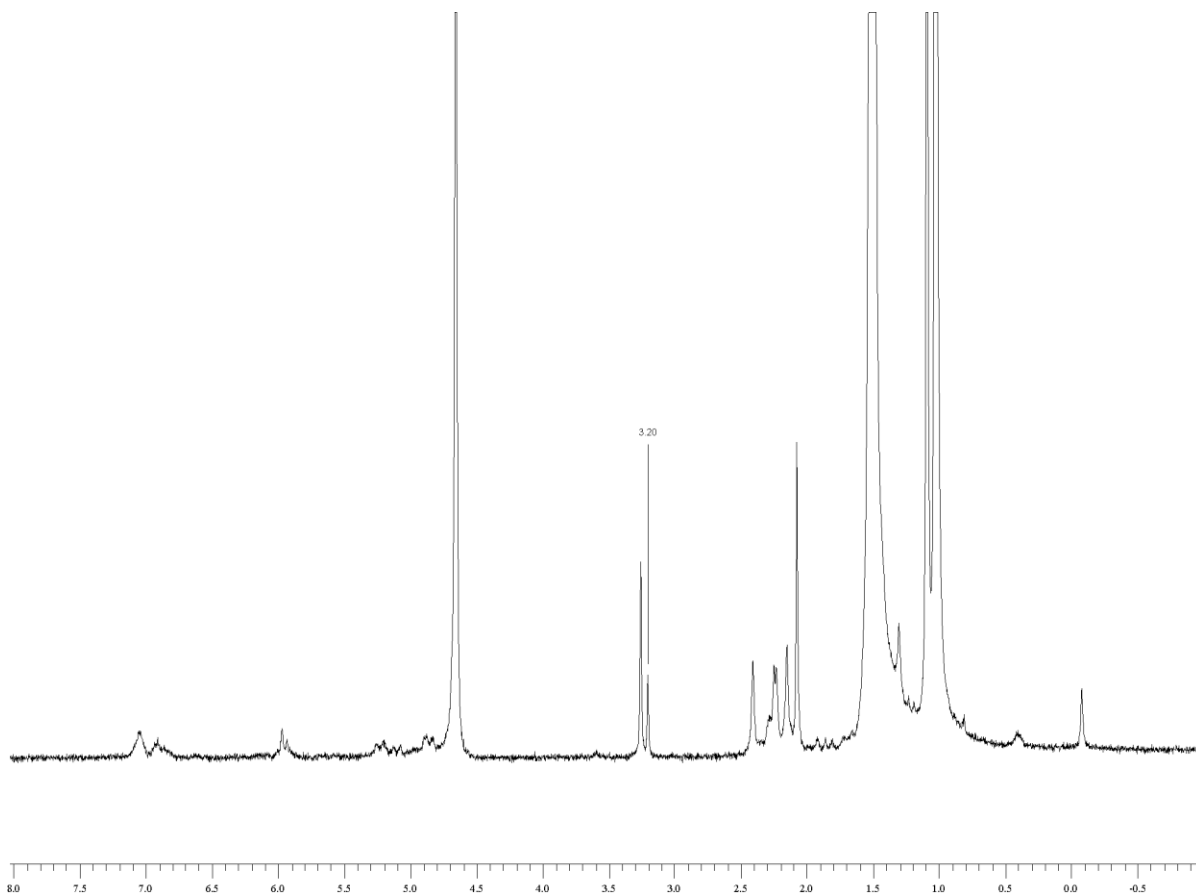
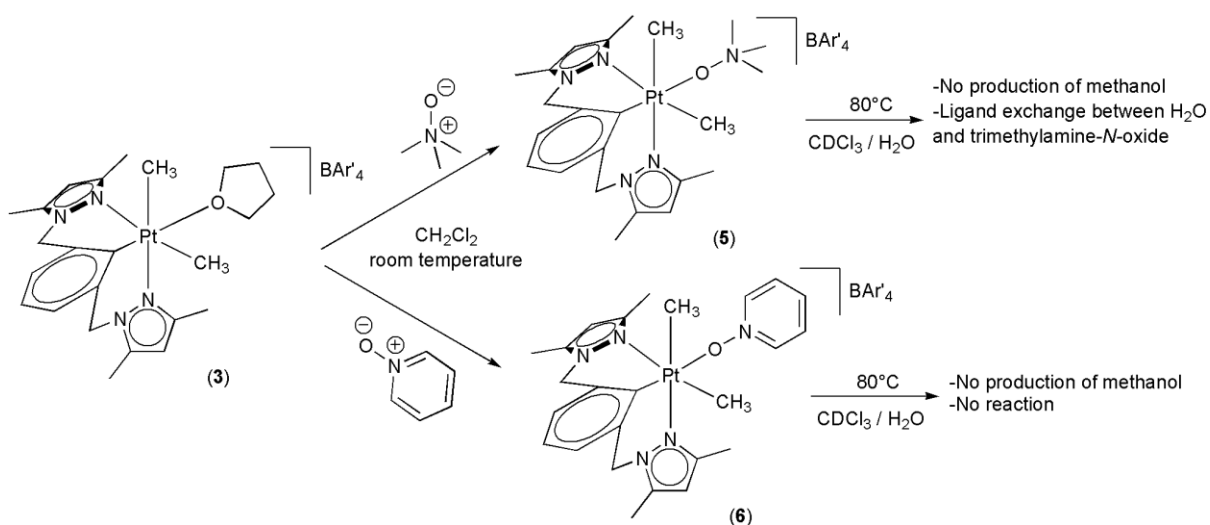


Figure 3.14. The reaction of $(\text{NCN}')\text{Pt}(\text{Me})_2\text{OTf}$ (**2**) with *tert*-butyl peroxide and the observation of resonance due to methanol.

Importantly, the oxygen of methanol is not from $\text{H}_2\text{O}/\text{D}_2\text{O}$, because there is no observation of the peaks around 3.34 ppm without presence of oxidants by heating **2** at 80 °C in neat D_2O . Furthermore, complex **2** is thermally stable due to no observation of changes in ^1H NMR upon heating at 80 °C in neat D_2O after 3 days. Thus, **2** is stable against water and heat in the absence of an oxidant.

The reactions of complex **3** with trimethylamine-*N*-oxide and pyridine-*N*-oxide result in ligand exchange between THF and the oxidants (Scheme 3.8). The new complexes, **5** and **6**, have a significant chemical shift difference from complex **3** in ^1H NMR spectra (Figure

3.12 and Figure 3.13). For example, coordinated ONMe₃ resonates at 3.20 ppm while free ONMe₃ resonates at 3.29 ppm. Also, coordinated pyridine-*N*-oxide resonates at 8.06 ppm (ortho), 7.65 ppm (para) and 7.46 ppm (meta), which present large chemical shift difference from free pyridine-*N*-oxide (8.25 ppm for ortho protons and 7.34 ppm for meta and para protons). When complex **5** was heated at 80°C in presence of water (approximately 20 equivalents), the formation of two metal complexes was observed. This may be due to ligand exchange of trimethylamine-*N*-oxide with H₂O. In the same condition with the previous reaction, complex **6** showed thermal stability, and no reaction occurred. These reactions did not produce any evidence of methanol resonance in ¹H NMR spectra.



Scheme 3.8. The reactions of complex **3** with trimethylamine-*N*-oxide and pyridine-*N*-oxide.

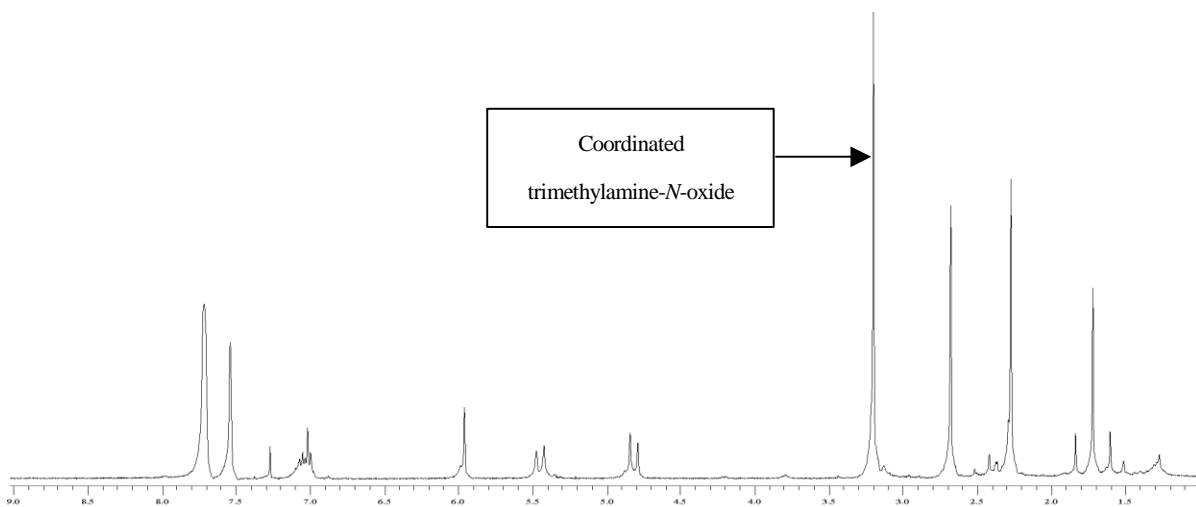


Figure 3.12. ^1H NMR spectrum of $[(\text{NCN}')\text{Pt}(\text{Me})_2(\text{ONCH}_3)][\text{BAR}'_4]$ (5) in CDCl_3 .

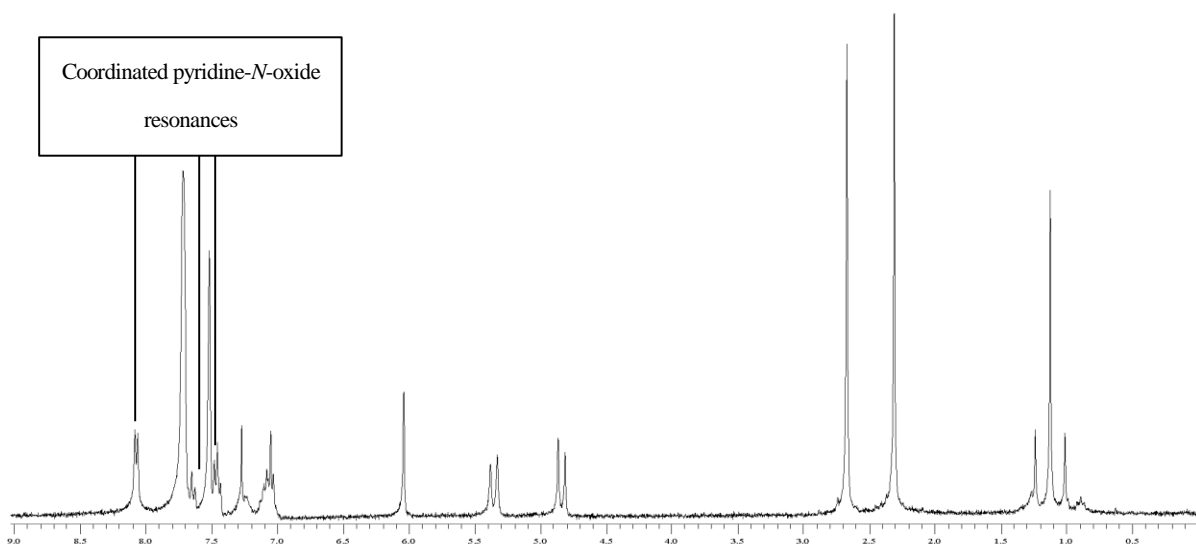


Figure 3.13. ^1H NMR spectrum of $[(\text{NCN}')\text{Pt}(\text{Me})_2(\text{O-pyridine})][\text{BAR}'_4]$ (6) in CDCl_3 .

3.3 Summary

Neither (NCN)Pt(Me)₂OTf (**1**) nor (NCN')Pt(Me)₂OTf (**2**) have been cleanly converted to the Pt amido complexes. A more reactive cationic species, [(NCN')Pt(Me)₂(THF)]BAr'₄ (**3**), was isolated and characterized. Complex **3** preferably reacts with NH₃ ligand, which is a stronger electron donor ligand than THF, to yield [(NCN')Pt(Me)₂(NH₃)] [BAr'₄] (**4**).

Preliminary results show that H₂O₂ and *tert*-butyl peroxide might coordinate to an open coordination site of **2** to insert oxygen atom into the Pt-Me bonds and release methanol via a hydrolysis reaction in D₂O.

3.4 Experimental procedures

Unless otherwise noted, all synthetic procedures were performed under anaerobic conditions in a nitrogen-filled glovebox or using standard Schlenk techniques. Glovebox purity was maintained by periodic nitrogen purges and was monitored by an oxygen analyzer (O₂ < 15 ppm for all reactions in glovebox). Benzene, tetrahydrofuran and diethyl ether (stored over 4 Å molecular sieves) were dried by distillation from sodium/benzophenone. Pentane was distilled over sodium. Acetonitrile and methanol were dried by distillation from CaH₂. Hexanes (stored over 4 Å molecular sieves) and methylene chloride were purified by passage through a column of activated alumina. Benzene-*d*₆, acetonitrile-*d*₃, and chloroform-*d*₁ were degassed using three freeze-pump-thaw cycles and stored under a nitrogen atmosphere over 4 Å molecular sieves. ¹H NMR spectra were recorded on a Varian Mercury 300 or 400 MHz spectrometer, and ¹³C NMR spectra (operating frequency 75 MHz) were

recorded on a Varian Mercury 300 MHz spectrometer. All ^1H and ^{13}C NMR spectra are referenced against residual proton signals (^1H NMR) or the ^{13}C resonances of the deuterated solvent (^{13}C NMR). ^{19}F NMR spectra were obtained on a Varian 300 MHz spectrometer (operating frequency 282 MHz) and referenced against an external standard of hexafluorobenzene ($\delta = -163.0$). Electrochemical experiments were performed under a nitrogen atmosphere using a BAS Epsilon Potentiostat. Cyclic voltammograms were recorded in a standard three-electrode cell from -2.00 V to +2.00 V with a glassy carbon working electrode and tetrabutylammonium hexafluorophosphate (TBAH) as electrolyte. Tetrabutylammonium hexafluorophosphate was dried under dynamic vacuum at 140 °C for 48 hours prior to use. All potentials are reported versus NHE (normal hydrogen electrode) using cobaltocenium hexafluorophosphate as an internal standard. Elemental analyses were performed by Atlantic Microlabs, Inc. The ligands 2,6-bis(pyrazol-1-ylmethyl)bromobenzene (NCN) 2,6-bisbromobenzene (NCN'), and $\{\text{PtMe}_2(\text{SEt}_2)\}_2$ were synthesized as previously reported.^{15, 30}

(NCN)Pt(Me)₂OTf (1). A 100 mL flask was charged with (NCN)Pt(Me)₂Br (0.517 g, 0.95 mmol) in 40 mL of THF. Upon addition of AgOTf (0.244 g, 0.95 mmol) a white precipitate (presumably AgBr) formed, and the mixture was stirred for 30 minutes. The volatiles were removed in vacuo, the residual material was dissolved in approximately 20 mL of CH₂Cl₂, and the solution was filtered through a plug of Celite. The filtrate volume was reduced to approximately 10 mL in vacuo and hexanes (approximately 40 mL) were added to form a precipitate. The product was collected via vacuum filtration through a fine porosity frit to give a white solid (0.273 g, 47%). ^1H NMR (CDCl₃, δ): 8.26, 7.56 (1:1 ratio, each a d,

$^3J_{\text{HH}} = 2$ Hz, pyrazolyl 3, 5-positions), 7.04 (3H, m, overlap of phenyl *meta* and *para* positions), 6.43 (2H, t, $^3J_{\text{HH}} = 2$ Hz, pyrazolyl 4-position), 5.86, 4.92 (each 2H, each a d, $^2J_{\text{HH}} = 15$ Hz, CH_2), 1.55 (6H, 33% d to ^{195}Pt , $^2J_{\text{Pt-H}} = 70$ Hz, $\text{Pt}(\text{CH}_3)_2$). ^{13}C NMR (CDCl_3 , δ): 140.8 (s, phenyl ortho position), 136.7 (s, phenyl meta), 131.8 (s, pyrazolyl 5 position), 129.3 (33% d to Pt, $^1J_{\text{CPt}} = 27$ Hz, phenyl ipso), 125.4 (s, pyrazolyl 3 position), 120.0 (q, $^1J_{\text{CF}} = 273$ Hz, CF_3 of OTf), 116.7 (s, pyrazolyl 4 position), 107.4 (s, phenyl para position), 58.4 (s, CH_2), -5.4 (m, 33% d to Pt, $^1J_{\text{Pt-C}} = 658$ Hz, $\text{Pt}(\text{CH}_3)_2$), ^{19}F NMR (CDCl_3 , δ): -74.7 (s, OTf). CV (THF, TBAH, 100 mV/s): $E_{\text{p,a}} = -1.47$ V, Pt(IV/III). Anal. Calc. for $\text{C}_{17}\text{H}_{19}\text{F}_3\text{N}_4\text{O}_3\text{PtS}$: C, 33.39; H, 3.13; N, 9.16. Found: C, 33.98; H, 3.35; N, 8.93.

(NCN')Pt(Me)₂OTf (2). A 100 mL flask was charged with (NCN')Pt(Me)₂Br (0.42 g, 0.71 mmol) in 40 mL THF. Upon addition of AgOTf (0.18 g, 0.70 mmol) a white precipitate (presumably AgBr) formed, and the mixture was stirred for 30 minutes. The volatiles were removed in vacuo the residual material was dissolved in approximately 20 mL of CH_2Cl_2 , and the solution was filtered through a plug of Celite. The filtrate volume was reduced to approximately 10 mL in vacuo, and hexanes (approximately 40 mL) were added to form a precipitate. The product was collected via vacuum filtration through a fine porosity frit to give a white solid (0.42 g, 96%). ^1H NMR (CDCl_3 , δ): 7.03 (3H, m, overlap of phenyl *meta* and *para* position), 6.01 (2H, s, pyrazolyl 4-position), 5.52, 4.82 (each 2H, each a d, $^2J_{\text{HH}} = 15$ Hz, CH_2), 2.63, 2.32 (each 6H, each a s, pyrazolyl 3-, 5- CH_3), 1.85 (6H, 33% d to ^{195}Pt , $^2J_{\text{Pt-H}} = 70$ Hz, $\text{Pt}(\text{CH}_3)_2$). ^{13}C NMR (CDCl_3 , δ): 152.3 (s, phenyl ortho position), 141.5 (s, phenyl meta), 137.3 (s, pyrazolyl 5 or 3 position), 129.2 (33% d to Pt, $^1J_{\text{CPt}} = 54$ Hz, phenyl ipso), 127.2 (q, $^1J_{\text{CF}} = 255$ Hz, CF_3 of OTf), 125.5 (s, pyrazolyl 3 or 5 position),

115.3 (s, pyrazolyl 4 position), 109.0 (s, phenyl para position), 54.4 (s, CH₂), 15.9, 12.5 (s, pyrazolyl 3-, 5-CH₃), -5.4 (m, 33% d to Pt, ¹J_{Pt-C} = 670 Hz, Pt(CH₃)₂), ¹⁹F NMR (CDCl₃, δ): -74.7 (s, OTf). CV (THF, TBAH, 100 mV/s): E_{p,a} = -1.52 V, Pt(IV/III).

[(NCN')Pt(Me)₂(THF)][BAr'₄] (3). A 100 mL round bottom flask was charged with (NCN')Pt(Me)₂OTf (**2**) (0.11 g, 0.165 mmol) and NaBAr'₄ (0.161 g, 0.181 mmol) in 30 mL of THF. After the mixture was stirred for 3 hours, the volatiles were removed in vacuo. The residual material was dissolved in approximately 20 mL of CH₂Cl₂, and the solution was filtered through a plug of Celite. The filtrate volume was reduced to approximately 5 mL in vacuo and hexanes (approximately 40 mL) were added to form a precipitate. The product was collected via vacuum filtration through a fine porosity frit to give a white solid (0.18 g, 75%). ¹H NMR (CDCl₃ δ): 7.71 (8H, br s, BAr'₄ ortho), 7.52 (4H, br s, BAr'₄ para), 7.03 (3H, m, overlap of phenyl *meta* and *para* position), 6.02 (2H, s, pyrazolyl 4-position), 5.41, 4.85 (each 2H, each a d, ²J_{HH} = 16 Hz, CH₂), 3.83 (4H, m, THF α-CH₂), 2.37, 2.29 (each 6H, each a s, pyrazolyl 3-, 5-CH₃), 1.97 (4H, THF β-CH₂), 1.51 (6H, 33% d to ¹⁹⁵Pt, ²J_{Pt-H} = 68 Hz, Pt(CH₃)₂). ¹³C NMR (CDCl₃, δ): 161.8 (1:1:1:1 quartet, ¹J_{CB} = 50 Hz, ipso C of BAr'₄), 151.3 (s, phenyl ortho position), 143.5 (s, phenyl meta), 136.3 (s, pyrazolyl 3 or 5 position), 134.9 (s, para-C of BAr'₄), 129.9 (s, phenyl ipso), 129.0 (q, ²J_{CF} = 34 Hz, meta-C of BAr'₄), 126.6 (s, pyrazolyl 3 or 5 position), 124.7 (q, ¹J_{CF} = 272 Hz, CF₃ of BAr'₄), 119.3 (s, pyrazolyl 4 position), 117.7 (s, ortho-C of BAr'₄), 109.3 (s, phenyl para), 69.6 (s, α-C of THF), 54.2 (s, CH₂), 25.2 (s, β-C of THF), 15.7, 12.3 (both s, pyrazolyl 3-, 5-CH₃), -1.5 (m, 33% d to Pt, ¹J_{Pt-C} = 670 Hz, Pt(CH₃)₂). ¹⁹F NMR (CDCl₃, δ): -58.9 (s,

BAR'₄). Anal. Calc. for C₅₆H₄₇BF₂₄N₄OPt: C, 46.24; H, 3.26; N, 3.85 (0.3 equivalent of cyclopentane present). Found: C, 48.00; H, 3.71; N, 3.79.

[(NCN')Pt(Me)₂(NH₃)] [BAR'₄] (4). A 100 mL round bottom flask was charged with [(NCN')Pt(Me)₂(THF)] [BAR'₄] (3) (0.18 g, 0.124 mmol) in 20 mL THF and approximately 10 mL of a saturated solution of NH₃ in THF (prepared by condensation of ammonia gas into THF) was added. After the mixture was stirred for 24 hours, the volatiles were removed in vacuo. The residual material was dissolved in approximately 20 mL of CH₂Cl₂, and the solution was filtered through a plug of Celite. The filtrate volume was reduced to approximately 5 mL in vacuo and hexanes (approximately 40 mL) were added to form a precipitate. The product was collected via vacuum filtration through a fine porosity frit to give a white solid (0.14 g, 80%). ¹H NMR (CDCl₃ δ): 7.71 (8H, br s, BAR'₄ ortho), 7.53 (4H, br s, BAR'₄ para), 7.11 (3H, m, overlap of phenyl *meta* and *para* position), 5.99 (2H, s, pyrazolyl 4-position), 5.37, 4.88 (each 2H, each a d, ²J_{HH} = 16 Hz, CH₂), 2.70 (3H, br s, NH₃), 2.32, 1.51 (each 6H, each a s, pyrazolyl 3-, 5-CH₃), 1.35 (6H, ²J_{Pt-H} = 70 Hz, Pt(CH₃)₂). ¹³C NMR (CDCl₃, δ): ¹³C NMR (CDCl₃, δ): 161.7 (1:1:1:1 quartet, ¹J_{CB} = 50 Hz, ipso C of BAR'₄), 150.0 (s, phenyl ortho position), 143.2 (s, phenyl meta), 136.7 (s, pyrazolyl 3 or 5 position), 134.9 (s, para-C of BAR'₄), 129.7 (s, phenyl ipso), 129.0 (q, ²J_{CF} = 31 Hz, meta-C of BAR'₄), 126.2 (s, pyrazolyl 4 position), 125.3 (s, pyrazolyl 3 or 5 position), 124.7 (q, ¹J_{CF} = 272 Hz, CF₃ of BAR'₄), 117.7 (s, ortho-C of BAR'₄), 109.6 (s, phenyl para), 54.9 (s, CH₂), 16.6, 12.5 (both s, pyrazolyl 3-, 5-CH₃), -3.2 (s, 33% d to Pt, ¹J_{Pt-C} = 670 Hz, Pt(CH₃)₂). ¹⁹F NMR (CDCl₃, δ): -58.7 (s, BAR'₄). CV (THF, TBAH, 100 mV/s): E_{p,a} = -1.93

V, Pt(IV/III). Anal. Calc. for C₅₂H₄₂BF₂₄N₅Pt: C, 44.63; H, 3.03; N, 5.01. Found: C, 44.50; H, 2.95; N, 4.62.

[(NCN')Pt(Me)₂(trimethylamine-*N*-oxide)][BAr'₄] (5). A 100 mL round bottom flask was charged with [(NCN')Pt(Me)₂(THF)][BAr'₄] (**3**) (0.11 g, 0.08 mmol) and trimethylamine-*N*-oxide (0.01 g, 0.15 mmol) in 20 mL of CH₂Cl₂. After the mixture was stirred for 3 hours, the volatiles were reduced to approximately 1 mL in vacuo. Hexanes (approximately 30 mL) were added to form a precipitate. The product was collected via vacuum filtration through a fine porosity frit to give a white solid (0.07 g, 62%). ¹H NMR (CDCl₃ δ): 7.71 (8H, br s, BAr'₄ ortho), 7.54 (4H, br s, BAr'₄ para), 7.02 (3H, m, overlap of phenyl *meta* and *para* position), 5.96 (2H, s, pyrazolyl 4-position), 5.45, 4.82 (each 2H, each a d, ²J_{HH} = 15 Hz, CH₂), 3.20 (9H, s, trimethylamine-*N*-oxide (CH₃)₃), 2.68, 2.27 (each 6H, each a s, pyrazolyl 3-, 5-CH₃), 1.72 (6H, 33% d to ¹⁹⁵Pt, ²J_{Pt-H} = 70 Hz, Pt(CH₃)₂). ¹³C NMR (CDCl₃, δ): 162.0 (1:1:1:1 quartet, ¹J_{CB} = 50 Hz, ipso C of BAr'₄), 151.9 (s, phenyl ortho position), 142.5 (s, phenyl meta), 137.6 (s, pyrazolyl 3 or 5 position), 135.1 (s, para-C of BAr'₄), 129.5 (s, phenyl ipso), 129.3 (q, ²J_{CF} = 32 Hz, meta-C of BAr'₄), 126.0 (s, pyrazolyl 4 position), 124.9 (q, ¹J_{CF} = 272 Hz, CF₃ of BAr'₄), 119.4 (s, pyrazolyl 3 or 5 position), 117.4 (s, ortho-C of BAr'₄), 109.4 (s, phenyl para), 60.5 (s, trimethylamine-*N*-oxide), 54.3 (s, CH₂), 15.8, 12.1 (both s, pyrazolyl 3-, 5-CH₃), -4.1 (s, 33% d to Pt, ¹J_{Pt-C} = 706 Hz, Pt(CH₃)₂). ¹⁹F NMR (CDCl₃, δ): -58.8 (s, BAr'₄).

[(NCN')Pt(Me)₂(pyridine-*N*-oxide)][BAr'₄] (6). A 100 mL round bottom flask was charged with [(NCN')Pt(Me)₂(THF)][BAr'₄] (**3**) (0.12 g, 0.083 mmol) and pyridine-*N*-oxide (0.01 g, 0.105 mmol) in 20 mL of chloroform. After the mixture was stirred for 2 hours, the

volatiles were removed in vacuo. The residual material was dissolved in approximately 20 mL of CH₂Cl₂, and the solution was filtered through a plug of Celite. The filtrate volume was reduced to approximately 2 mL in vacuo and hexanes (approximately 40 mL) were added to form a precipitate. The product was collected via vacuum filtration through a fine porosity frit to give a grey solid (0.09 g, 70%). ¹H NMR (CDCl₃ δ): 8.06 (2H, d, ²J_{HH} = 7 Hz, pyridine-*N*-oxide ortho), 7.70 (8H, br s, BAr'₄ ortho), 7.65 (1H, t, ²J_{HH} = 7 Hz, pyridine-*N*-oxide para), 7.50 (4H, br s, BAr'₄ para), 7.46 (2H, t, ²J_{HH} = 7 Hz, pyridine-*N*-oxide meta), 7.05 (3H, m, overlap of phenyl *meta* and *para* position), 6.04 (2H, s, pyrazolyl 4-position), 5.35, 4.84 (each 2H, each a d, ²J_{HH} = 16 Hz, CH₂), 2.67, 2.31 (each 6H, each a s, pyrazolyl 3-, 5-CH₃), 1.12 (6H, 33% d to ¹⁹⁵Pt, ²J_{Pt-H} = 70 Hz, Pt(CH₃)₂). ¹³C NMR (CDCl₃, δ): 161.9 (1:1:1:1 quartet, ¹J_{CB} = 50 Hz, ipso C of BAr'₄), 152.1 (s, phenyl ortho), 142.5 (s, phenyl meta), 142.2 (s, pyridine-*N*-oxide ortho), 137.4 (s, pyrazolyl 3 or 5 position), 135.2 (s, pyridine-*N*-oxide meta), 135.0 (s, para-C of BAr'₄), 130.2 (s, phenyl ipso), 129.3 (s, pyridine-*N*-oxide para), 128.8 (q, ²J_{CF} = 31 Hz, meta-C of BAr'₄), 127.1 (s, pyrazolyl 4 position), 126.1 (s, pyrazolyl 3 or 5 position), 124.7 (q, ¹J_{CF} = 271 Hz, CF₃ of BAr'₄), 117.7 (s, ortho-C of BAr'₄), 109.5 (s, phenyl para), 54.4 (s, CH₂), 15.3, 12.2 (both s, pyrazolyl 3-, 5-CH₃), -2.8 (m, 33% d to Pt, ¹J_{Pt-C} = 700 Hz, Pt(CH₃)₂). ¹⁹F NMR (CDCl₃, δ): -58.9 (s, BAr'₄).

Reaction of (NCN')Pt(Me)₂OTf (2) and oxidants. (NCN')Pt(Me)₂OTf (2) (0.01 g, 0.015 mmole) and approximately 5 equivalents of each oxidant (H₂O₂, *tert*-butyl-peroxide, KIO₄ and trimethylamine-*N*-oxide) were combined in a screw cap NMR tube in D₂O (0.5 mL). The reaction was followed by ¹H NMR until no further decomposition of the metal

complex was noted. Methanol production was confirmed by addition of trace amount of free methanol to the NMR reaction tube.

REFERENCES

1. Kubas, G. J., *Metal Dihydrogen and σ -Bond Complexes*. Kluwer Academic/Plenum Publishers: New York, 2001; p 259-296.
2. Labinger, J. A.; Bercaw, J. E. *Nature* **2002**, 417, 507-514.
3. Arndtsen, B. A.; Bergman, R. G.; Mobley, T. A.; Peterson, T. H. *Acc. Chem. Res.* **1995**, 28, 154-162.
4. Jones, W. D.; Feher, F. J. *Acc. Chem. Res.* **1989**, 22, 91-100.
5. Crabtree, R. H. *Chem. Rev.* **1985**, 85, 245-269.
6. Crabtree, R. H. *Chem. Rev.* **1995**, 95, (4), 987-1007.
7. Goldberg, K. I.; Goldman, A. S., *Activation and Functionalization of C-H Bonds*. American Chemical Society: Washington, DC, 2004; Vol. 885.
8. Feng, Y.; Lail, M.; Barakat, K. A.; Cundari, T. R.; Gunnoe, T. B.; Petersen, J. L. *J. Am. Chem. Soc.* **2005**, 127, 14174-14175.
9. Tenn, I., W. J.; Young, K. J. H.; Bhalla, G.; Oxgaard, J.; Goddard III, W. A.; Periana, R. A. *J. Am. Chem. Soc.* **2005**, 127, 14172-14173.
10. Davies, D. L.; Donald, S. M. A.; Macgregor, S. A. *J. Chem. Soc. Chem.* **2005**, 127, (40), 13754-13755.
11. Feng, Y.; Lail, M.; Foley, N. A.; Gunnoe, T. B.; Barakat, K. A.; Cundari, T. R.; Petersen, J. L. *J. Am. Chem. Soc.* **2006**, 128, 7982-7994.
12. Gunnoe, T. B. *Eur. J. Inorg. Chem.* **2007**, (9), 1185-1203.
13. Kloek, S. M.; Heinekey, D. M.; Goldberg, K. L. *Angew. Chem. Int. Ed.* **2007**, 46, (25), 4736-4738.
14. Zhang, Y. G. *Inorg. Chem.* **1982**, 21, (11), 3886-3889.
15. Canty, A. J.; Patel, J.; Skelton, B. W.; White, A. H. *J. Organomet. Chem.* **2000**, 599, (2), 195-199.
16. Zhang, J. Synthesis and reactivity of ruthenium and platinum amido and carbene complexes: application toward carbon-nitrogen bond forming reactions. North Carolina State University, Raleigh, 2005.

17. Schlecht, S.; Magull, J.; Fenske, D.; Dehnicke, K. *Angew. Chem. Int. Ed. Engl.* **1997**, 36, (18), 1994-1995.
18. Butts, M. D.; Scott, B. L.; Kubas, G. J. *J. Am. Chem. Soc.* **1996**, 118, (47), 11831-11843.
19. Thomas, J. C.; Peters, J. C. *J. Am. Chem. Soc.* **2001**, 123, (21), 5100-5101.
20. Brown, S. N.; Mayer, J. M. *J. Am. Chem. Soc.* **1996**, 118, (48), 12119-12133.
21. Vanasselt, A.; Burger, B. J.; Gibson, V. C.; Bercaw, J. E. *J. Am. Chem. Soc.* **1986**, 108, (17), 5347-5349.
22. Parkin, G.; Bunel, E.; Burger, B. J.; Trimmer, M. S.; Asselt, A. V.; Bercaw, J. E. *J. Mol. Catal.* **1989**, 41, 21-39.
23. Tahmassebi, S. K.; Conry, R. R.; Mayer, J. M. *J. Am. Chem. Soc.* **1993**, 115, (16), 7553-7554.
24. Bottomley, F.; Sutin, L. *Adv. Organomet. Chem.* **1988**, 28, 339-396.
25. Spaltenstein, E.; Erikson, T. K. G.; Critchlow, S. C.; Mayer, J. M. *J. Am. Chem. Soc.* **1989**, 111, (2), 617-623.
26. Herrmann, W. A. *Angew. Chem. Int. Ed. Engl.* **1988**, 27, (10), 1297-1313.
27. Conley, B. L.; Ganesh, S. K.; Gonzales, J. M.; Tenn, W. J.; Young, K. J. H.; Oxgaard, J.; Goddard, W. A.; Periana, R. A. *J. Am. Chem. Soc.* **2006**, 128, (28), 9018-9019.
28. Murahashi, S. I.; Ono, S.; Imada, Y. *Angew. Chem. Int. Ed.* **2002**, 41, (13), 2366-2368.
29. Gottlieb, H. E.; Kotlyar, V.; Nudelman, A. *J. Org. Chem.* **1997**, 62, (21), 7512-7515.
30. Kuyper, J.; Vanderlaan, R.; Jeanneaus, F.; Vrieze, K. *Transition Met. Chem.* **1976**, 1, (4), 199-204.